

Atmospheric Physics

Stephan de Roode

Delft University of Technology

Version, May 10, 2020

Preface

Weather and climate are becoming increasingly important to the society. Industrialization has led to a gradual increase of greenhouse gases like carbon dioxide and water vapor, which is having an effect on the global radiation balance. The energy transition from fossil fuels to renewables nowadays demands the best and most accurate predictions of sun and wind. At the same time a better understanding of the formation of clouds and precipitation in time and space is relevant to farming, transportation planning, and the recreational industry. Continuous improvements of weather forecast and climate models, in addition to new technology for measuring atmospheric properties, provide unprecedented data that need a careful and thoughtful analysis by skilful experts.

At TU Delft, the course *Environmental Physics* offered by the Faculty of Applied Sciences since 2000, was one of the first courses that touched upon a few of these topics. In 2012 some of its classes were also given in the course *Physics of the Earth and Atmosphere* which was launched in 2012 as a compulsory course in the new MSc track 'Geosciences and Remote Sensing' at the Faculty of Civil Engineering and Remote Sensing. Another course of this program is *Atmospheric Science* which currently focusses strongly on applications for which the atmospheric boundary layer and turbulence play a key role, such as wind energy. In 2016 another MSc track 'Environmental Engineering' was started. Here students get an introduction to *Transport Processes* at the soil-atmosphere interface, and *Introduction to Meteorology*. Students who wish to specialize in the global water cycle can also follow *Water in the Atmosphere* and *From Field Observations to Modelling*.

Part I of this syllabus summarizes the topics that students need as prior knowledge for the course 'Water in the Atmosphere'.

<hr/>	
Chapter	
1	Global Energy Balance
2	Atmospheric Thermodynamics
3	Governing Equations
4	Large-scale dynamics
5	Reynolds Averaging
6	Atmospheric Stability

The table below gives an overview of courses in which (a part of it) is being taught.

Part II discusses the atmospheric boundary layer, which is defined as the lower part of the atmosphere. Much attention will be paid to processes like evaporation and turbulent mixing, which both control the possible formation of clouds. Also changes in radiative transfer as a result of cloud

Course	Code	Chapter					
		1	2	3	4	5	6
Env. Phys.	AP3141	X	X	X	X	X	X
Phys. of Atm.	CIE4601	X	X	X		X	X
Atmos. Sci.	CIE4605			X	X	X	
Transp. Procs.	CIE4701				X	X	
Intro Meteo.	CIE4706	X	X	X		X	X

formation will be discussed. The contents of Parts I and II are necessary to be able to follow the specialization course *From Field Observations to Modelling*.

Contents

Contents	2
I Governing equations for the atmosphere	5
Part I	7
1 The global energy balance	7
1.1 Some key elements of radiation	8
1.2 A simple model for the Earth's energy balance	10
2 Atmospheric thermodynamics	15
2.1 Gas law	15
2.2 The Clausius-Clapeyron equation	19
2.3 Hydrostatic pressure	21
2.4 Conservation of energy	24
2.5 The potential temperature	27
2.6 Moist adiabatic temperature lapse rate	28
2.7 Summary and outlook	29
3 Governing equations	31
3.1 Governing equations for atmospheric dynamics	32
3.2 Summary and Outlook	34
4 Reynolds decomposition	37
4.1 Reynolds averaging rules	38
4.2 Why does warm (or moist) air rise?	39
4.3 Reynolds decomposition of the gas law	40
4.4 Reynolds-averaged equations	41
4.5 Summary	43
5 Thermal wind relation and Ekman pumping	45

5.1	Scaling	45
5.2	Large-scale circulation	49
5.3	Governing equations	49
5.4	Thermal wind	50
5.5	Large-scale vertical velocity	50
6	Atmospheric Stability	55
6.1	Stability of the dry atmosphere	56
6.2	Stability of the moist atmosphere	58
II Part II. Clear and Cloud-Topped Atmospheric Boundary Layers		61
Part II. The Atmospheric Boundary Layer		63
7	Preface	63
8	The clear convective boundary layer	65
8.1	Evolution of the boundary-layer depth	66
8.2	Turbulence	69
8.3	Summary and outlook	72
9	An introduction to boundary-layer clouds	75
9.1	Summary and outlook	83
10	Mixed-layer model	85
10.1	Summary and outlook	88
Bibliography		91

Part I

Governing equations for the atmosphere

Chapter 1

The global energy balance

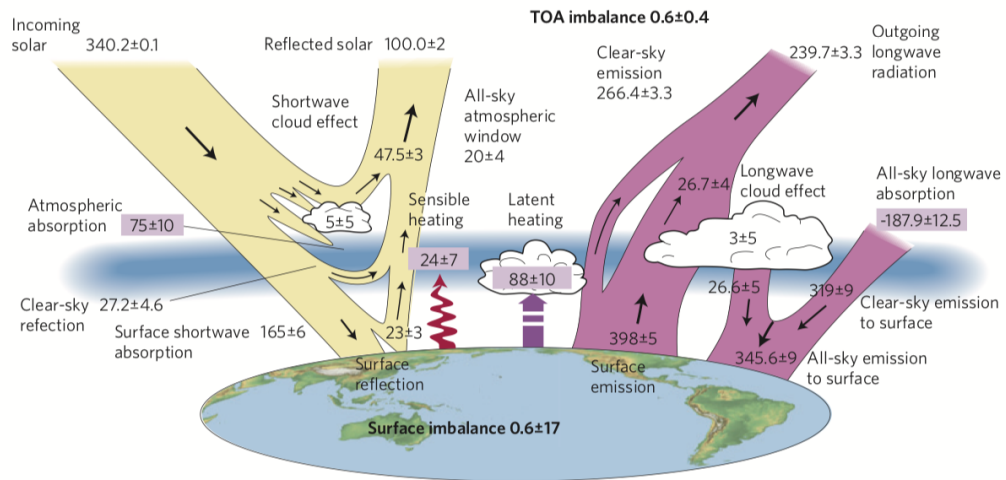


Figure 1.1: The global annual mean energy budget of Earth for the approximate period 2000–2010. All fluxes are in W m^{-2} . Solar fluxes are in yellow and infrared fluxes in pink. The four flux quantities in purple-shaded boxes represent the principal components of the atmospheric energy balance (Stephens et al. 2012).

Fig. 1.1 shows the global mean energy balance. The sun is the engine of the system. The atmosphere absorbs and reflects back to space a part of the solar radiation that is received at the top of the atmosphere (TOA). Clouds have a very strong capacity to reflect solar radiation, but also the molecules in the atmosphere cause a net backscattering of solar radiation, for example by Rayleigh scattering. In addition, gases like water vapor do also absorb solar radiation.

On annual time scales, the amount of energy that is received at the ground surface must be lost in order to achieve a mean equilibrium state. Otherwise, heat would pile up in the soil, leading to an ever increasing temperature. The global mean surface energy balance can be expressed by stating that the sum of all incoming (downward 'dn') and outgoing (upward 'up') energy fluxes must be equal,

$$\text{SW}_{\text{dn}} + \text{LW}_{\text{dn}} = \text{SW}_{\text{up}} + \text{LW}_{\text{up}} + \text{SHF} + \text{LHF}, \quad (1.1)$$

with SW the solar radiation flux, LW the infrared radiation flux, and the so-called sensible and latent heat fluxes (SHF and LHF, respectively). The SHF directly heats the atmosphere. The LHF is the same as evaporation of water vapor from the ground surface in units of W m^{-2} . An evaporation rate of 1 mm day^{-1} corresponds roughly to about 30 W m^{-2} . As evaporation requires

energy, it leads to a cooling of the ground surface. However, once water vapor starts to condense in clouds, energy is released, which, in turn, heats the atmosphere.

The **albedo**, or reflection of solar radiation is defined as,

$$R = \frac{SW_{\text{up}}}{SW_{\text{dn}}}. \quad (1.2)$$

The albedo can be defined at any height, for example at the top of the atmosphere, above a cloud layer, or at the ground surface. For fresh snow the ground surface is rather large ($R \sim 0.9$). For oceans, which cover the largest area on Earth, the albedo is about 0.06.

The numbers for the various components of the infrared radiative fluxes are striking. For example, the radiative flux emitted from the ground surface of the Earth is larger than the value of mean downward solar radiation flux at the top of the atmosphere. This is actually an effect of the presence of the atmosphere. Some gases like water vapor, carbondioxide and methane, but also clouds absorb a fraction of the radiation that is emitted by the Earth. The atmosphere, in turn, emits infrared radiation in both downward and upward directions. This 'trapping' effect strongly enhances the total amount of energy received at the ground surface, and is called the **greenhouse** effect.

The strength with which the atmosphere can absorb and emit infrared radiation depends on the greenhouse gas concentrations. The stronger the greenhouse effect, the larger the value of LW_{dn} received at the ground surface. On the basis of the global mean surface energy balance (Eq. eq:SEB) one could speculate about possible scenarios of how an increase in LW_{dn} might affect the global climate. For example, imagine a scenario in which the LHF increases. This will have a direct effect on the global mean precipitation P since the global water balance states

$$\text{LHF} = P. \quad (1.3)$$

Therefore, in the situation that the global mean value of the LHF increases, the global mean precipitation will increase, too. In another possible scenario a stronger evaporation may cause an increase in global cloudiness. Because this would enhance the reflectivity of solar radiation, more clouds would lead to a decrease in SW_{dn} , thereby reducing, or even completely offsetting the enhanced greenhouse effect (Randall et al. 1984). On the other hand, a part of an enhanced LW_{dn} may promote larger values of LW_{up} or SHF, both of which cause a warming of the atmosphere. Since a warmer atmosphere may contain more water vapor, one could reason that this might reduce the amount of clouds thereby amplifying global warming.

Dufresne and Bony (2008) analysed results from different climate models. In particular, they assessed how changes in the greenhouse gas concentrations, surface albedo, and global cloudiness each contribute to a global warming. They found that any of their changes do all support a global warming effect. In their study they distinguished between water vapor and all other greenhouse gases like carbondioxide and methane. The positive water vapor feedback can be explained as follows. Because a warming of the atmosphere allows more water vapor to be present, and because water vapor itself is a strong greenhouse gas, the gradual increase in atmospheric water vapor is an important positive feedback to the increase in CO_2 concentrations. The positive surface albedo feedback is due to the melting of snow and ice which allows for an enhanced absorption of solar radiation. The strength of the cloud feedback varies strongly among the different models, but, in any case, they do all predict a positive feedback. Although the atmosphere will moisten under conditions of global warming, the positive cloud feedback however suggests a decrease in global cloud amount.

1.1 Some key elements of radiation

The intensity of the radiative flux I_λ for a black body as a function of the wavelength λ and the temperature T is given by the Planck's law (Liou 2002)

$$I_\lambda(\lambda, T) = \frac{2hc^2}{\lambda^5} \frac{1}{e^{hc/kT\lambda} - 1} \quad (1.4)$$

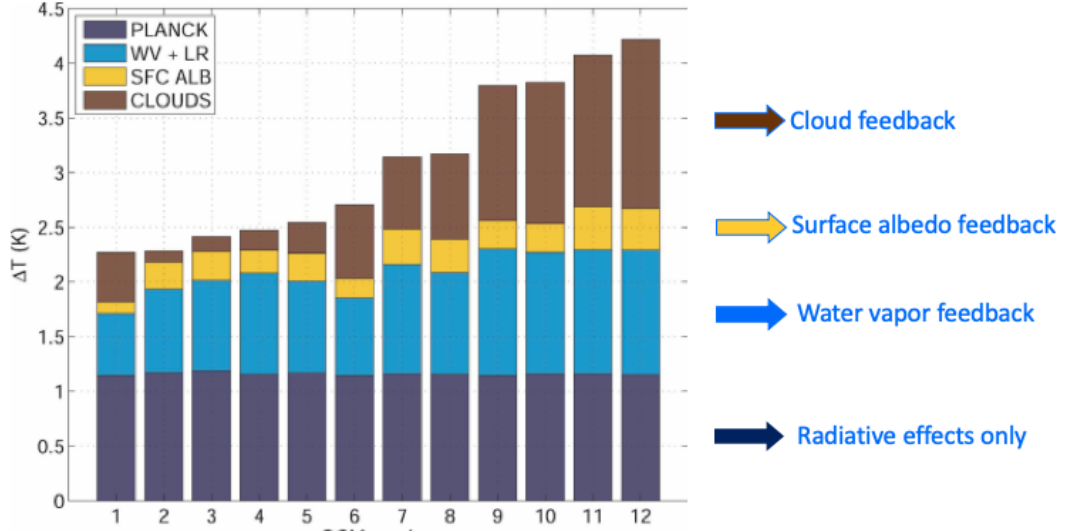


Figure 1.2: Results from 12 different global climate models (Dufresne and Bony 2008). It shows the change in the global mean temperature as a result of a change in the greenhouse gas concentrations (radiative effects only), the resulting changes in water vapor, surface albedo, and cloud amount (cloud feedback).

	$T(K)$	R (m)	$L_{ES}(m)$
Sun	5778	6.96342×10^8	
Earth	288	6.371×10^6	1.496×10^{11}

Table 1.1: The mean temperature and radius of the Earth and the sun, and distance L_{ES} between the Earth and the sun.

with $c = 3 \times 10^8 \text{ m s}^{-1}$ the speed of light, the Planck constant $h = 6.625 \times 10^{-34} \text{ Js}$ and the Boltzmann constant $k = 1.38 \times 10^{-23} \text{ JK}^{-1}$.

Planck's law can be used to derive the wavelength of maximum emission, by differentiating the Planck function with respect to wavelength, and setting the result to zero,

$$\frac{\partial I_\lambda}{\partial \lambda} = 0. \quad (1.5)$$

Wien derived theoretically

$$\lambda_{\max} = \frac{a}{T}, \quad (1.6)$$

where $a = 2.897 \times 10^{-3} \text{ mK}$. The total black-body radiative flux is

$$F(T) = \int_0^\infty \pi I_\lambda d\lambda = \sigma T^4 \quad (1.7)$$

with the Stefan-Boltzmann constant $\sigma = 5.67 \times 10^{-8} \text{ Wm}^{-2}\text{K}^{-4}$. The factor π is needed to convert the *isotropic* radiance I_λ , to irradiance F which is defined to be *perpendicular* component of the emitting or receiving surface. Here we note that the irradiance F is relevant flux which appears in the heat equation.

Fig. 1.3 shows the Planck function. The area under each graph, which represents to total radiative flux, grows with increasing temperature. In accord with Wien's displacement law Eq. (1.6) the plot also shows how the spectral peak tends to shift toward larger wavelengths for lowering temperatures. The colors that the human eye sees are in the waveband in which the sun has its

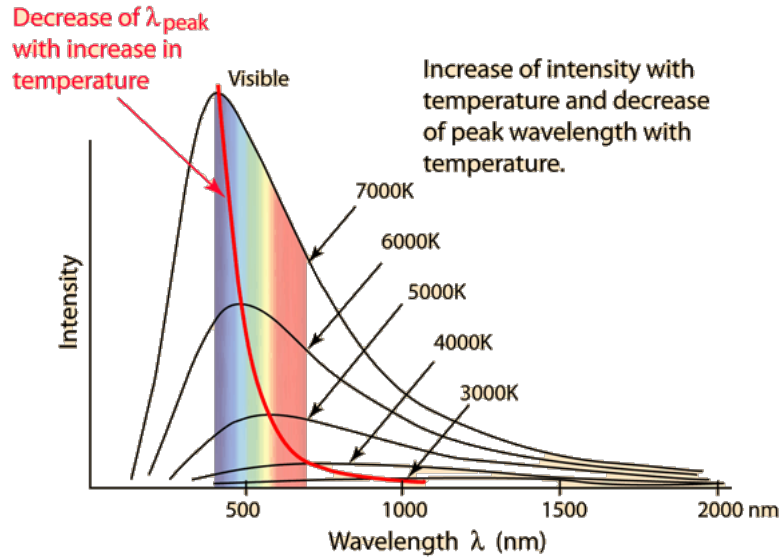


Figure 1.3: The Planck function for different temperatures. Copied from <http://hyperphysics.phy-astr.gsu.edu/hbase/wien.html>.

maximum intensity, so solar radiation is often called visible radiation. Fig. 1.4 shows the Planck curves as emitted by the sun and the Earth. Because of the large temperature difference between them, they radiate at very different wavelengths, with only a little bit of overlap near $4 \mu\text{m}$. This separation is the reason why solar radiation is sometimes called shortwave radiation, as it is present at wavelengths much shorter than for the radiation that is emitted by the Earth. This 'terrestrial' radiation predominantly takes place in the infrared, or longwave waveband.

Fig. 1.3 also shows the scattering cross section σ_{sca} for air molecules ("Rayleigh scattering") and absorption cross sections σ_{abs} for a few strongly absorbing gases. Both σ_{sca} and σ_{abs} are quantities that give a measure for the probability of a scattering or absorption event, respectively. The net decrease of the radiative intensity is also proportional to the concentration of the particular scattering or absorbing molecule.

Water vapor, carbon dioxide, methane and ozone are all strong absorbing gases. If a gas absorbs infrared radiation this means that some fraction of the radiation that is emitted by the Earth's ground surface cannot escape to space but will be absorbed by the atmosphere. The figure shows that the peak in the infrared spectrum coincides with the waveband in which CO_2 strongly absorbs.

Rayleigh scattering of photons is most efficient for short wavelengths. This is the reason why the sky colors blue during daytime. More 'blue' than 'red' photons are scattered out of the direct solar beam, and this diffuse light reaches our eyes from random directions.

Ozone is a particularly strong absorber at short wavelengths. The photons in the UV waveband are very powerful, and are harmful to life as they can destroy DNA. Fortunately, ozone is filtering out most of the UV radiation. The observed decrease in stratospheric ozone with respect to typical values that were present a few decades ago, most notably in the area over Antarctica (the ozone 'hole'), is therefore a matter of concern to human health. Fortunately, the CFK gases that are responsible for the destruction of stratospheric ozone are not emitted anymore, and ozone concentrations are slowly getting back to their undisturbed values.

1.2 A simple model for the Earth's energy balance

We will make use of the Stefan-Boltzmann equation (1.7) to estimate the equilibrium temperature of the Earth's surface T_E . We will first ignore the presence of an atmosphere, and in the second case

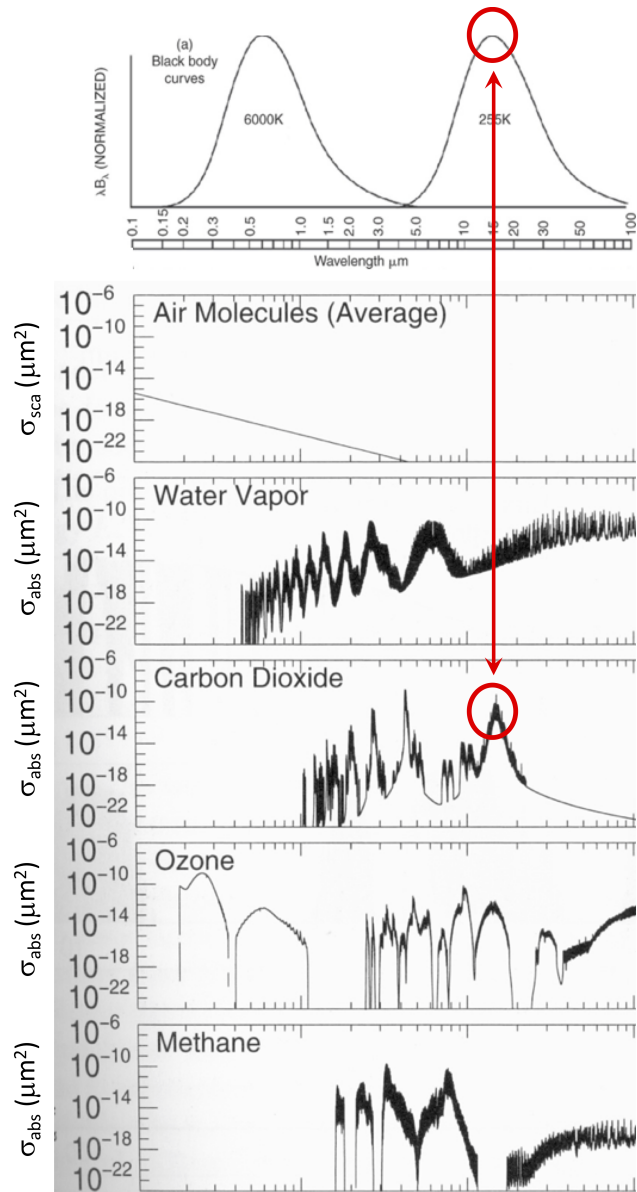


Figure 1.4: The Planck function for temperatures that are close to the mean values of the sun and the Earth. The graphs have been normalized for easy comparison. The lower panels show the absorption cross sections for a few of the most strongly absorbing gases and average scattering cross section for air molecules. Figure adapted from Liou (2002).

we will take into account the emission and absorption of the atmosphere in the infrared waveband.

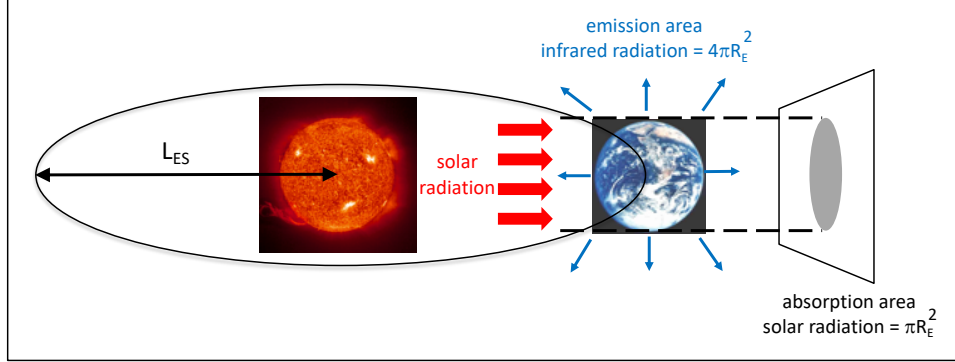


Figure 1.5: Radiative fluxes in the Earth-sun system.

Figure 1.5 shows a schematic of the absorption of solar radiation by the Earth, and the loss of energy by emission of infrared radiation. First of all, it is obvious that we will need to compute how much solar radiation is received at the position of the Earth. Secondly, the schematic illustrates that the maximum amount of solar radiation that the Earth will be able to absorb is determined by its cross section, πR_E^2 , which is a factor of 4 smaller than the total surface area of the Earth, $4\pi R_E^2$.

As a first step we will need to assess the solar radiative flux that reaches Earth. Given the temperature of the sun T_{sun} , Eq. (1.7) can be applied to calculate the solar radiative flux, $F_{\text{sun}} = \sigma T_{\text{sun}}^4$. Recalling that F_{sun} has units of W m^{-2} , a multiplication with the surface area of the sun gives its power, $P = 4\pi R_{\text{sun}}^2 F_{\text{sun}}$. Using the fact that no radiation is absorbed in the space between the sun and the Earth, energy conservation dictates that the solar radiative flux S_0 at a distance L_{ES} from the sun, integrated over a sphere with radius L_{ES} should equal the solar power,

$$P = 4\pi L_{\text{ES}}^2 S_0 \iff S_0 \equiv \left(\frac{R_{\text{sun}}}{L_{\text{ES}}}\right)^2 \sigma T_{\text{sun}}^4 \quad (1.8)$$

S_0 is referred to as the solar constant of a planet and for the Earth $S_0 = 1361 \text{ W m}^{-2}$. It decreases proportionally to the square of the distance between the planet and the sun.

Radiative energy balance. (I) No atmosphere

Since we now know the solar radiative flux reaching the Earth, we can now make a first estimation of the equilibrium temperature of the Earth, T_E . As depicted in Fig. 1.5 the total intercepted amount of solar radiation is proportional to the solar constant and the cross section of the Earth. In an equilibrium state the outgoing flux, which in this case is equal to the emitted longwave radiative flux multiplied by the total surface area of the Earth, must be equal to the intercepted flux,

$$\pi R_E^2 S_0 = 4\pi R_E^2 \sigma T_E^4 \iff T_E = \left(\frac{S_0}{4\sigma}\right)^{1/4} = \left(\frac{1}{2} \frac{R_{\text{sun}}}{L_{\text{ES}}}\right)^{1/2} T_{\text{sun}}, \quad (1.9)$$

The value $S_0/4 = 340 \text{ W m}^{-2}$ is consistent with the global mean solar radiation received at the TOA shown in Fig. 1.1. Although the neglect of an atmosphere causes the solar radiation received at the ground surface to be about twice as large as observed, the simple energy balance gives a global mean temperature T_E of 255 K, which is much lower than the observed value of 288 K.

Radiative energy balance. (II) A single-slab atmosphere

We will now include a single slab homogeneous atmosphere with a mean temperature T_A (see Fig. 1.6). We will assume that the atmosphere absorbs a fraction α of the infrared radiation that is

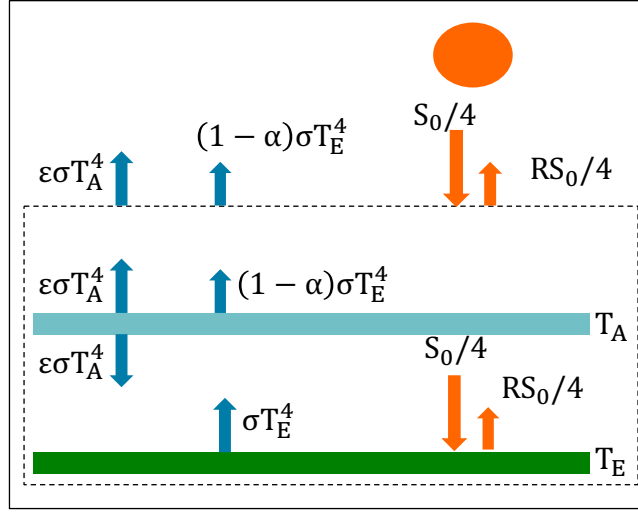


Figure 1.6: The single slab atmosphere global energy balance model.

emitted by the Earth's surface. The atmosphere will also lose energy, which we will assume to be proportional to the energy emitted by black body radiation, $\epsilon\sigma T_A^4$. In the model we will also allow the ground surface to reflect a fraction R of the incident solar radiative flux.

In an equilibrium state a gain of energy must be balanced by an opposite loss. Applying this to the ground surface and the atmosphere gives, respectively,

$$(1 - R) \frac{S_0}{4} + \epsilon\sigma T_A^4 = \sigma T_E^4, \quad (1.10)$$

$$\alpha\sigma T_E^4 = 2\epsilon\sigma T_A^4. \quad (1.11)$$

We have two equations with which can solve the two unknown temperatures T_A and T_E . Before doing so, we wish to make another simplification. Absorption of radiation by molecules occurs at particular wavelengths, α_λ (see Fig. 1.3). Molecules that absorb radiation, also emit, and according to Kirchhoff's law the spectral absorption and emission coefficients are equal, $\epsilon_\lambda = \alpha_\lambda$. Analogous to this relation, we will set the broadband absorptivity equal to the broadband emissivity

$$\alpha = \epsilon \quad (1.12)$$

This gives

$$T_E = \left[\left(\frac{1 - R}{1 - \epsilon/2} \right) \frac{S_0}{4\sigma} \right]^{1/4}. \quad (1.13)$$

For zero albedo and zero emissivity the solution is identical to the one that neglected the atmosphere Eq. (1.9). We find that the global mean temperature will decrease if a fraction of the incident solar radiation is reflected. The key result is that T_E will increase if the atmospheric absorptivity increases (shown in Fig. 1.7). This is what is called the enhanced greenhouse effect. The concentration of greenhouse gases like CO_2 has increased since pre-industrial times (see Fig. 1.8). This has led to more absorption, but, following Kirchhoff's law, also an enhanced emission of infrared radiation. The simple single-slab atmosphere model predicts a rise of the global mean temperature. A feedback may be provided by a subsequent change in the reflectivity R , which in reality may be due to a change in the surface albedo, for example by the change in the global snow and ice cover, or by a change in the global cloud amount.

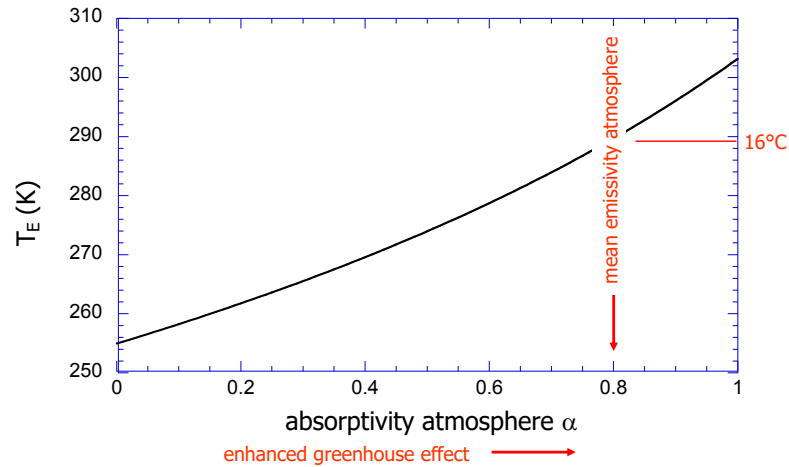


Figure 1.7: The equilibrium temperature of the Earth's surface as a function of the atmospheric absorptivity for a mean albedo $R = 0.29$.

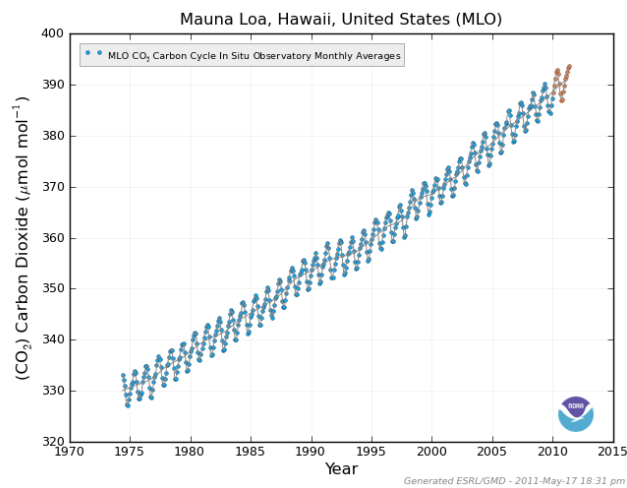


Figure 1.8: The gradual increase of the atmospheric CO_2 concentration as monitored from the Mauna Loa (19°N , 155°W) Observatory (MLO) since 1958. The oscillations are due to the seasonal growth cycle of plants and trees. The latest observations of CO_2 concentrations from MLO can be found at <https://www.esrl.noaa.gov/gmd/ccgg/insitu/index.html>.

Chapter 2

Atmospheric thermodynamics

Water is a very important component of the Earth's atmosphere as its condensation forms the clouds that strongly affect radiative fluxes and produce the rain that is needed for the presence of life on the continents. Here a short summary of basic thermodynamics will be presented.

We will first discuss how the gas law should be applied to the atmosphere which consists of a mixture of different gases. In particular, we will convert the ideal gas law, in which the amount of gas is expressed in moles, to a formula that uses densities. To assess the maximum amount of water vapor that can be present in air the Clausius-Clapeyron relation will be explained. The hydrostatic pressure balance is another important relation that knits together the pressure, height and density of air.

2.1 Gas law

The equation of state for an ideal gas law relates its pressure p , volume V and temperature T by

$$pV = NkT = \nu R^*T, \quad (2.1)$$

where N is the number of identical molecules, ν is the number of moles of gas, $k = 1.3806 \times 10^{-23} \text{JK}^{-1}$ is Boltzmann's constant, $R^* \equiv N_a k = 8.341 \text{ J mol}^{-1} \text{K}^{-1}$ is the universal gas constant, with $N_a = 6.022 \times 10^{23} \text{ mol}^{-1}$ Avogadro's number. The interpretation of the equation is as follows. Consider a box filled with molecules that move through this volume (see Fig 2.1). The pressure is equal to the force exerted by the molecules hitting and rebounding from a unit area of the gas box surface. The temperature is equivalent to the kinetic energy of the molecules. Note that the ideal gas law (2.1) does not include the mass of the molecules. In other words, the pressure exerted by a given number of molecules does *not* depend on the molecular mass.

Dry air (excluding water)

The Earth's atmosphere is a mixture of gases, mostly nitrogen, oxygen and argon, trace gases like carbon dioxide, ozone and methane, and variable amounts of water in its three physical phases (see Fig. 2.2). The concentrations of the mixture of gases that we define as dry air (see Table 2.1) are very closely constant up to a height of about 100 km. The dry atmosphere can be taken to a very good approximation as an ideal gas.

In general, it is useful to formulate the thermodynamic relations in terms of *intensive* variables. An intensive variable is one whose value does not depend on the amount of matter in the system, like the temperature or pressure. In contrast, an *extensive* variable, depends on the size of the system. For instance, the internal energy of a gas is an extensive variable since if we double its size, all else being kept equal, its internal energy will double. Given a system whose volume V contains an amount of mass M ,

$$v = \frac{V}{M} \quad (2.2)$$

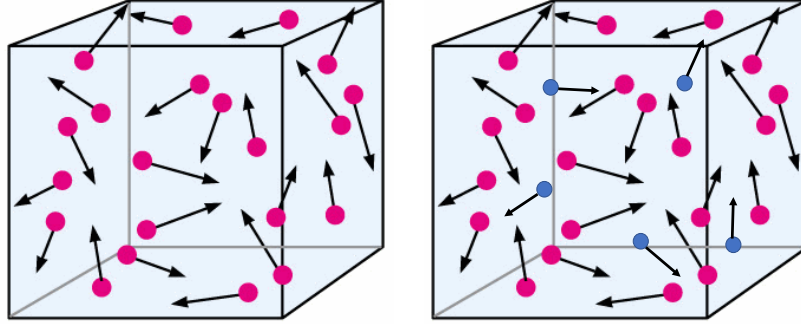


Figure 2.1: Schematic of a box filled with molecules that each move in a random direction. In the left box we have a single type of molecules, and the pressure is dictated by the ideal gas law (2.1). In case we have a mixture of gases such as in the right box, Dalton's law (2.6) states that the total pressure can be obtained by adding the partial pressures of each kind of molecule.

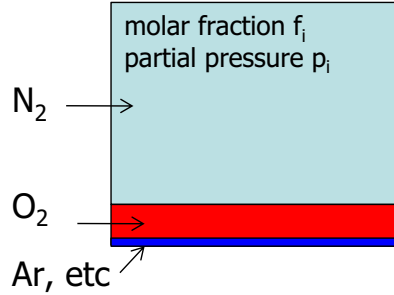


Figure 2.2: The main components of the atmosphere are nitrogen and oxygen.

Gas	Molecular weight M_i (g mol ⁻¹)	Molar fraction	Mass fraction m_i/m_{tot}	Specific gas constant R_i (J kg ⁻¹ K ⁻¹)	$(m_i/m_{tot})R_i$ (J kg ⁻¹ K ⁻¹)
NO ₂	28.013	0.7809	0.7552	296.80	224.15
O ₂	31.999	0.2095	0.2315	259.83	60.15
Ar	39.948	0.0093	0.0128	208.13	2.66
CO ₂	44.010	0.0003	0.0005	188.92	0.09
total		1.0000	1.0000		287.05

Table 2.1: Main components of dry atmospheric air (source *Smithsonian Meteorological Tables*). The molar fractions are approximately constant with height up to 100 km. By contrast, the molar fraction of water vapor is highly variable in time and space. The molecular weight of water vapor $M_v = 18.07$ g mol⁻¹.

denotes the *specific volume* of the system. In principle, every extensive variable can be converted to its corresponding intensive form by normalizing it by the amount of matter it describes. In the remainder of this text we will use lower case letters to denote specific intensive quantities, as opposed to their non-intensive counterpart for which we will use capital letters, e.g. the specific volume v and the volume V .

We would like to write the gas law in terms of kilograms rather than moles. To this end, we need use the molecular weight of a species i , M_i (g/mol), and gives the mass of 1 mole of identical molecules in grams. If the total mass of the gas is m_i , we can express the gas law as,

$$pV = \frac{m_i}{M_i} R^* T. \quad (2.3)$$

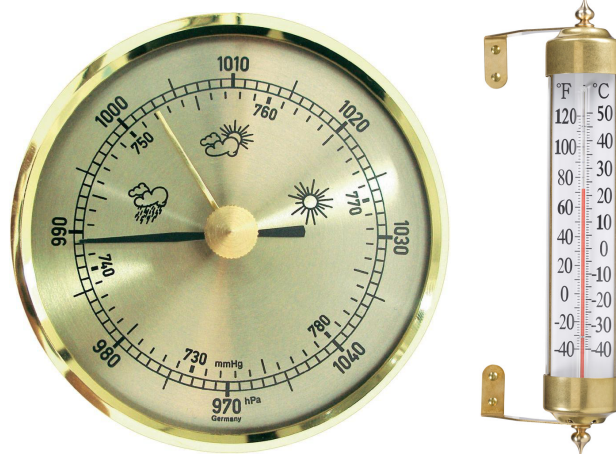


Figure 2.3: Measurements obtained with classical instruments like a barometer and a thermometer allow to determine the density of air by means of the gas law (2.7).

The molecular weight can be substituted out by using the *specific gas constant* R_i for a species i , which is defined as

$$R_i \equiv R^*/M_i. \quad (2.4)$$

For a mixture of gases the **partial pressure** p_i of the i^{th} gas is defined as the pressure p_i that it would have if the same mass (m_i) existed alone at the same temperature T and occupying the same volume V . By (2.3) and (2.4) the partial pressure for an ideal gas can thus be expressed as

$$p_i = \frac{T}{V} m_i R_i. \quad (2.5)$$

According to Dalton's law of partial pressures, the total pressure p of a mixture of (ideal) gases is the sum of the pressures $\sum p_i$ of each species i as if it alone occupied a volume V ,

$$p = \frac{T}{V} \sum_i m_i R_i = \rho R_m T, \quad (2.6)$$

in which $m_{\text{tot}} = \sum_i m_i$ the total mass, $R_m = 1/m_{\text{tot}} \sum_i m_i R_i$ the specific gas constant for the mixture, and $\rho = m_{\text{tot}}/V$ is the density. Eq. (2.6) is the form of the gas law generally used in meteorology. Table 2.1 shows the value of the specific **gas constant for dry air** $R_d = 287.05 \text{ J kg}^{-1} \text{ K}^{-1}$. Hence, in the absence of water the gas law reads

$$p_d = \rho_d R_d T. \quad (2.7)$$

where we deliberately use the subscript 'd' to denote p_d as the 'dry' pressure that is due to all gases excluding the pressure exerted by water vapor, and likewise $\rho_d = m_d/V$ is the density of dry air. Only if the air is void of water the total pressure $p = p_d$.

There are two important reasons to use the gas law in this form rather than (2.1). First of all, the air pressure p and temperature can be well measured with devices like a barometer and a thermometer, respectively. If these quantities are known the density of air can be computed straightforwardly. As will be shown the equation of motion includes the density, which is the second reason why the gas law expressed as (2.7) is preferred.

Air including water

The water vapor pressure is usually denoted by the symbol e , which can be expressed as

$$e = \rho_v R_v T, \quad (2.8)$$

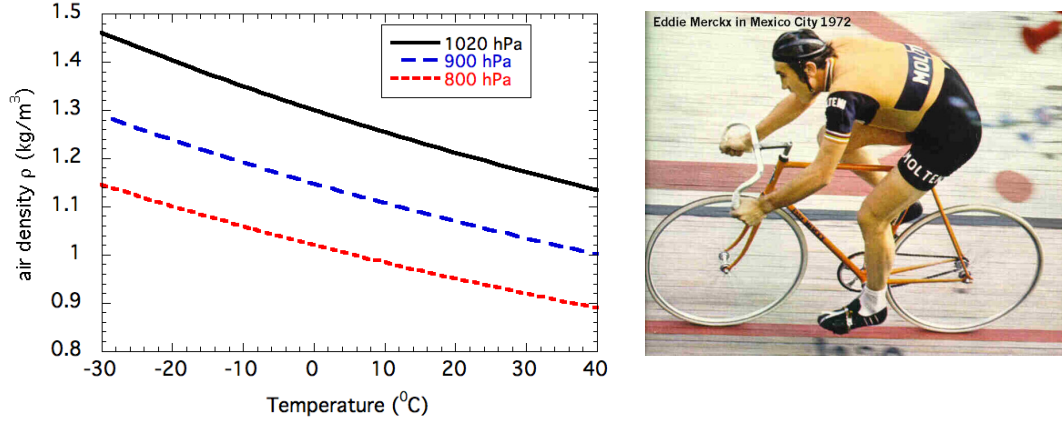


Figure 2.4: The density of air as a function of temperature for three different pressure values (see legend). A value of 1020 hPa is representative for a height near sea level, while pressures of 900 and 800 hPa are roughly at 1 and 2 km above sea level, respectively. The aerodynamic resistance of a moving object is linearly proportional to the density of air. Because the air density at higher altitudes is lower, sportsmen prefer to beat speed records well above sea level height. Eddy Merckx set the cycling hour record of 49.431 km at an altitude of 2300 m in Mexico City. Note that the optimal height is also determined by the oxygen concentration which also tends to decrease with height.

where ρ_v is the density of water vapor, and the specific gas constant for water vapor can be computed from (2.4) to give $R_v = 461.5 \text{ J kg}^{-1} \text{ K}^{-1}$. Following Dalton's law the total pressure p is the sum of the pressure exerted by the dry air and water vapor,

$$p = p_d + e = \rho_d R_d T + \rho_v R_v T, \quad (2.9)$$

with $\rho_v = m_v/V$. As we are usually interested in the total pressure and the total density of air,

$$\rho = \frac{m_{\text{tot}}}{V} = \frac{m_d + m_v}{V} = \frac{\rho_d + \rho_v}{V}. \quad (2.10)$$

we manipulate (2.9) to arrive at

$$p = \rho T \left(\frac{\rho_d}{\rho} R_d + \frac{\rho_v}{\rho} R_v \right) = \rho R_d T (1 + \epsilon_I q_v), \quad (2.11)$$

with the water vapor specific humidity q_v defined by

$$q_v = \frac{m_v}{m_v + m_d}, \quad (2.12)$$

and the constant $\epsilon_I = R_v/R_d - 1 \approx 0.608$. The presence of the water vapor contribution to the gas law is sometimes absorbed in the virtual temperature,

$$T_v \equiv T(1 + \epsilon_I q_v). \quad (2.13)$$

We can draw an important conclusion from the gas law including water vapor, namely that for a given pressure and temperature an air parcel containing water vapor ($q_v > 0$) will have a lower density than a dry air parcel. This is a direct consequence of the fact that the ideal gas law (2.1) does not care about the molecular mass but rather the number of molecules that are present in the volume. Suppose that we have a mixture of dry and water molecules. If we replace all the water molecules by dry molecules while maintaining the same pressure, temperature and volume, the air

parcel without water will have larger mass simply because the molecular weight of a dry molecule such as the dominant components NO_2 and O_2 is larger than that of water vapor (see Table 2.1).

Example Consider air with a temperature of 20°C , a pressure 1020 hPa and $q_v = 0.02 \text{ kg kg}^{-1}$. From (2.11) we find that the density of air is 1.2975 kg m^{-3} . If we would have neglected q_v we would have obtained $\rho = 1.21206 \text{ kg m}^{-3}$, which is about 1.2% higher. For accuracy reasons, in the atmospheric sciences it is common practice to include the presence of water vapor in the gas law. This is actually obligatory if one studies buoyant (density driven) convection in the atmosphere, in which both temperature and humidity may have a comparable contribution to the density.

2.2 The Clausius-Clapeyron equation

Sometimes it is argued that when air cools clouds form because cold air cannot hold as much water vapor as warm air. Since, for instance, cumulus clouds develop in surface-driven thermals that have gradually cooled during their ascent, it appears that there is a causal relation between cooling and saturation so that this argument is making sense. However, the underlying notion that air is some kind of imaginary sponge that can absorb an amount of water vapor depending on its temperature is a misconception¹.

Water molecules are constantly coursing back and forth between phases (another word for the three states: vapor, liquid, and solid). If more molecules are leaving a liquid surface than arriving, there is a net evaporation; if more arrive than leave, a net condensation. It is these relative flows of molecules which determine whether a cloud forms or evaporates. The rate at which vapor molecules arrive at a surface of liquid (cloud drop) or solid (ice crystal) depends upon the vapor pressure. The rate at which vapor molecules leave the surface depends upon the characteristics of the surface. What appears to be cloud-free air (virtually) always contains sub microscopic drops, but as evaporation exceeds condensation, the drops do not survive long after an initial chance clumping of molecules. As air is cooled, the evaporation rate decreases more rapidly than does the condensation rate with the result that there comes a temperature (the dew point temperature) where the evaporation is less than the condensation and a droplet can grow into a cloud drop. Evaporation increases with temperature, not because the holding capacity of the air changes, but because the more energetic molecules can evaporate more readily (with, of course, the caveat that evaporation is also influenced by things other than temperature, as described above).

In case the concentration of water vapor is at its saturation value we can define the corresponding saturation vapor pressure by e_{sat} . A familiar quantity to many is the relative humidity RH of air, which is defined as

$$\text{RH} = \frac{e}{e_{\text{sat}}}. \quad (2.14)$$

Clearly, the relative humidity gives a measure of the ratio of two partial pressures. If we define the saturation water vapor specific humidity $q_{\text{sat}} = m_{\text{sat}}/(m_{\text{sat}} + m_{\text{d}})$ with m_{sat} the mass of the water vapor at its saturation value, we may express the relative humidity as

$$\text{RH} = \frac{\rho_v R_v T}{\rho_{\text{sat}} R_v T} = \frac{m_v}{m_{\text{sat}}} = \frac{m_v/m_{\text{tot}}}{m_{\text{sat}}/m_{\text{tot}}} = \frac{q_v}{q_{\text{sat}}}. \quad (2.15)$$

It can be theoretically shown that the saturation vapor pressure e_{sat} can be expressed as (Emanuel 1994)

$$\frac{de_{\text{sat}}}{dT} = \frac{1}{T} \frac{L_v}{(v_v - v_l)}, \quad (2.16)$$

¹see <http://www.ems.psu.edu/fraser/BadMeteorology.html> from which the explanation above is taken, and more nice examples of 'bad' meteorology

with v_v (v_v) the specific volume that is occupied by water vapor (liquid water). This equation is called the Clausius-Clapeyron equation. Note that the saturation pressure depends only on temperature. If we assume that the specific volume of the liquid water is much smaller than that for the water vapor, $v_l \ll v_v$, and because water vapor is to a good approximation an ideal gas, $e_{\text{sat}}v_v = R_vT$, we can rewrite Eq. (2.16) as

$$\frac{1}{e_{\text{sat}}} \frac{de_{\text{sat}}}{dT} \approx \frac{L_v}{R_vT^2}. \quad (2.17)$$

For typical temperatures in the atmospheric boundary layer one may use the following approximate form for e_{sat} (Stull 1988)

$$e_{\text{sat}} = 610.78 \exp \left[\frac{17.2694(T - 273.16)}{T - 35.86} \right] \quad [\text{Pa}], \quad (2.18)$$

for absolute temperature T [K].

The saturated water vapor specific humidity q_{sat} is a more frequently used quantity. It is related to e_{sat} as follows,

$$q_{\text{sat}} = \frac{e_{\text{sat}}}{\frac{R_v}{R_d}(p - e_{\text{sat}}) + e_{\text{sat}}} = \frac{\epsilon e_{\text{sat}}}{p + e_{\text{sat}}(\epsilon - 1)}. \quad (2.19)$$

with

$$\epsilon \equiv \frac{R_d}{R_v}. \quad (2.20)$$

This relation can be derived from Dalton's law and some 'handy' substitutions,

$$p = \rho_d R_d T + e_{\text{sat}} = (\rho - \rho_{\text{sat}}) R_d T + e_{\text{sat}} = \rho(1 - q_{\text{sat}}) R_d T + e_{\text{sat}} \quad (2.21)$$

$$= p \frac{1 - q_{\text{sat}}}{1 + (1/\epsilon - 1)q_{\text{sat}}} + e_{\text{sat}}, \quad (2.22)$$

where in the last step the gas law (2.11) is used. After sorting terms with q_{sat} one can arrive at (2.19). In the free troposphere $p \gg e$, with which we can approximate,

$$q_{\text{sat}} \approx \epsilon \frac{e_{\text{sat}}}{p}. \quad (2.23)$$

An example of the dependency of q_{sat} on the temperature is displayed in Fig. 2.5. During nights with weak winds fog may develop when air just above the ground surface is strongly cooled by infrared radiation. The lack of vertical mixing keeps the saturation specific humidity approximately constant with time. At some point the the air becomes cold enough to become saturated with water vapor. Mixing fog (the red arrow) occurs when warm, moist but unsaturated air is mixed with cold, moist unsaturated air. If the mixture is above the value of q_{sat} saturation will occur.

Water paths

The total amount of water vapor that is present in the column can be conveniently expressed in terms of the column **Water Vapor Path** (WVP),

$$\text{WVP} = \int_0^\infty \rho q_v dz. \quad (2.24)$$

Note that WVP has units kg m^{-2} . Likewise, the **Liquid Water Path** (LWP) is defined as

$$\text{LWP} = \int_0^\infty \rho q_l dz. \quad (2.25)$$

In practice the bulk amount of water is present in the lower few kilometers of the atmosphere. The density of liquid water is 1000 kg m^{-3} , so if a liquid water mass of 1000 kg would occupy a horizontal surface area of 1 m^2 its height would be 1 m . The WVP is strongly related to precipitation (see Fig. 2.7).

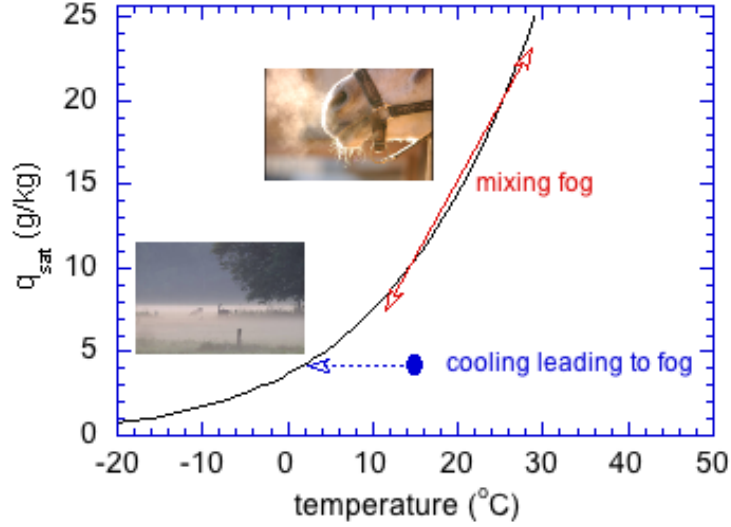


Figure 2.5: The water vapor saturation specific humidity as a function of temperature for a pressure of 1020 hPa. The photos show examples of the properties of air parcels when mixing of warm and cold moist air (mixing fog, red arrow) occurs, and the radiative cooling of air leading to fog formation during calm nights with weak winds (blue arrow).

2.3 Hydrostatic pressure

Fig. 2.8 depicts a column of air. Let us consider the layer in the middle which has a horizontal surface area A . The pressure and gravitation are the only forces that are acting. If the air is motionless the forces balance,

$$-p(z + \Delta)A + p(z)A - \rho g A \Delta z = 0. \quad (2.26)$$

We can take the limit $\Delta z \rightarrow 0$ to give the equation of **hydrostatic equilibrium**,

$$\frac{\partial p}{\partial z} = -\rho g. \quad (2.27)$$

We have seen from the gas law that the density of air depends on the pressure, temperature and the specific humidity. Eliminating the density yields

$$\frac{\partial p}{\partial z} = -\frac{pg}{R_d T_v} \iff \frac{\partial \ln p}{\partial z} = -\frac{g}{R_d T_v}, \quad (2.28)$$

where we recall that in the absence of moisture ($q_v = 0$) the virtual temperature becomes equal to the temperature, $T = T_v$.

Isothermal atmosphere

For an atmospheric layer with a constant temperature and no moisture the pressure profile is given by,

$$p(z) = p_{\text{sf}} e^{-z/H} \quad (2.29)$$

with the scale height $H = R_d T/g$. For $T = 290\text{K}$ $H = 8.5\text{km}$. This actually states that 63% of the air is present in a rather thin layer (as compared with the radius of the Earth ($R = 6400\text{km}$)).

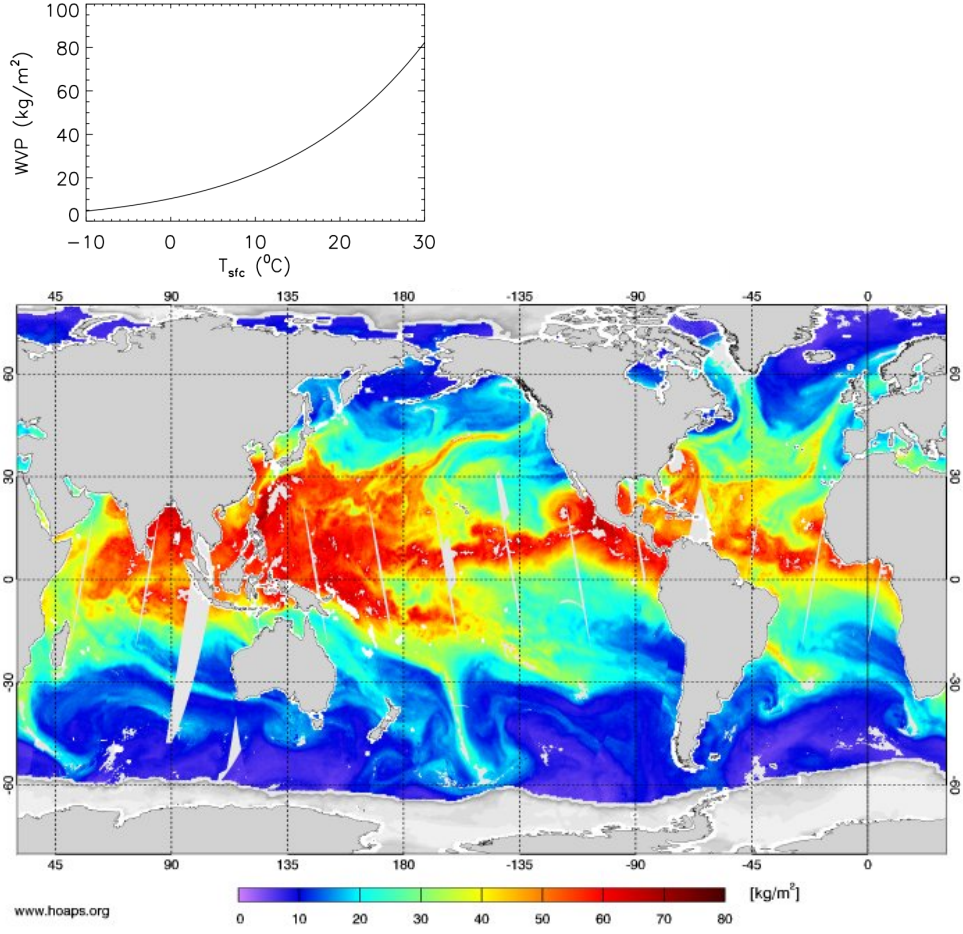


Figure 2.6: The maximum WVP as a function of the surface temperature assuming a fixed vertical temperature gradient of -6 K km^{-1} (upper plot). The lower plot shows the measured WVP on 18 September 2003. There is a distinct north-south gradient associated with the warm temperatures near the equator and cold temperatures at high latitudes. Note the presence of 'vapor tongues' that extend from the subtropics to the mid-latitudes.

Constant vertical gradient of temperature

Suppose the temperature varies with height according to

$$T(z) = T_{\text{sfc}} + \gamma_T z, \quad (2.30)$$

with constant slope

$$\gamma_T \equiv \frac{dT}{dz}. \quad (2.31)$$

Substitution in Eq. (2.28) gives

$$d \ln p = -\frac{g}{\gamma_T R_d} d \ln(T_{\text{sfc}} + \gamma_T z). \quad (2.32)$$

Integration from the ground surface $z = 0$ upwards to height z yields

$$\ln \left(\frac{p(z)}{p_{\text{sfc}}} \right) = -\frac{g}{\gamma_T R_d} \ln \left(1 + \frac{\gamma_T z}{T_{\text{sfc}}} \right) = \ln \left(1 + \frac{\gamma_T z}{T_{\text{sfc}}} \right)^{-\frac{g}{\gamma_T R_d}} \quad (2.33)$$

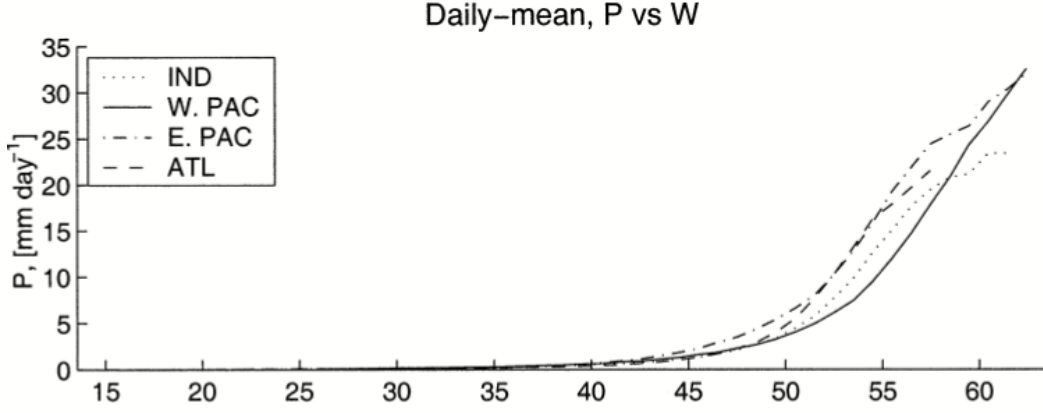


Figure 2.7: Mean daily averaged precipitation P in 1-mm-wide bins of water vapor path W , for the four tropical ocean regions (Indian Ocean, West and East Pacific, and the Atlantic) for all months in 1998-2001 (copied from Bretherton et al. (2004)).

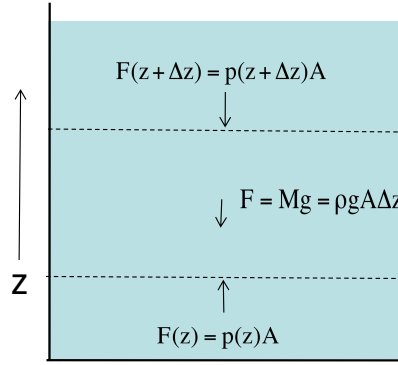


Figure 2.8: Schematic of the pressure and gravitational forces acting on a motionless fluid parcel.

or likewise without the logarithms,

$$p(z) = p_{\text{sfc}} \left(1 + \frac{\gamma_T z}{T_{\text{sfc}}} \right)^{-\frac{g}{\gamma_T R_d}} \quad (2.34)$$

This equation is valid for any layer with constant lapse rate of temperature.

Constant vertical gradient of temperature

Note that in practice temperature and humidity always vary irregularly with height and consequently (2.28) needs to be evaluated numerically. For example, consider a situation in which we have an observation of the temperature and the humidity as a function of height, so we know $T_v(z)$. We may discretize Eq. (2.28) by dividing the atmosphere into layers with a finite depth $\Delta z^{k+1/2} = z^{k+1} - z^k$ with k indicating the number of the layer. This gives,

$$p^{k+1} = p^k \exp \left[\frac{-g(z^{k+1} - z^k)}{R_d T_v^{k+1/2}} \right]. \quad (2.35)$$

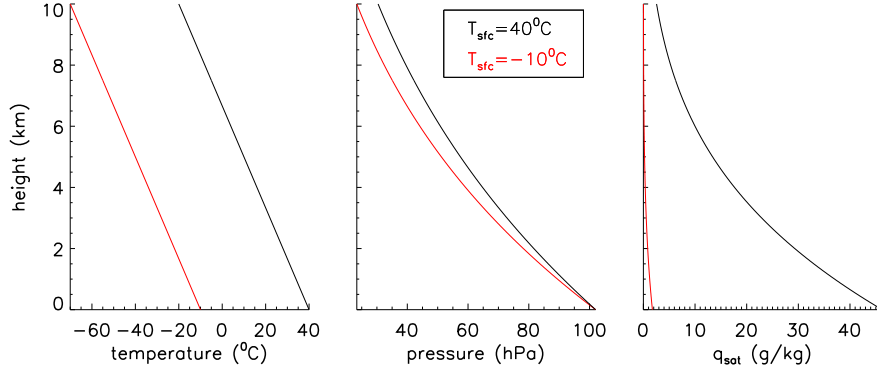


Figure 2.9: Examples of the pressure and saturation specific humidity as a function of height for two temperatures (see legend). The surface pressure was set to 1020 hPa.

Fig. 2.9 gives an example of the variation of the pressure with height for a warm and a cold atmosphere, $T_{\text{sfc}} = 300$ and 260 K, respectively assuming a fixed vertical temperature gradient of -6 K km^{-1} . It is found that if two columns of air have a different temperature, horizontal pressure gradients will arise simply due to the fact that their density profiles are different. In a nutshell this example explains why the atmosphere is in a continuous motion. At the equator it is much warmer than at the poles, and it is this temperature difference that creates a large-scale force, namely a horizontal pressure gradient. The vertical profile of the maximum (saturation) specific humidity shows a strong temperature dependency of the maximum amount of water vapor that can be present.

The pressure at a certain height depends on the temperature of the air column, and large-scale horizontal pressure gradients depend on the horizontal distribution of temperatures. For these reasons meteorologists plot maps that show the height of the 500 hPa pressure level. Fig. 2.10.

2.4 Conservation of energy

The First Law of Thermodynamics states that energy is conserved,

$$dQ = dU + dW \quad (2.36)$$

where dQ is the added heat, $dU = mc_v dT$ is the change in the internal energy is $dW = pdV$ is the work. After division by the mass m and using

$$d\left(\frac{V}{m}\right) = d\frac{1}{\rho} = -\frac{1}{\rho^2}d\rho, \quad (2.37)$$

to give

$$dq = c_v dT + pdv = c_v dT - \frac{p}{\rho^2} d\rho, \quad (2.38)$$

with $dQ = mdq$ and $v = V/\rho$.

The dry case

We need some manipulations to arrive at an expression that relates the temperature to the height z . To this end we perturb the gas law for dry air,

$$dp = R_d T d\rho + \rho R_d dT \quad (2.39)$$

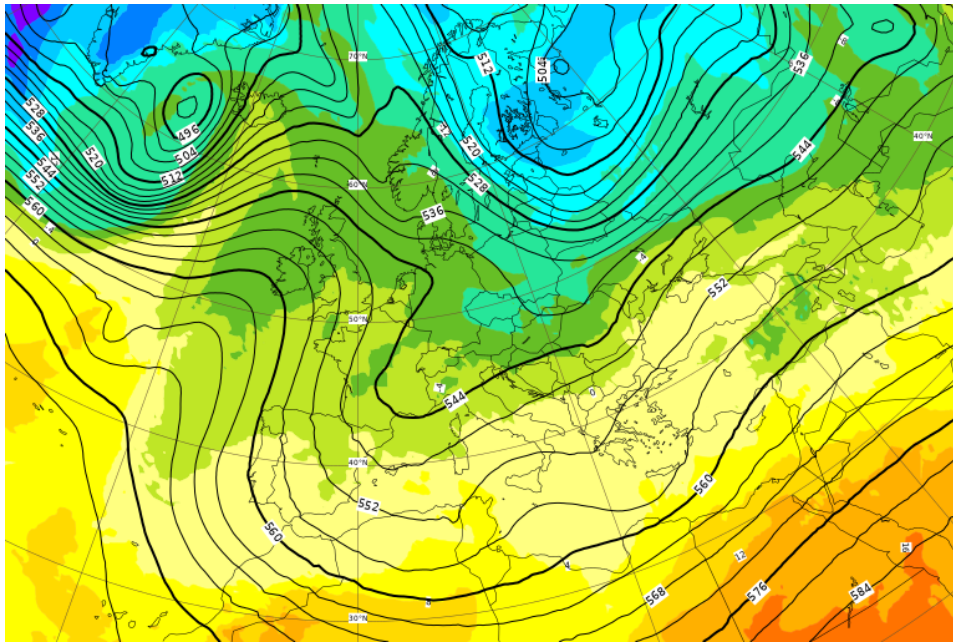


Figure 2.10: The 500 hPa geopotential height (contours) and temperature at 850 hPa (shading) from the ECMWF model for 21 January 2019. The most recent predictions can be found at www.ecmwf.int. The ECMWF explains its use as follows. The geopotential height of the 500 hPa pressure surface shows approximately how far one has to go up in the atmosphere before the pressure drops to 500 hPa (i.e. 500 millibars). On average this level is around 5.5 km above sea level, and it is often referred to as a steering level, because the weather systems beneath, near to the Earth's surface, roughly move in the same direction as the winds at the 500 hPa level. Height contours are labelled in tens of metres (=decametres, ="dam") with an interval of 4 dam. The contours effectively show the main tropospheric waves that "control" our weather - low heights indicate troughs and cyclones in the middle troposphere whilst high heights indicate ridges and anticyclones. Colour shading indicates temperature at the 850 hPa level in °C, in 4°C colour bands. This is the temperature approximately 1.5 km above sea level, usually just above the boundary layer. At this level the diurnal (daily) cycle in temperature is generally negligible. Therefore temperature at 850 hPa can be used to indicate frontal zones (i.e. areas of large temperature gradient, where the isotherms are more closely packed together), and naturally also to distinguish between warm and cold air masses. Sometimes temperature at 850 hPa can be used to roughly assess the maximum temperature at sea level by adding 10 to 15°C, and for higher ground one can interpolate. However there are situations when this method does not apply, particularly in winter.

and its subsequent substitution gives

$$dq = c_p dT - \frac{dp}{\rho}, \quad (2.40)$$

with the specific heat of dry air at constant pressure $c_p \equiv c_v + R_d$. The fact that $c_p > c_v$ has the following interpretation. Suppose we want to heat air with a fuel that produces an amount of heat dq . If we keep the volume of air constant, $dv = 0$, then (2.38) is the equation to be used. However, if we keep the pressure constant, $dp = 0$, dq is used to heat the air in addition to expanding the air parcel. It is this amount of work that explains the difference between c_v and c_p . In the atmosphere processes take place at constant pressure, so in the remainder you will most frequently see heat budgets that involve c_p .

We can actually go one step further with our manipulations. Suppose that the atmosphere is in a hydrostatic equilibrium (2.27). In this case the (2.40) becomes

$$dq = c_p dT + g dz. \quad (2.41)$$

This form of the energy conservation equation has a nice interpretation. The first term on the rhs indicates the **enthalpy** and the second term represents the potential energy of the air parcel due to the presence of the Earth's gravitational field. A parcel that does not mix properties with its surroundings and to which no external heat is added ($dq = 0$) is called an **adiabatic** parcel. Consider an air parcel that is lifted, $dz > 0$. This raises its potential energy. However, energy conservation dictates that $c_p dT = -g dz < 0$. In other words, the air parcel must cool in order to keep its total energy constant,

$$\left(\frac{dT}{dz}\right)_{\text{dry adiabat}} = -\frac{g}{c_p} = -9.8 \text{ K km}^{-1}, \quad (2.42)$$

which is widely known as the **dry adiabatic lapse rate**. The **dry static energy** is defined by

$$s_d \equiv c_p T + g z. \quad (2.43)$$

The strength of the dry static energy is that it is a so-called **conserved thermodynamic variable**, which means that it is constant for an adiabatic vertical displacement of a dry air parcel. This means that when we know, for example from a measurement, the temperature and height of an air parcel, say T_0 and z_0 , we will be able to estimate its temperature T_1 at another height z_1 . If this shows that the parcel will be warmer than the actual temperature at height z_1 , the displaced parcel will be accelerated in the upward direction. This situation is called unstable. Another, similar quantity is the potential temperature which will be derived below.

The moist case: effects of condensation or evaporation

Effects of latent heat release due to condensation of water vapor (a loss of water vapor $dq_v < 0$ but a gain in liquid water $dq_l > 0$) need to be taken into account by adding it as an energy source,

$$dq = c_p dT + g dz + L_v dq_v, \quad (2.44)$$

and likewise the **moist equivalent static energy** is defined as

$$s_e = c_p T + g z + L_v q_v. \quad (2.45)$$

Following the definition of an adiabatic parcel its total amount of water ($q_t = q_v + q_l$) is constant (since no mixing with its environment is assumed) and consequently

$$dq_v = -dq_l, \quad (2.46)$$

with the **liquid static energy**

$$s_l = c_p T + g z - L_v q_l. \quad (2.47)$$

The large value of L_v has a significant impact on the temperature lapse rate if water is condensed in the sense that the so-called moist adiabatic lapse rate is strongly reduced,

$$\left(\frac{dT}{dz}\right)_{\text{moist adiabatic}} = -\frac{g}{c_p} + L_v \frac{dq_1}{dz}. \quad (2.48)$$

Example Fossil fuels are popular because of their capacity to produce large amounts of heat. For example, the heat of combustion for petrol is $48 \times 10^6 \text{ J kg}^{-1}$. The global water cycle is an eternal process of evaporation of water from the surface, condensation of cloud droplets in the atmosphere and the subsequent formation of rain which partly evaporates in the atmosphere before reaching the ground surface. To put things into perspective, let us compute how much petrol it takes to evaporate 1 kg of liquid water at room temperature (20°C). The latent heat of vaporization of water is $L_v = 2.5 \times 10^6 \text{ J kg}^{-1}$. Assuming an efficiency of 100% this means that about 52 g of petrol is needed to evaporate the water. This is a non-negligible number, and illustrates the vast amount of energy associated with phase changes of water. For this reason one may call water the 'fuel' that releases the heat that drives the strong vertical motions in clouds.

Example. For a pressure of 1000 hPa and a temperature of 15°C the moist adiabatic temperature gradient is -4.67 K km^{-1} . The liquid static energy in low clouds is often observed to be approximately constant with height, $s_1(z) = \text{cst}$, it follows from Eq. (2.63) that $dq_1/dz = 2.05 \text{ g kg}^{-1} \text{ km}^{-1}$. Let us consider a stratocumulus cloud layer, which is rather thin ($\sim 200 - 500 \text{ m}$), yet it tends to reflect more than 50% of the downwelling solar radiation. Because this is such a large effect, one may wonder how much liquid water is causing this. To this end let us compute the cloud LWP. Assuming that cloud liquid water is only present in a layer with a thickness of 300 m gives $\text{LWP} = 1.2 \times 0.615 \times 0.5 = 0.37 \text{ kg m}^{-2} = 0.37 \text{ mm}$ (the factor 0.5 follows from the fact that q_1 is increasing linearly with height and $\rho = 1.2 \text{ kg m}^{-3}$). It is striking to conclude that an amount of less than 1 mm of liquid water has such a strong effect on the reflection of sunlight!

2.5 The potential temperature

We have derived the dry static energy by applying energy conservation, and the assumption of hydrostatic equilibrium provided us with a relation that tells how the temperature of an adiabatic air parcel will vary with height. The potential temperature gives the temperature of an air parcel is it vertically displaced from a pressure level p_1 to a *reference* pressure p_0 . Let us start with Eq. (2.40)², and eliminate ρ with aid of the gas law,

$$dq = c_p dT - R_d T \frac{dp}{p}. \quad (2.49)$$

If we set $dq = 0$, we obtain

$$\frac{dT}{T} = \frac{R_d}{c_p} \frac{dp}{p} \iff d \ln T = \frac{R_d}{c_p} d \ln p. \quad (2.50)$$

Integration from a state '0' to '1' gives

$$\ln T_1 - \ln T_0 = \frac{R_d}{c_p} (\ln p_1 - \ln p_0) \iff \ln \left(\frac{T_1}{T_0}\right) = \frac{R_d}{c_p} \ln \left(\frac{p_1}{p_0}\right) = \ln \left(\frac{p_1}{p_0}\right)^{\frac{R_d}{c_p}} \quad (2.51)$$

The potential temperature θ is defined as follows,

$$\theta \equiv T_0 = T \left(\frac{p_0}{p}\right)^{\frac{R_d}{c_p}}, \quad (2.52)$$

and it is equal to the temperature of an air parcel with a temperature T at pressure p that is displaced to a reference pressure p_0 , which is typically taken to 1000 hPa.

²Formally the potential temperature is derived from the second law of thermodynamics, $T ds \geq 0$, with the entropy s , and $ds = dq/T$. For an isentropic process $ds = 0$, which is equivalent to $dq = 0$.

The potential temperature is a conserved variable for dry adiabatic displacements. Like the dry static energy, the potential temperature of a dry adiabatic parcel is *constant with height*. In the lower part of the atmosphere they are approximately related as

$$\theta \approx \frac{s_d}{c_p}. \quad (2.53)$$

For any pressure level, Eq. (2.52) can be used to compute the temperature of the parcel. Last, we introduce the **Exner** function,

$$\Pi \equiv \left(\frac{p}{p_0}\right)^{\frac{R_d}{c_p}} = \frac{T}{\theta}. \quad (2.54)$$

2.6 Moist adiabatic temperature lapse rate

The heat that is released when phase changes of water occurs has a strong impact on the temperature. Here we will derive the vertical gradient of temperature for an adiabatic parcel in the presence of latent heat release due to phase changes of water. According to Eq. (2.19) q_{sat} depends on the partial water vapor saturation pressure e_{sat} and the mean pressure p we can express

$$dq_{\text{sat}} = \frac{dq_{\text{sat}}}{de_{\text{sat}}} de_{\text{sat}} + \frac{dq_{\text{sat}}}{dp} dp = \frac{dq_{\text{sat}}}{de_{\text{sat}}} \frac{de_{\text{sat}}}{dT} dT + \frac{dq_{\text{sat}}}{dp} dp. \quad (2.55)$$

Differentiating Eq. (2.19) with respect to e_{sat} and p yields, respectively,

$$\frac{dq_{\text{sat}}}{de_{\text{sat}}} = \frac{\epsilon p}{[p + e_{\text{sat}}(\epsilon - 1)]^2}, \quad (2.56)$$

$$\frac{dq_{\text{sat}}}{dp} = -\frac{e_{\text{sat}}\epsilon}{[p + e_{\text{sat}}(\epsilon - 1)]^2}. \quad (2.57)$$

Substituting these two expressions, and Eq. (2.17) into Eq. (2.55) gives

$$dq_{\text{sat}} = \frac{q_{\text{sat}}}{p + e_{\text{sat}}(\epsilon - 1)} \left(\frac{pL_v}{R_v T^2} dT - dp \right). \quad (2.58)$$

If we rewrite Eq. (2.19) as

$$e_{\text{sat}} = \frac{q_{\text{sat}} p}{\epsilon + q_{\text{sat}}(1 - \epsilon)}, \quad (2.59)$$

then we can eliminate e_{sat} from Eq. (2.58),

$$dq_{\text{sat}} = \left(1 + \frac{1 - \epsilon}{\epsilon} q_{\text{sat}} \right) \left(\frac{q_{\text{sat}} L_v}{R_v T^2} dT - q_{\text{sat}} \frac{dp}{p} \right). \quad (2.60)$$

The potential temperature depends on the temperature and the pressure, thus

$$d\theta = \frac{d\theta}{dT} dT + \frac{d\theta}{dp} dp = \frac{\theta}{T} dT - \frac{R_d \theta}{c_p p} dp. \quad (2.61)$$

We have now expressed dq_{sat} and $d\theta$ in terms of dT and dp . As we are interested in the vertical derivative of the temperature, dT/dz , we will need use the vertical pressure gradient relation (2.28), to write the moist-adiabatic lapse rate as

$$\frac{dT}{dz} = - \left[\frac{\frac{\theta}{T} \frac{g}{c_p} + \frac{L_v}{c_p} (1 + (1/\epsilon - 1)q_{\text{sat}}) \frac{gq_{\text{sat}}}{R_d T_v}}{\frac{\theta}{T} + \frac{L_v}{c_p} (1 + (1/\epsilon - 1)q_{\text{sat}}) \frac{L_v q_{\text{sat}}}{R_v T^2}} \right]. \quad (2.62)$$

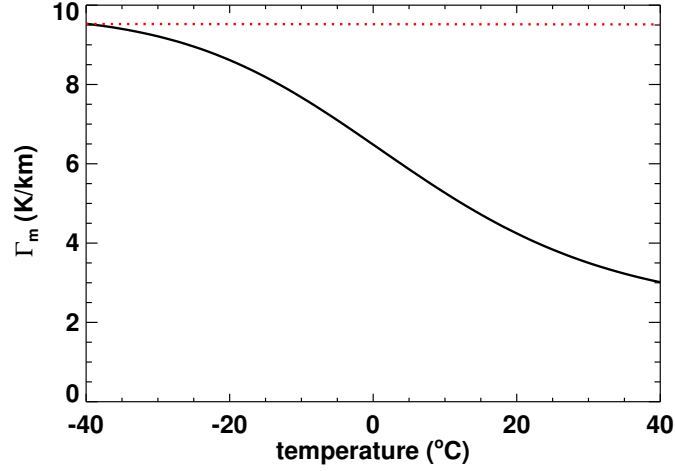


Figure 2.11: The moist adiabatic lapse rate Γ_m (solid line) as a function of the temperature and for a pressure of 1000 hPa. The red dotted line indicates the dry adiabatic temperature lapse rate Γ_d .

In the literature one often finds a simplified expression. In particular, if one approximates $\theta/T \approx 1$, $T_v \approx T$, and uses the fact that in the atmosphere typically $q_{\text{sat}} < 4 \times 10^{-2} \text{ kg kg}^{-1}$, the moist-adiabatic lapse rate Γ_m can be simplified as

$$\Gamma_m = -\frac{dT}{dz} = \Gamma_d \left[\frac{1 + \frac{L_v q_{\text{sat}}}{R_d T}}{1 + \frac{L_v^2 q_{\text{sat}}}{c_p R_v T^2}} \right] < \Gamma_d, \quad (2.63)$$

with the dry adiabatic temperature lapse rate

$$\Gamma_d = \frac{g}{c_p}. \quad (2.64)$$

The inequality is satisfied whenever $L_v \epsilon > c_p T$. Because of the high value of L_v for water, this inequality is always valid in the atmosphere. The release of latent heat in a saturated parcel explains why the moist adiabatic lapse rate Γ_m is always smaller than the dry adiabatic lapse rate Γ_d . Its actual value depends strongly on the temperature, and to a lesser extent on the mean pressure. For $T = 288 \text{ K}$ and $p = 1000 \text{ hPa}$ we find $\Gamma_m = 4.3 \text{ K km}^{-1}$. For lower temperatures however the difference between Γ_m and Γ_d becomes progressively smaller.

2.7 Summary and outlook

Fig. 2.12 shows vertical profiles for an adiabatic parcel. In the absence of saturation, $q_1 = 0$, and consequently $q_v = q_t$. The temperature follows the dry adiabatic lapse rate, $\partial T/\partial z = -g/c_p$, and the dry static energy and potential temperature of the parcel are constant with height. If the parcel contains moisture, it will become saturated at the height where $q_v = q_{\text{sat}}(T, p)$. This height is called the cloud Lifting Condensation Level (LCL). For shallow cumulus clouds the LCL is typically very close to the actual cloud base height. Using the concept of adiabatic parcels and near surface observations of relative humidity, temperature and pressure can be used to obtain the LCL. More specifically, for unsaturated parcels the quantities s_d and q_v are constant with height up to the LCL. With aid of the hydrostatic pressure p can be calculated, which, in turn, can be used to compute

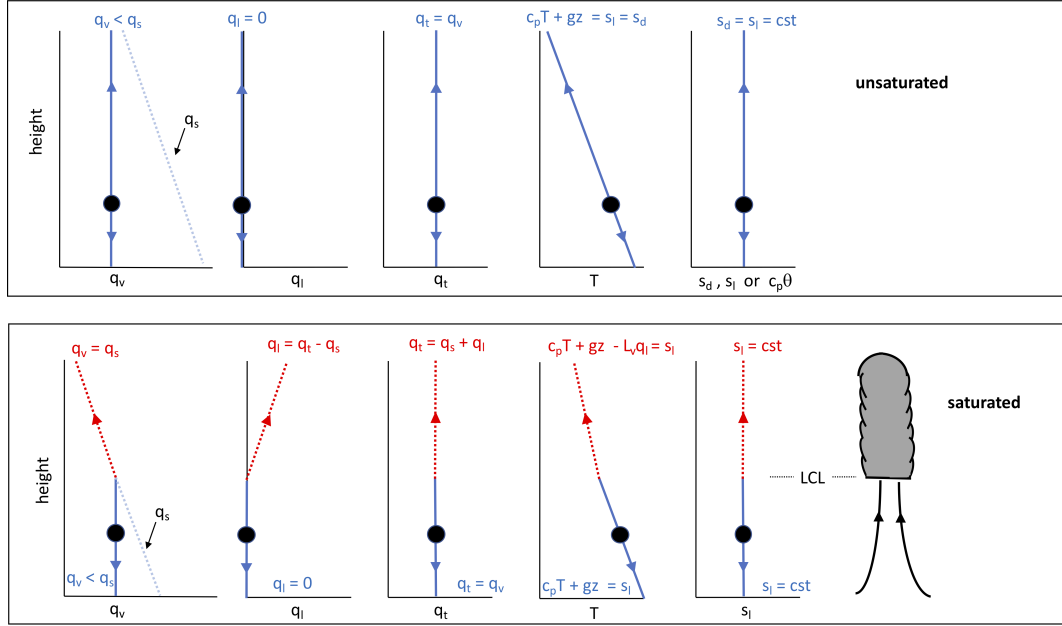


Figure 2.12: Vertical profiles for adiabatic parcels for the water vapor specific humidity q_v , the liquid water specific humidity q_l , the total water specific humidity q_t , the temperature T , the dry static energy s_d and the potential temperature θ , and the liquid static energy s_l . The upper panel shows profiles for an unsaturated parcel, and the lower panel for a parcel that is moist enough for saturation to occur.

the vertical profile of q_{sat} . The LCL can be assessed from the crossing point where $q_v = q_{\text{sat}}(T, p)$. Above the LCL the conserved thermodynamic variables q_t and s_l are constant with height. For any temperature and pressure q_{sat} can be computed from Eq. (2.19). Since for a saturated parcel $q_v = q_{\text{sat}}$, the liquid water specific humidity can be diagnosed from an iterative procedure. For given p , q_{sat} can be calculated for any T , and q_l can be obtained from the unique set $q_{\text{sat}}(T), T$ that satisfies both of the following two equations

$$\begin{aligned} s_l &= c_p T + gz - L_v (q_t - q_{\text{sat}}(T, p)), \\ q_t &= q_{\text{sat}}(T, p) + q_l. \end{aligned} \quad (2.65)$$

In addition to estimating the cloud base height, we will see that the concept of adiabatic parcels has some great applications. Because it gives the temperature with height, it may be used as a tool to diagnose whether air parcels will be able to rise spontaneously. In other words, it can predict whether the atmosphere state allows for convective plumes, but also the formation of cumulus clouds, and even the possibility of thunderstorms. To this end we will first need to introduce the (vertical) momentum equation, and we will have to introduce the Reynolds averaging technique which specifically considers effects of fluctuations in a turbulent flow.

Chapter 3

Governing equations

The state of the atmosphere changes not only by diabatic processes like radiation and precipitation, but also by advection including turbulent motions. The basic approach to derive a simplified set of equations describing turbulent flows involves Reynolds-averaging. This technique splits variables into a mean and a fluctuation part, the latter being associated with the turbulent motions. The turbulent transport of heat, moisture, pollutants and chemical species is then represented by so-called Reynolds-averaged fluxes. In this chapter we will present the governing equations for *shallow* convection. A more elaborate description of the material contained in this chapter can be found in the book 'An introduction to Boundary layer Meteorology', by Stull (1988).

Notation

Tensor notation

We will use the tensor notation so that u_i is the velocity vector in a Cartesian coordinate system x_i with $i \in \{1, 2, 3\}$ such that $\vec{u} = (u_1, u_2, u_3) \equiv (u, v, w)$ and $\vec{x} = (x_1, x_2, x_3) \equiv (x, y, z)$ where z aligned with the gravitational acceleration vector. In addition, δ_{ij} indicates the Kronecker's delta function

$$\delta_{ij} \begin{cases} +1 & \text{for } m = n \\ 0 & \text{for } m \neq n, \end{cases} \quad (3.1)$$

and ϵ_{ijk} the alternating unit tensor (or the Levi-Civita symbol),

$$\epsilon_{ijk} \begin{cases} +1 & \text{for } ijk = 123, 231 \text{ or } 312 \\ -1 & \text{for } ijk = 321, 213 \text{ or } 132 \\ 0 & \text{for any two or more indices alike.} \end{cases} \quad (3.2)$$

Material derivative

Consider a fluid parcel with a time dependent velocity \vec{u} (see Fig. 3.1). Since the position of the parcel also depends on time, $\vec{x} = (x(t), y(t), z(t))$, we can express the wind vector as, $\vec{u} = \vec{u}(\vec{x}, t)$. Following the chain rule for differentiation,

$$\frac{dy(x(t))}{dt} = \frac{dy}{dx} \frac{dx}{dt}, \quad (3.3)$$

we can write

$$\frac{du(x(t), y(t), z(t), t)}{dt} = \frac{\partial u}{\partial t} + \frac{\partial u}{\partial x} \frac{\partial x}{\partial t} + \frac{\partial u}{\partial y} \frac{\partial y}{\partial t} + \frac{\partial u}{\partial z} \frac{\partial z}{\partial t}, \quad (3.4)$$

and likewise for v and w . Since

$$\frac{\partial x_i}{\partial t} = u_i, \quad (3.5)$$

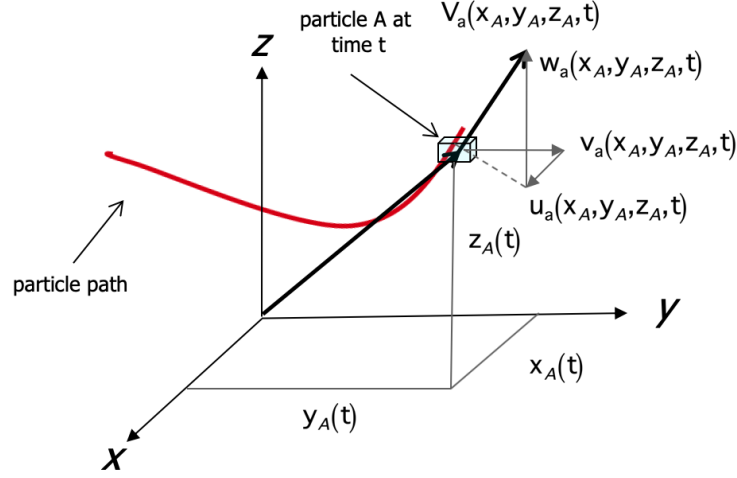


Figure 3.1: Schematic of the moving position of a fluid parcel. At time t its position is at (x_A, y_A, z_A) , and its velocity $V_A = (u_A, v_A, w_A)$.

we can rewrite

$$\frac{du(x(t), y(t), z(t), t)}{dt} = \frac{\partial u}{\partial t} + u \frac{\partial u}{\partial x} + v \frac{\partial u}{\partial y} + w \frac{\partial u}{\partial z}. \quad (3.6)$$

Taking the derivative with respect to time gives rise to non-linear terms, which are sometimes called the **advection** or **convection** terms. The first term in the equation above is called the **local** derivative, or the **tendency** term. One could think of 'local' as the change that one would observe at a fixed position in space. In tensor notation the **material derivative** or **total derivative** reads

$$\frac{d}{dt} \equiv \frac{\partial}{\partial t} + u_j \frac{\partial}{\partial x_j}. \quad (3.7)$$

Fig. 3.2 shows the eastward advection of cold air, with $\partial T / \partial x = 1^\circ \text{Ckm}^{-1}$, $u = 10 \text{km h}^{-1}$. Let us consider the temperature change for an observer in an air balloon and another one at a fixed position. For any arbitrary scalar ϕ the total derivative reads,

$$\frac{d\phi}{dt} = \frac{\partial \phi}{\partial t} + u \frac{\partial \phi}{\partial x} + v \frac{\partial \phi}{\partial y} + w \frac{\partial \phi}{\partial z} = S_\phi, \quad (3.8)$$

where S_ϕ is a source function like, which may represent the effect of radiation in case ϕ represents temperature, and which we assume to be zero. First, let us consider a measurement location at a fixed position. The equation above states that $\partial \phi / \partial t = -u \partial \phi / \partial x$, so the horizontal advection by the wind will lead to an observed *local* change. However, now suppose that the observer is flying in a hot air balloon. In that case the properties of the air surrounding the balloon will not change, $d\phi / dt = 0$. Therefore, the material derivative is the change *one would observe if one moves along with the air parcel*.

3.1 Governing equations for atmospheric dynamics

In addition to the gas law, we will need conservation equations for momentum, heat, moisture and mass.

The gas law

The gas law in terms of the virtual temperature T_v and the density of moist air ρ reads

$$p = \rho R_d T_v. \quad (3.9)$$

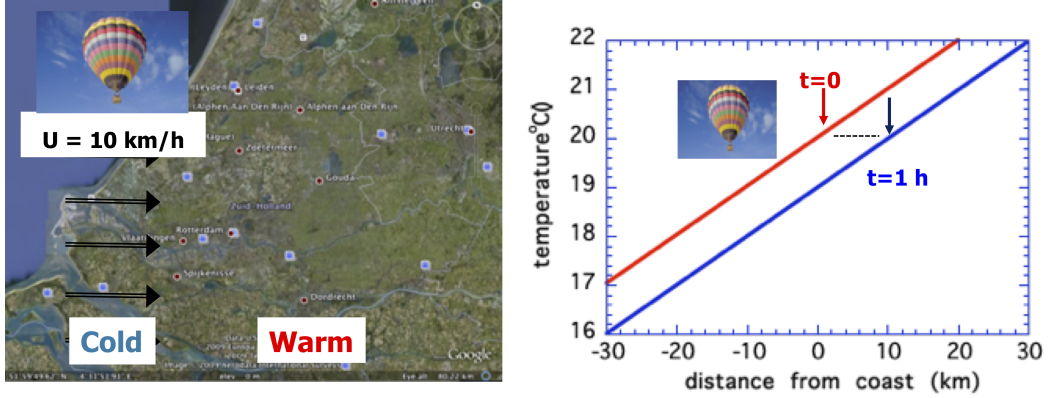


Figure 3.2: Schematic of eastward advection of cold air. The graph indicates the temperature at two times.

Conservation of mass

The conservation for mass, or the continuity equation, is given by

$$\frac{\partial \rho}{\partial t} + \frac{\partial \rho u_j}{\partial x_j} = 0 \quad \Longleftrightarrow \quad \frac{\partial u_j}{\partial x_j} = -\frac{1}{\rho} \frac{d\rho}{dt}. \quad (3.10)$$

Let us denote U and L as typical velocity and length scales for the boundary layer, c_s the velocity of sound and f the frequency of any pressure wave that might occur. The density drops out of the continuity equation if the following conditions are satisfied, (1) $U \ll 100 \text{ ms}^{-1}$, (2) $L \ll 12 \text{ km}$, (3) $L \ll c_s^2/g$, and (4) $L \ll c_s/f$. For the boundary layer these conditions are usually met which allows to approximate the continuity equation (3.10) as:

$$\frac{\partial u_j}{\partial x_j} = 0. \quad (3.11)$$

This form of the continuity equation states that in shallow convection compressibility effects that are embodied in $d\rho/dt$ can be neglected. Intuitively, this may come as a surprise. Indeed, the density of air is known to decrease by about 90% from sea level to a height of 10 km. One is also usually aware of the notion that warm air rises as it is having a smaller density than the air in its vicinity. To appropriately deal with the latter, in practice one often uses a constant density, except in the buoyancy term that is present in the vertical momentum equation.

Conservation of momentum

The conservation of momentum reads

$$\frac{du_i}{dt} = -\delta_{i3}g + f\epsilon_{ij3}u_j - \frac{1}{\rho} \frac{\partial p}{\partial x_i} + \nu \frac{\partial^2 u_i}{\partial x_j^2}. \quad (3.12)$$

The Coriolis parameter $f = 2\omega \sin \phi$, where ϕ is the latitude and since the period of rotation of the Earth $T_{\text{Earth}} = 86400\text{s}$, $\omega = 2\pi/T_{\text{Earth}} = 7.27 \times 10^{-5} \text{ s}^{-1}$ is the angular velocity of the Earth. The value of the kinematic viscosity ν is given in Table 3.1.

Conservation of heat

In Chapter 2 we derived a form of the conservation of heat, Eq. (3.13), which we repeat here for convenience,

$$dq = c_p dT + gdz + L_v dq_v, \quad (3.13)$$

T (°C)	ν	κ_T m^2s^{-1}	κ_{q_v}
20	1.53×10^{-5}	2.16×10^{-5}	2.57×10^{-5}

Table 3.1: The kinematic viscosity ν , the thermal diffusivity κ_T of dry air, and the molecular diffusivity of water vapor κ_{q_v} in dry air, at $p = 1000$ hPa (Garratt 1994).

Taking the time derivative gives,

$$\frac{dT}{dt} = -\frac{g}{c_p} \frac{dz}{dt} - \frac{1}{\rho c_p} \frac{\partial F_j}{\partial x_j} - \frac{L_p E}{c_p} + \kappa_T \frac{\partial^2 T}{\partial x_j^2}, \quad (3.14)$$

with κ_T the thermal diffusivity in air. Heat can be added to air by an energy flux F_j , for example by a non-adiabatic process like radiation. The variable E represents the mass of water vapor per unit mass of air per unit time being created by a phase change from liquid or solid, L_p is the latent heat associated with the phase change of E , with the subscript $p \in \{v, f, s\}$ (L_v was already used for the condensation of liquid water). A specific example of the latent heat release term is the evaporation of liquid water. In that case the loss of liquid is a gain of water vapor, $E = \partial q_v / \partial t = -\partial q_l / \partial t$, and the negative sign states that for positive E the process of evaporation leads to a cooling tendency. The values for latent heat at 0°C are $L_v = 2.50 \times 10^6$ J/kg (gas→liquid), $L_f = 3.34 \times 10^5$ J/kg (liquid→solid) and $L_s = 2.83 \times 10^6$ J/kg of water (gas→solid). The first term on the rhs is a consequence of energy conservation, stating that a change in the potential energy of an air parcel, proportional to gz , must be accompanied by an opposite change in its enthalpy, $c_p T$. In the end of this Chapter alternative, and more compact forms of the heat equation will be presented. This is achieved by using quantities like the dry static energy or potential temperature instead of the temperature T .

The conservation equations for the water vapor specific humidity (q_v) reads

$$\frac{dq_v}{dt} = \kappa_{q_v} \frac{\partial^2 q_v}{\partial x_j^2} + E, \quad (3.15)$$

with ν_q the molecular diffusivity for water vapor in the air.

Conservation of an arbitrary chemical species

Likewise, the conservation equation for an arbitrary chemical species c reads (Fick's second law),

$$\frac{dc}{dt} = \nu_c \frac{\partial^2 c}{\partial x_j^2} + S_c \quad (3.16)$$

where S_c represents a loss/gain term due to a chemical reaction.

3.2 Summary and Outlook

For atmospheric flow changes in the air properties are hardly affected by molecular processes. Although they occur, their effect is negligibly small with respect to changes due to advection (by the wind) or radiation. In the conservation equation presented in this Chapter molecular diffusion can therefore be neglected. In atmospheric sciences the heat equation is usually expressed in terms of conserved variables for adiabatic displacements, like the dry static energy or the total water specific humidity.

Conservation of momentum

Splitting the wind vector in its three components $u_i = (u, v, w)$ gives

$$\begin{aligned}\frac{du}{dt} &= fv - \frac{1}{\rho} \frac{\partial p}{\partial x} \\ \frac{dv}{dt} &= -fu - \frac{1}{\rho} \frac{\partial p}{\partial y} \\ \frac{dw}{dt} &= -\rho g - \frac{1}{\rho} \frac{\partial p}{\partial z}.\end{aligned}\tag{3.17}$$

The different signs in the Coriolis acceleration terms guarantee an acceleration to the right (left) of the moving parcel on the northern (southern) hemisphere.

Conservation of heat

Let us start with the energy conservation equation (3.14),

$$\frac{dT}{dt} = -\frac{g}{c_p} w + \frac{L_v}{c_p} \frac{dq_l}{dt} - \frac{1}{\rho c_p} \frac{\partial F_i}{\partial x_i}\tag{3.18}$$

where we used the definition of the vertical velocity of the air parcel, $w = dz/dt$, and we confine ourselves to phase change of water vapor to liquid water and vice versa, such that

$$\frac{L_p E}{c_p} = \frac{L_v}{c_p} \frac{dq_v}{dt} = -\frac{L_v}{c_p} \frac{dq_l}{dt}.\tag{3.19}$$

If we use the definition of the dry static energy and liquid static energy (Eqs. (2.43) and (2.47)), we can rewrite the above equation as, respectively,

$$\frac{ds_{\text{dry}}}{dt} = L_v \frac{dq_l}{dt} - \frac{1}{\rho} \frac{\partial F_i}{\partial x_i},\tag{3.20}$$

and

$$\frac{ds_l}{dt} = -\frac{1}{\rho} \frac{\partial F_i}{\partial x_i}.\tag{3.21}$$

Interestingly, changes in the vertical position of the air parcel, or phase changes of water are absorbed in the static energy variables. How does this work in practice? For a given radiative flux profile, first the change in the static energy is computed. After the total water specific humidity is computed, the liquid water specific humidity q_l is *diagnosed*. The key difference with the energy equation in a form like Eq. (3.14) is that in the latter the change in q_l is a source term in the form of Eq. (3.19) which needs to be *prognosed*.

Likewise, in terms of the potential temperature the equations look almost the same except for a factor c_p and the Exner function Π (Eq. (2.54)),

$$\frac{d\theta}{dt} = \frac{L_v}{c_p \Pi} \frac{dq_l}{dt} - \frac{1}{\rho c_p} \frac{\partial F_i}{\partial x_i},\tag{3.22}$$

$$\frac{d\theta_l}{dt} = -\frac{1}{\rho c_p \Pi} \frac{\partial F_i}{\partial x_i}.\tag{3.23}$$

We recall that a static energy gives the temperature for an adiabatic displacement across a vertical distance z , whereas the potential temperature does the same for a change between two pressure levels. In this respect the liquid water potential temperature has a similar interpretation as the liquid static energy, and is defined as

$$\theta_l \approx \theta - \frac{L_v}{c_p \Pi} q_l.\tag{3.24}$$

Although this Chapter summarizes the key conservation equations, we have not yet arrived at a form that is widely used in models. Because turbulence causes strong fluctuations in the variables, one has developed a mathematical technique called Reynolds averaging, which aims to split turbulent fluctuations from the mean signal. This will be the subject of the next Chapter.

Chapter 4

Reynolds decomposition

A means to separate large-scale (synoptic) fluctuations from turbulent motions is provided by the Reynolds-averaging procedure. In practice, one often measures time series of quantities like wind, temperature or humidity. This may be done from a measurement site such as Cabauw, but also from aircraft¹ (Fig. 4.1).

Consider an arbitrary variable ϕ that is split into a mean part ($\bar{\phi}$) and a fluctuating part ϕ' , $\phi = \bar{\phi} + \phi'$. For a set of N data points from observations this is computed as follows,

$$\bar{\phi} = \frac{1}{N} \sum_{i=1}^N \phi_i, \quad (4.1)$$

$$\phi'_i = \phi_i - \bar{\phi}. \quad (4.2)$$

In practice, the results following from Reynolds decomposition do depend on the time periods used for the analyses. This can intuitively be understood by realizing that quantities like the temperature are influenced by a diurnal cycle. For example, when the atmosphere is heated during the morning, the mean value of the temperature will typically become higher if a longer time period is used. Because of the presence of trends in variables, the time period should not be too long. At the same time, neither a period too short should be used, as this may lead to an undersampling of the large,

¹<https://www.youtube.com/watch?v=FHeOykff5Hs>



Figure 4.1: The UKMO Hercules C130 research aircraft. The photo on the right is taken during the Surface Heat Budget of the Arctic Ocean (SHEBA) experiment and show a sonic anemometer installed on a 2 m mast on the Arctic sea ice. In the background the icebreaker 'Des Groseilliers' is visible.

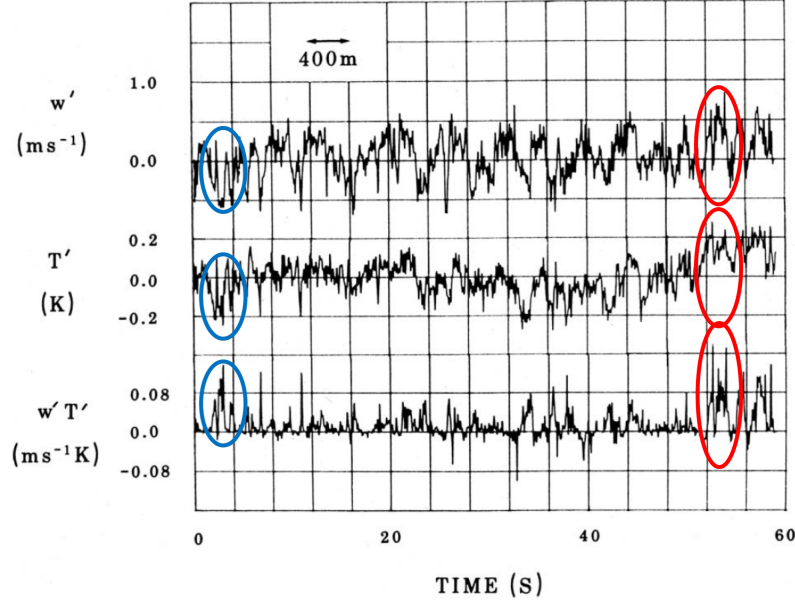


Figure 4.2: Vertical-velocity fluctuation (w') data and temperature fluctuation (T') data from part of a run near cloud top by the UK C-130 on 30 June 1987. The date encircled in blue and red indicate a cold downdraft and a warm updraft, respectively. The instantaneous heat flux ($w'T'$) is almost all upward at this level. Figure taken from Albrecht et al. (1988).

dominant turbulent eddies. For observations collected at a fixed point, the decomposition is often based on time series of about 10 minutes. For aircraft flights, turbulence statistics are often based on horizontal legs of about 60 km. Figure 4.2 shows an example for the fluctuations of the vertical velocity w and temperature T .

4.1 Reynolds averaging rules

If we let c denote an arbitrary constant, then the Reynolds-averaging rules read

$$\begin{aligned}
 \overline{c\phi} &= c\bar{\phi}, \\
 \overline{(\phi)} &= \bar{\phi}, \\
 \overline{(w\phi)} &= \bar{w}\bar{\phi}, \\
 \overline{w + \phi} &= \bar{w} + \bar{\phi}, \\
 \overline{\left(\frac{d\phi}{dt}\right)} &= \frac{d\bar{\phi}}{dt}.
 \end{aligned} \tag{4.3}$$

Averaging yields

$$\bar{\phi} = \overline{(\bar{\phi} + \phi')} = \bar{\phi} + \bar{\phi'}, \tag{4.4}$$

which, $\overline{(\phi)} = \bar{\phi}$, can only be equal if

$$\bar{\phi'} = 0. \tag{4.5}$$

This rule states that the mean of fluctuations is zero. Things become less straightforward if we consider multiplications, e.g. $w\phi$,

$$\overline{w\phi} = \overline{(\bar{w} + w')(\bar{\phi} + \phi')} = \bar{w}\bar{\phi} + \overline{w'\phi'}. \tag{4.6}$$



Figure 4.3: Photograph of a golden eagle and a schematic illustration of soaring in a thermal to gain height then gliding to the next thermal. Copied from <http://www.petercavanagh.us/>.

This result is at the heart of Reynolds decomposition. Although the mean of the fluctuations is zero, the mean of the *product* of fluctuations generally is nonzero. The great advantage of this whole procedure is that we have split the total *transport* of flow in a mean part, $\overline{w\phi}$, and a part that is mainly due to turbulence, $\overline{w'\phi'}$.

4.2 Why does warm (or moist) air rise?

It is generally known that rising plumes are present in the atmosphere. Birds like eagles (see Fig. 4.3) take benefit of these updrafts. Here we will apply Reynolds decomposition to the vertical momentum equation (3.17) to derive the relation between the density of air and its vertical acceleration,

$$\frac{dw}{dt} = -g - \frac{1}{\rho} \frac{\partial p}{\partial z}. \quad (4.7)$$

We have estimated that the order of magnitude of the mean vertical velocity is on the order of 0.1 ms^{-1} , which is about a factor of 100 smaller than the magnitude of g . This implies that the atmosphere must be very close to a mean hydrostatic equilibrium,

$$\frac{\partial \bar{p}}{\partial z} = -\bar{\rho}g. \quad (4.8)$$

Let us assume that the mean atmosphere is in a perfect hydrostatic equilibrium ($\bar{w} = 0$). Let us now apply Reynolds decomposition,

$$(\bar{\rho} + \rho') \frac{dw'}{dt} = -g(\bar{\rho} + \rho') - \frac{\partial(\bar{p} + p')}{\partial z}. \quad (4.9)$$

We can eliminate the mean hydrostatic pressure by substitution of Eq. (4.8). Next, we divide the equation above by the mean density. The *Boussinesq approximation* makes use of the fact that $\rho'/\bar{\rho}$ is on the order 3.33×10^{-3} , such that $1 + \rho'/\bar{\rho} \approx 1$, from which follows,

$$\frac{dw'}{dt} = -g \frac{\rho'}{\bar{\rho}} - \frac{1}{\bar{\rho}} \frac{\partial p'}{\partial z}. \quad (4.10)$$

This finding states that air with a smaller density than its surroundings will tend to accelerate in the upward direction. Although we have now arrived at the main point of being able to explain how density differences control vertical accelerations we want to briefly consider the gas law. As argued before, unlike the density of air, temperature and humidity can be measured straightforwardly by relatively simple devices. For this reason the density in Eq. (4.10) is often replaced by the virtual temperature,

$$\frac{dw'}{dt} = \frac{T'_v}{T_v} g - \frac{1}{\bar{\rho}} \frac{\partial p'}{\partial z}. \quad (4.11)$$

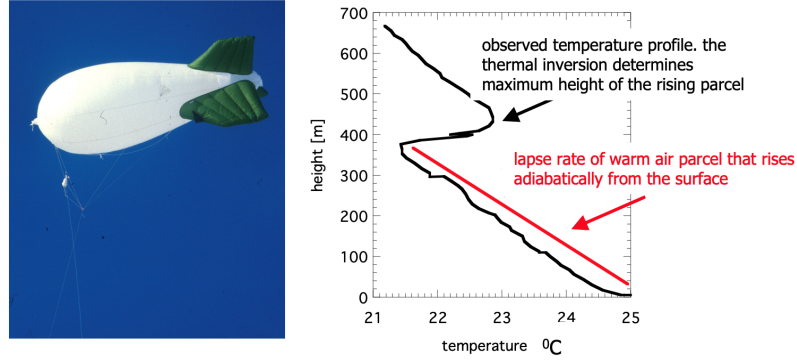


Figure 4.4: Vertical profile (black) of the temperature at Cabauw as observed from a tethered balloon during the Baltex Bridge Campaign (Crewe et al. 2004). The red line indicates the lapse rate of parcel that rises adiabatically from the ground surface.

with $T'_v \approx T' + \epsilon_I \bar{T} q'_v$ derived in the next section. This confirms that warm air tends to rise. In addition, we learn that vertical motions may also be triggered by moisture fluctuations. In particular, if air is moist, $q'_v > 0$, it will tend to accelerate upwards. If we multiply the buoyancy term by Π/Π , then the Exner function allows to use the virtual potential temperature,

$$\frac{dw'}{dt} = \frac{\theta'_v}{\theta_v} g - \frac{1}{\bar{\rho}} \frac{\partial p'}{\partial z}, \quad (4.12)$$

which is considered more convenient as θ_v is a conserved quantity for unsaturated air parcels.

Fig. 4.4 shows an example of the vertical profile of the temperature. The red line indicates the temperature of a parcel that rises from the ground surface, having an initial temperature that is higher than its environment. If the parcel would not mix with its environment during its ascent, its temperature fluctuation would be positive up to the inversion layer. As a result, convective plumes will typically reach a height of about 400 m. The fact that the observed temperature is very close to the dry adiabatic lapse rate is not a coincidence. On the contrary, such a profile is typically observed during daytime under conditions of clear skies, and is the result of turbulent eddies that tend to mix (or 'stir') air between the ground surface and the inversion layer. This topic will be further elaborated.

4.3 Reynolds decomposition of the gas law

The remaining question to be addressed is how the density term in the vertical momentum equation can be replaced by virtual temperature. Application of Reynolds decomposition to the gas law (3.9) gives,

$$\frac{\bar{p}}{R_d} + \frac{p'}{R_d} = \bar{\rho} \bar{T}_v + \bar{\rho} T'_v + \rho' \bar{T}_v + \rho' T'_v. \quad (4.13)$$

which after Reynolds averaging yields

$$\frac{\bar{p}}{R_d} = \bar{\rho} \bar{T}_v + \overline{\rho' T'_v} \approx \bar{\rho} \bar{T}_v, \quad (4.14)$$

which states that the gas law holds in the mean because $\overline{\rho' T'_v} \ll \bar{\rho} \bar{T}_v$. In the following this form of the gas law will be used twice. First we subtract it from (4.13),

$$\frac{p'}{R_d} = \bar{\rho} T'_v + \rho' \bar{T}_v + \rho' T'_v. \quad (4.15)$$

Second, division both sides of Eq. (4.15) by Eq. (4.14) gives,

$$\frac{p'}{\bar{p}} = \frac{\rho'}{\bar{\rho}} + \frac{T'_v}{\bar{T}_v} + \frac{\rho' T'_v}{\bar{\rho} \bar{T}_v}. \quad (4.16)$$

The last term on the right-hand side is much smaller than the others and can be neglected. In that case we arrive at the *linearized perturbation ideal gas law*:

$$\frac{p'}{\bar{p}} = \frac{\rho'}{\bar{\rho}} + \frac{T'_v}{\bar{T}_v}. \quad (4.17)$$

In the boundary layer the pressure fluctuation term is very small in comparison to T'_v/\bar{T}_v . In the *shallow convection approximation* the pressure effect in (4.17) is therefore neglected:

$$\frac{\rho'}{\bar{\rho}} = -\frac{T'_v}{\bar{T}_v}. \quad (4.18)$$

The virtual temperature is defined as $T_v = T(1 + \epsilon_I q_v)$. Applying Reynolds decomposition gives

$$\bar{T}_v + T'_v = (\bar{T} + T')(1 + \epsilon_I(\bar{q}_v + q'_v)). \quad (4.19)$$

Taking the mean of this expression yields,

$$\bar{T}_v = \bar{T}(1 + \epsilon_I \bar{q}_v), \quad (4.20)$$

where again we used the fact that the product of fluctuations is much smaller than the product of mean values, $T'q'_v \ll \bar{T}\bar{q}_v$. This leads to the desired result, $T'_v \approx T' + \epsilon_I \bar{T}q'_v$.

4.4 Reynolds-averaged equations

Reynolds decomposition allows to split the effect of large-scale advection and turbulent transport on the mean properties of air.

Mass conservation

The continuity equation for mass assumes an incompressible mean flow (constant density in time),

$$\frac{\partial \bar{u}}{\partial x} + \frac{\partial \bar{v}}{\partial y} + \frac{\partial \bar{w}}{\partial z} = 0. \quad (4.21)$$

Applying Reynolds decomposition to the continuity equation (3.11), gives after subtraction of the equation above,

$$\frac{\partial u'}{\partial x} + \frac{\partial v'}{\partial y} + \frac{\partial w'}{\partial z} = 0. \quad (4.22)$$

Note that the latter form enables to express the advection terms that arises from Reynolds decomposition

$$u' \frac{\partial \phi'}{\partial x} + v' \frac{\partial \phi'}{\partial y} + w' \frac{\partial \phi'}{\partial z}, \quad (4.23)$$

into a so-called flux form by addition of a 'zero' term $\phi'(\partial u'/\partial x + \partial v'/\partial y + \partial w'/\partial z)$,

$$u' \frac{\partial \phi'}{\partial x} + v' \frac{\partial \phi'}{\partial y} + w' \frac{\partial \phi'}{\partial z} + \phi' \left(\frac{\partial u'}{\partial x} + \frac{\partial v'}{\partial y} + \frac{\partial w'}{\partial z} \right) = \frac{\partial u' \phi'}{\partial x} + \frac{\partial v' \phi'}{\partial y} + \frac{\partial w' \phi'}{\partial z}. \quad (4.24)$$

The effect of turbulence is usually expressed like the term on the rhs of the above equation.

Momentum budget

The Reynolds-averaged momentum equation reads

$$\frac{\partial \bar{u}_i}{\partial t} + \bar{u}_j \frac{\partial \bar{u}_i}{\partial x_j} = -\delta_{i3}g + f\epsilon_{ij3}\bar{u}_j - \frac{1}{\bar{\rho}} \frac{\partial \bar{p}}{\partial x_i} - \frac{\partial \overline{u'_i u'_j}}{\partial x_j}. \quad (4.25)$$

If turbulence is horizontally homogeneous, the terms including horizontal transport of wind fluctuations, for example a term like $\partial \overline{u'v'}/\partial y$, are negligibly small with respect to the other terms in the equations. This gives

$$\begin{aligned} \frac{\partial \bar{u}}{\partial t} + \bar{u} \frac{\partial \bar{u}}{\partial x} + \bar{v} \frac{\partial \bar{u}}{\partial y} + \bar{w} \frac{\partial \bar{u}}{\partial z} &= f\bar{u} - \frac{1}{\bar{\rho}} \frac{\partial \bar{p}}{\partial x} - \frac{\partial \overline{u'w'}}{\partial z}, \\ \frac{\partial \bar{v}}{\partial t} + \bar{u} \frac{\partial \bar{v}}{\partial x} + \bar{v} \frac{\partial \bar{v}}{\partial y} + \bar{w} \frac{\partial \bar{v}}{\partial z} &= -f\bar{v} - \frac{1}{\bar{\rho}} \frac{\partial \bar{p}}{\partial y} - \frac{\partial \overline{v'w'}}{\partial z}, \\ 0 &= -\rho g - \frac{\partial \bar{p}}{\partial z}. \end{aligned} \quad (4.26)$$

The latter equations states that the mean state is in an hydrostatic equilibrium, which, in turn, implies that the mean vertical velocity acceleration is negligibly small. In a non-hydrostatic situation, i.e. one in which deviations of hydrostatic equilibrium occurs, vertical turbulent gusts will develop at small scales.

Heat budget

For temperature we obtain,

$$\frac{\partial \bar{T}}{\partial t} + \bar{u}_j \frac{\partial \bar{T}}{\partial x_j} = -\bar{w} \frac{g}{c_p} - \frac{1}{\bar{\rho}c_p} \frac{\partial \bar{F}_j}{\partial x_j} - \frac{L_p}{c_p} \bar{E} - \frac{\partial \overline{w'T'}}{\partial x_j} \quad (4.27)$$

Figure 4.2 shows an example of the product of the fluctuations of the vertical velocity w and temperature T . Although the signals seems rather irregular, the mean value of $w'T'$ is positive. This can be interpreted as follows. If air parcels warmer than the mean environment rise, they will have $w' > 0$ and $T' > 0$. Likewise, cold, sinking air parcels will have $w' < 0$ and $T' < 0$. For both cases the product $w'T' > 0$. If $\overline{w'T'} > 0$, this means the net effect of turbulent eddies is that they transport heat in the vertical direction. Suppose that the vertical flux is the only process. Eq. (4.27) states that only if $\overline{w'T'}$ changes with height this will result in a change of the slab mean temperature,

$$\frac{\partial \bar{T}}{\partial t} = -\frac{\partial \overline{w'T'}}{\partial z}. \quad (4.28)$$

In terms of conserved variables for adiabatic displacements and horizontally homogeneous turbulence conditions we can express the Reynolds-averaged heat equation as

$$\frac{\partial \bar{s}_1}{\partial t} + \bar{u} \frac{\partial \bar{s}_1}{\partial x} + \bar{v} \frac{\partial \bar{s}_1}{\partial y} + \bar{w} \frac{\partial \bar{s}_1}{\partial z} = -\frac{1}{\bar{\rho}c_p} \frac{\partial \bar{F}_j}{\partial x_j} - \frac{\partial \overline{w's'_1}}{\partial z} + S_{s_1}, \quad (4.29)$$

$$\frac{\partial \bar{\theta}_1}{\partial t} + \bar{u} \frac{\partial \bar{\theta}_1}{\partial x} + \bar{v} \frac{\partial \bar{\theta}_1}{\partial y} + \bar{w} \frac{\partial \bar{\theta}_1}{\partial z} = -\frac{1}{\bar{\rho}c_p\Pi} \frac{\partial \bar{F}_j}{\partial x_j} - \frac{\partial \overline{w'\theta'_1}}{\partial z} + S_{\theta_1}, \quad (4.30)$$

where S_{s_1} and S_{θ_1} represent source terms of heat different from radiation or phase changes of water vapor to liquid water. It is important to recall that in the absence of liquid water, the liquid static energy reduces to the dry static energy $c_p T + gz$, and likewise $\theta_1 = \theta$.

Water budget

The budget for the total specific humidity reads,

$$\frac{\partial \bar{q}_t}{\partial t} + \bar{u} \frac{\partial \bar{q}_t}{\partial x} + \bar{v} \frac{\partial \bar{q}_t}{\partial y} + \bar{w} \frac{\partial \bar{q}_t}{\partial z} = -\frac{\partial \overline{w'q'_t}}{\partial z} + S_{q_t}. \quad (4.31)$$

What does the source term S_{q_t} represent? Some models define $q_t = q_v + q_l$, which excludes ice or rain. So if ice melts, or evaporates like rain, this may increase either q_v or q_l .

Name	Variable	Relevant equation	Purpose
Temperature	T	Gas law (2.7)	
Virtual temperature	T_v	Gas law (2.13)	Moisture effect on density
Virtual potential temperature	θ_v	Vertical velocity (4.12)	Buoyancy, including moisture
Potential temperature	θ	Heat (4.30)	Gives temperature for a change in pressure (by a vertical displacement)
Liquid potential temperature	θ_l	Heat (4.30)	Like θ , but takes latent heat release due to phase changes of water

Table 4.1: Variables that have temperature in their names. The dry (liquid) static energy is analogous to the (liquid) potential temperature except for that it gives the temperature for vertical changes in height.

4.5 Summary

In summary, the derivation of the prognostic equation (4.10) for the vertical velocity fluctuation w' follows from a Reynolds decomposition of the ideal gas law and the vertical momentum equation. The major assumptions made are that we effectively neglect the role of pressure perturbations on the density in the linearized gas law, and that the mean state of the boundary layer is in a hydrostatic equilibrium. In any case, if we want to predict the evolution of the mean state of the atmosphere we will have to take into account the effect of turbulence.

In this Chapter, and in the Chapters on "Atmospheric Thermodynamics" and the "Governing Equations" we have seen a couple of variables that have 'temperature' in their names. Table 4.5 gives a summary.

Chapter 5

Thermal wind relation and Ekman pumping

Geostrophic flow is at the heart of dynamical meteorology. It elucidates why in a synoptic system of (low) high pressure on the northern hemisphere the wind vector is close to tangent to the isobars in a (counter-)clockwise direction. We will investigate this balance a bit more in detail to explore the relation of horizontal temperature gradients on the vertical structure of wind. Second, we will explain how turbulence controls the large-scale vertical velocity.

5.1 Scaling

Due to the presence of multiple forces acting on an parcel it is worthwhile to ask whether any term might be neglected, for example, by demonstrating that it is much smaller than other terms. To this end it is instructive to make the equations dimensionless. To this end let us introduce dimensionless variables, indicated with superscripted star symbols,

$$\begin{aligned} t^* &= \frac{t}{\mathcal{T}}, \\ (x^*, y^*, z^*) &= \left(\frac{x}{\mathcal{L}}, \frac{y}{\mathcal{L}}, \frac{z}{\mathcal{H}} \right), \\ (u^*, v^*, w^*) &= \left(\frac{u}{\mathcal{V}}, \frac{v}{\mathcal{V}}, \frac{w}{\mathcal{W}} \right). \end{aligned} \tag{5.1}$$

Here we have normalized the actual position and velocity by the *characteristic* horizontal and vertical scales of length (\mathcal{L} and \mathcal{H} , respectively) and velocity (\mathcal{V} and \mathcal{W}) of the flow, and likewise the nondimensional time t^* with \mathcal{T} . We will see that we do not need to care whether \mathcal{V} is 7.2 or 8.3 ms^{-1} , we merely will need its *approximate order of magnitude*.

We will start with a simple example. Let us consider the midlatitudes. We know from observations that the typical order of magnitude of the horizontal wind speed is 10 ms^{-1} . A very small value of 1 ms^{-1} may sometimes be observed in a very strong system of high pressure, but this is rather the exception than the rule. A wind speed of 100 ms^{-1} is also rarely observed. In the midlatitudes the typical length scale of synoptic system is about 1000 km. On the basis of this information we are able to estimate the typical order of magnitude of the vertical wind. To this end let us apply the nondimensionalization to the continuity equation. By the chain rule we have

$$\frac{\partial u^*}{\partial x^*} = \frac{1}{\mathcal{V}} \frac{\partial u(x(x_*))}{\partial x_*} = \frac{1}{\mathcal{V}} \frac{\partial u}{\partial x} \frac{\partial x}{\partial x^*} = \frac{\mathcal{L}}{\mathcal{V}} \frac{\partial u}{\partial x} \iff \frac{\partial u}{\partial x} = \frac{\mathcal{V}}{\mathcal{L}} \frac{\partial u^*}{\partial x^*}, \tag{5.2}$$

with which we can express the nondimensional form of the continuity equation as

$$\frac{\mathcal{V}}{\mathcal{L}} \left(\frac{\partial u^*}{\partial x^*} + \frac{\partial v^*}{\partial y^*} \right) + \frac{\mathcal{W}}{\mathcal{H}} \left(\frac{\partial w^*}{\partial z^*} \right) = 0. \tag{5.3}$$

The factors \mathcal{V}/\mathcal{L} and \mathcal{W}/\mathcal{H} give the respective order of magnitudes of the terms within brackets and must have similar magnitudes in order to balance, $\mathcal{W} \sim \mathcal{V}\mathcal{H}/\mathcal{L}$. The presence of a stably stratified

tropopause causes the vertical transport to take place predominantly within the lower $\sim 10\text{km}$ of the atmosphere (see Fig. 5.1). If we set \mathcal{H} to this value we estimate $\mathcal{W} = 0.01\mathcal{V} \sim 10\text{ cm s}^{-1}$. This example tells us that if the length scale of horizontal motion is much larger than the one in the vertical direction, mass conservation dictates that the characteristic vertical velocity must be much smaller than the characteristic horizontal velocity.

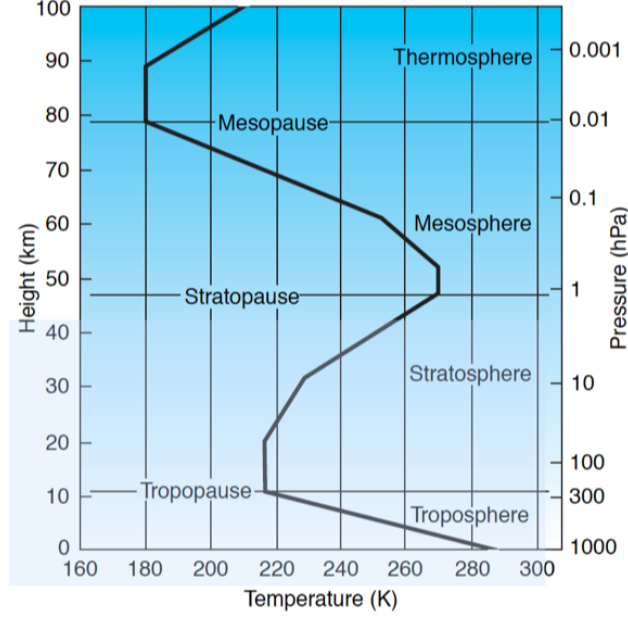


Figure 5.1: A typical midlatitude vertical temperature profile, as represented by the U.S. Standard Atmosphere (Wallace and Hobbs 2006).

The conservation of momentum equation involves higher-order derivatives. In general,

$$\begin{aligned} \frac{\partial^n u^*}{\partial x^{*n}} &= \frac{1}{\mathcal{V}} \frac{\partial^n u(x(x^*))}{\partial x^{*n}} = \frac{1}{\mathcal{V}} \frac{\partial^{n-1}}{\partial x^{*n-1}} \frac{\partial u(x(x^*))}{\partial x^*} = \frac{\mathcal{L}}{\mathcal{V}} \frac{\partial^{n-1}}{\partial x^{*n-1}} \frac{\partial u}{\partial x} \\ &= \frac{\mathcal{L}}{\mathcal{V}} \frac{\partial}{\partial x} \frac{\partial^{n-1} u}{\partial x^{*n-1}} = \frac{\mathcal{L}^n}{\mathcal{V}} \frac{\partial^n u}{\partial x^n} \iff \\ \frac{\partial^n u}{\partial x^n} &= \frac{\mathcal{V}}{\mathcal{L}^n} \frac{\partial^n u^*}{\partial x^{*n}}, \end{aligned} \quad (5.4)$$

where we used Eq. (5.3), and we changed the order of differentiation,

$$\frac{\partial^2 f(x, y)}{\partial x \partial y} = \frac{\partial^2 f(x, y)}{\partial y \partial x}. \quad (5.5)$$

Applying this to the momentum equation in the x -direction gives,

$$\begin{aligned} \frac{\mathcal{V}}{\mathcal{T}} \frac{\partial u^*}{\partial t^*} + \frac{\mathcal{V}^2}{\mathcal{L}} \left(u^* \frac{\partial u^*}{\partial x^*} + v^* \frac{\partial u^*}{\partial y^*} + w^* \frac{\partial u^*}{\partial z^*} \right) = \\ f\mathcal{V}v^* - \frac{\delta P}{\rho \mathcal{L}} \frac{\partial p^*}{\partial x^*} + \frac{\nu \mathcal{V}}{\mathcal{L}^2} \left(\frac{\partial^2 u^*}{\partial x^{*2}} + \frac{\partial^2 u^*}{\partial y^{*2}} + \frac{\mathcal{L}^2}{\mathcal{H}^2} \frac{\partial^2 u^*}{\partial z^{*2}} \right), \end{aligned} \quad (5.6)$$

where we denoted δP to be the characteristic magnitude of pressure fluctuation in the system under consideration, and we used $\mathcal{W} = \mathcal{V}\mathcal{H}/\mathcal{L}$ found earlier from the continuity equation. As next steps,

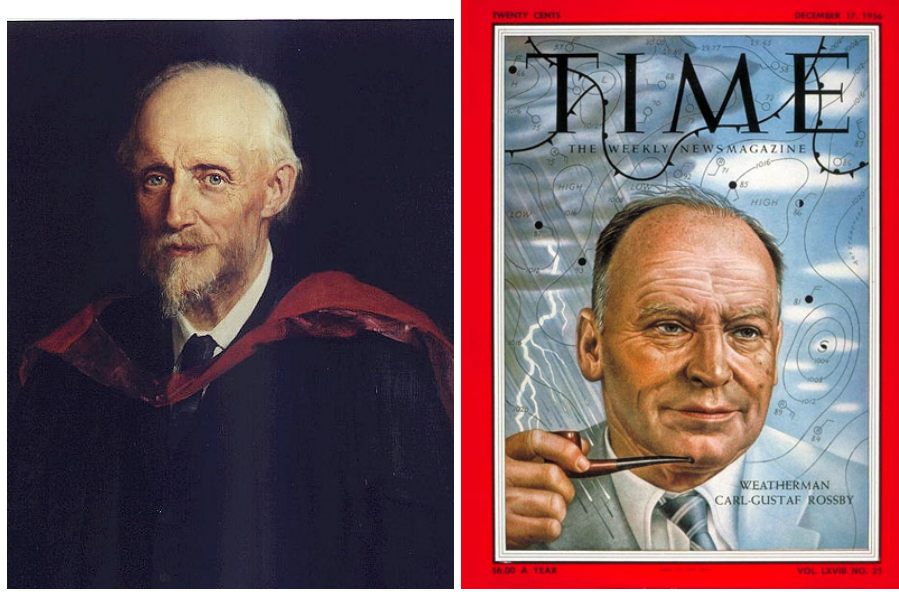


Figure 5.2: A painting of Reynolds and a picture of Rossby on the cover of TIME magazine. Osborne Reynolds (1842–1912) was a pioneer in the field of fluid dynamics and turbulent flows. He investigated the transition of a laminar to turbulent flows in pipes. The Reynolds number and the technique of Reynolds-averaging of turbulent flows are named after him. Carl-Gustaf Arvid Rossby (1898–1957) was a Swedish-born American meteorologist who first explained the large-scale motions of the atmosphere in terms of fluid mechanics. He identified and characterized both the jet stream and the long waves in the westerlies that were later named Rossby waves.

we estimate the time scale $\mathcal{T} = \mathcal{L}/\mathcal{V}$, and we multiply with a factor $\mathcal{L}/\mathcal{V}^2$ to give

$$\frac{\partial u^*}{\partial t^*} + u^* \frac{\partial u^*}{\partial x^*} + v^* \frac{\partial u^*}{\partial y^*} + w^* \frac{\partial u^*}{\partial z^*} = \frac{1}{\text{Ro}} v^* - \frac{\mathcal{V}^2 \delta P}{\rho} \frac{\partial p^*}{\partial x^*} + \frac{1}{\text{Re}} \left(\frac{\partial^2 u^*}{\partial x^{*2}} + \frac{\partial^2 u^*}{\partial y^{*2}} + \frac{\mathcal{L}^2}{\mathcal{H}^2} \frac{\partial^2 u^*}{\partial z^{*2}} \right), \quad (5.7)$$

with the Reynolds (Re) and Rossby (Ro) numbers, respectively,

$$\text{Re} \equiv \frac{\mathcal{V}\mathcal{L}}{\nu}, \quad (5.8)$$

$$\text{Ro} \equiv \frac{\mathcal{V}}{f\mathcal{L}}. \quad (5.9)$$

These numbers are named after Osborne Reynolds and Carl-Gustav Rossby (Fig. 5.2). The weakest flows are perhaps observed during calm, stable nights. For these situations the conditions in the atmosphere may be characterized by $\mathcal{L} = 1 \text{ m}$ and $\mathcal{V} = 0.1 \text{ m s}^{-1}$. The ratio of the magnitudes of the molecular diffusion to the total derivative is $1/\text{Re} \sim 10^{-4}$. Hence, with the exception of the lowest few cm above the ground surface, the molecular diffusion term may be neglected. This also holds for the molecular diffusion terms in the equations for heat, moisture and chemical species.

For the following conditions of synoptic scale flow at the midlatitudes, $f \sim 10^{-4} \text{ s}^{-1}$, $\mathcal{L} \sim 1000 \text{ km}$, and $\mathcal{V} = 10 \text{ m s}^{-1}$, the Rossby number will be about 0.1, and consequently we may neglect the non-linear advection terms. This gives the so-called **geostrophic balance**, which, in dimensional form, reads,

$$u = -\frac{1}{\rho} \frac{\partial p}{\partial y}, \quad v = \frac{1}{\rho} \frac{\partial p}{\partial x}. \quad (5.10)$$

It is important to note that in the presence of a noticeable effect of the rotation of the Earth, i.e. away from equatorial areas, the geostrophic balance implies that the wind vector *not* directed from high to low pressure, $u \neq \sim \partial p / \partial x$.

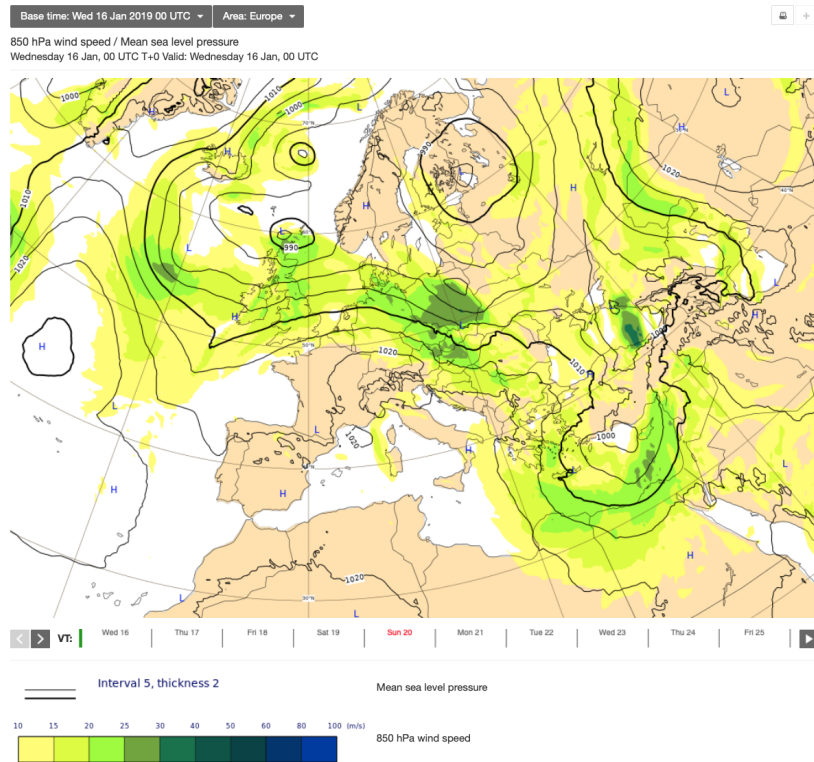


Figure 5.3: ECMWF weather map showing isolines of surface pressure and the windspeed at a height where the pressure is 850 hPa.

The Rossby number can also be used to falsify the infamous misconception that the direction of bath tub flow is controlled by the Earth rotation. If we take $\mathcal{V} = 0.1 \text{ m s}^{-1}$, $\mathcal{L} = 0.1 \text{ m}$ and $f = 10^{-4}$ for the midlatitudes, we find $\text{Ro} = 10^4$, which indicates that the effect of Earth rotation is negligibly small.

Fig. 5.3 shows a weather prediction from the ECMWF. We see that the areas with the largest wind speeds are found at places with the distances between the **isobars** (lines of equal pressure) are relatively small. At those locations the horizontal pressure gradients are largest, and, according to Eq. (5.10), the magnitude of the wind speed is directly proportional to the horizontal pressure gradient. Secondly, in a geostrophic equilibrium situation the wind vector is exactly parallel to the isobars. This is why in the northern hemisphere the wind flows in a clockwise direction around the center of a high pressure system, and counterclockwise in a low pressure system. These weather systems are therefore key in the redistribution of warm air from low to high latitudes, and likewise cold air from high to low latitudes. This net flow of heat towards the high latitudes is required to balance the surplus of radiation received near the equator, and the net loss of radiation at the poles.

The geostrophic balance is a powerful means to explain the main flow features in large-scale weather systems, but we should keep in mind that it is a highly idealized situation. In practice the presence of turbulence causes a slight deviation from a flow directed parallel to the isobars. We will learn later that there is a net horizontal of air from high pressure to low pressure, which, in turn, causes a mean downwards motion in a high pressure system, and a mean upwards velocity in a low pressure system. If air rises, it cools, and its capacity to hold water will decrease. This is the reason why low pressure systems are often rainy, and nice, sunny weather can be expected in a high pressure system.

5.2 Large-scale circulation

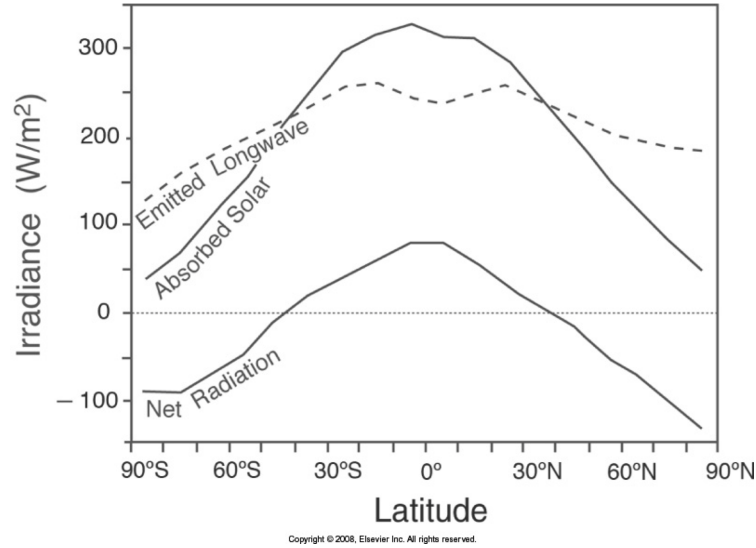


Figure 5.4: The zonal mean emitted infrared, absorbed solar and the net radiative flux. Figure copied from Marshall and Plumb (2016))

Large-scale transport by the wind is driven by an imbalance in the global distribution of net radiation. The global distribution of the annual mean solar radiation is maximum near the equator (see Fig. 5.4). This is due to the fact that towards higher latitudes the solar beam is spread out over a larger horizontal area. The imbalance in net radiation results from a somewhat lower emission of infrared radiation than absorption of solar radiation near the tropics, and vice versa at high latitudes. If no processes other than radiation would act, the poles would cool down to 0 K and the equatorial oceans would start to boil. This is obviously not happening because wind and ocean flow transport heat from low to high latitudes. The interplay between radiation and advective transport leads to the mean zonal temperature structure as depicted in Fig. 5.5.

The effect of Earth rotation on deflecting the wind prohibits a direct transport from the Equatorial region to high latitudes. As illustrated by Fig. 5.6 the mean flow structure in each hemisphere consists of three distinct cells. The subtropical circulation is called the Hadley cell. The maximum insolation near the equator causes an upward transport by deep convective clouds. Near the top of the troposphere this flow bends towards higher latitudes, and sinks down in the subtropics. The near surface winds in the subtropics are directed toward the equator, and are called the 'trade-winds' by early sailors who navigated between Europe and Asia.

Another distinct feature of the large-scale circulation is the presence of strong westerly winds at the midlatitudes with maximum values near the top of the troposphere (see Fig. 5.5). We will derive that this structure is due to the presence of a large-scale temperature gradient.

5.3 Governing equations

Because turbulence plays a key role in controlling the large-scale vertical velocity we will apply the Reynolds-averaged equations, where we will use capital symbols to indicate mean values, for example, for wind U , V , and W . The conservation equations for mass and momentum read,

$$\frac{\partial U}{\partial x} + \frac{\partial V}{\partial y} + \frac{\partial W}{\partial z} = 0. \quad (5.11)$$

$$\frac{dU}{dt} = fV - \frac{1}{\rho} \frac{\partial P}{\partial x} - \frac{\partial \overline{u'w'}}{\partial z}, \quad (5.12)$$

$$\frac{dV}{dt} = -fU - \frac{1}{\rho} \frac{\partial P}{\partial y} - \frac{\partial \overline{v'w'}}{\partial z}, \quad (5.13)$$

$$\frac{\partial P}{\partial z} = -\rho g, \quad (5.14)$$

with P the pressure, f the Coriolis parameter, and $\overline{u'w'}$ and $\overline{v'w'}$ the Reynolds averaged momentum fluxes. We already derived that for large-scale flow away from the equator, $f \neq 0$, for frictionless flow the geostrophic balance holds, which defines the geostrophic wind as follows,

$$U_g \equiv -\frac{1}{\rho} \frac{\partial P}{\partial y}, \quad V_g \equiv \frac{1}{\rho} \frac{\partial P}{\partial x}. \quad (5.15)$$

We will use this set to 1) investigate the effect of a horizontal density gradient, and 2) the effect of turbulent friction on the vertical velocity.

5.4 Thermal wind

The easiest route to understanding the impact of a large-scale horizontal temperature gradient on wind is provided by expressing the density field by a constant value ρ_{ref} superposed by fluctuations ρ' in the horizontal directions,

$$\rho(x, y, z) = \rho_{\text{ref}} + \rho'(x, y), \quad (5.16)$$

with $\rho'/\rho_{\text{ref}} \ll 1$. This expression thus ignores vertical variations in the density. It is inspired from oceanography where vertical variations in the density are actually very small across the water column. We will use this strong simplification for the atmosphere, as it will give the desired physical explanation in just one step.

Let us consider a geostrophic balance,

$$f\rho U = -\frac{\partial p}{\partial y}. \quad (5.17)$$

Differentiating with respect to height gives the **thermal wind** relation,

$$f\rho \frac{\partial U}{\partial z} = -\frac{\partial^2 p}{\partial z \partial y} = g \frac{\partial \rho'}{\partial y} \quad (5.18)$$

where changed the order of differentiation, and applied hydrostatic balance.

As the air in the equator is warmer than at the poles, the horizontal density gradient $\partial \rho'/\partial y > 0$. At the northern hemisphere $f > 0$, and consequently we conclude that the zonal wind must increase with height, $\partial U/\partial z > 0$.

5.5 Large-scale vertical velocity

In the previous section we have seen how a horizontal density gradient controls vertical shear. Now we will investigate the effect of turbulent friction. For simplicity we will assume a horizontally homogeneous atmosphere.

Solution for geostrophic flow

The mean vertical velocity is controlled by the large-scale divergence of horizontal wind,

$$D \equiv \frac{\partial U}{\partial x} + \frac{\partial V}{\partial y} = -\frac{\partial W}{\partial z}. \quad (5.19)$$

If we substitute the solutions for the wind that satisfy a geostrophic balance we find

$$D = \frac{1}{\rho f} \left(-\frac{1}{\rho} \frac{\partial^2 P}{\partial x \partial y} + \frac{1}{\rho} \frac{\partial^2 P}{\partial y \partial x} \right) = 0. \quad (5.20)$$

We conclude that a pure geostrophic flow *does not support any large-scale vertical motions*.

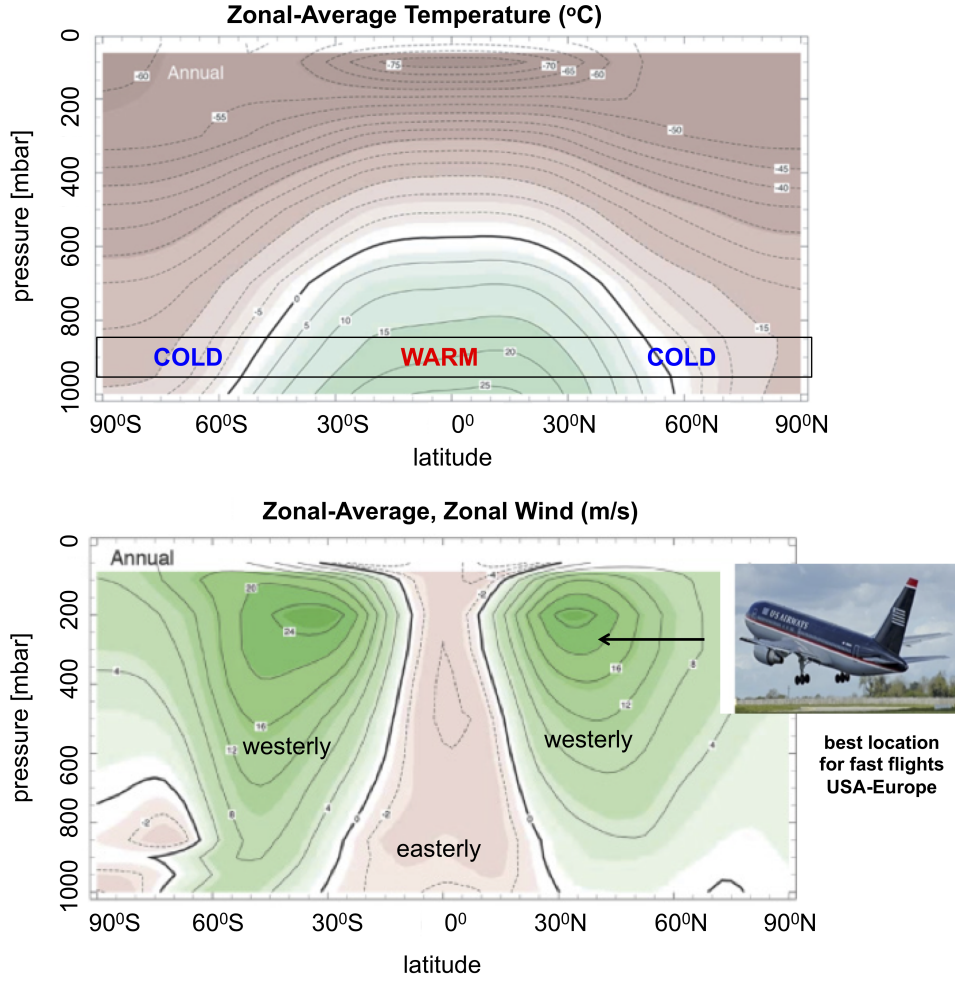


Figure 5.5: Zonal mean structure of the temperature (upper plot) and zonal wind (lower plot) (copied from Marshall and Plumb (2016)).

Solution with turbulent friction

The importance of turbulence on the vertical motion becomes clear after a differentiation of Eqs. (5.12) and (5.13) with respect to y and x , respectively,

$$\frac{\partial}{\partial z} \left[fW - \frac{\partial \overline{u'w'}}{\partial y} + \frac{\partial \overline{v'w'}}{\partial x} \right] = 0. \quad (5.21)$$

Here we used Eq. (5.11) and we ignored latitudinal variations in f . A vertical integration from the surface, indicated by the subscript 'sfc', upwards to height h , above which the atmosphere is assumed to be free of turbulence, demonstrates that a vertical velocity will be induced by turbulence,

$$W|_h = \frac{1}{f} \left(\frac{\partial \overline{u'w'}_{\text{sfc}}}{\partial y} - \frac{\partial \overline{v'w'}_{\text{sfc}}}{\partial x} \right), \quad (5.22)$$

where we used $W = 0$ at the ground surface.

Many experimental field campaigns have been dedicated to finding empirical relations between turbulent fluxes and mean state properties. For example, the surface flux for a variable ϕ , which

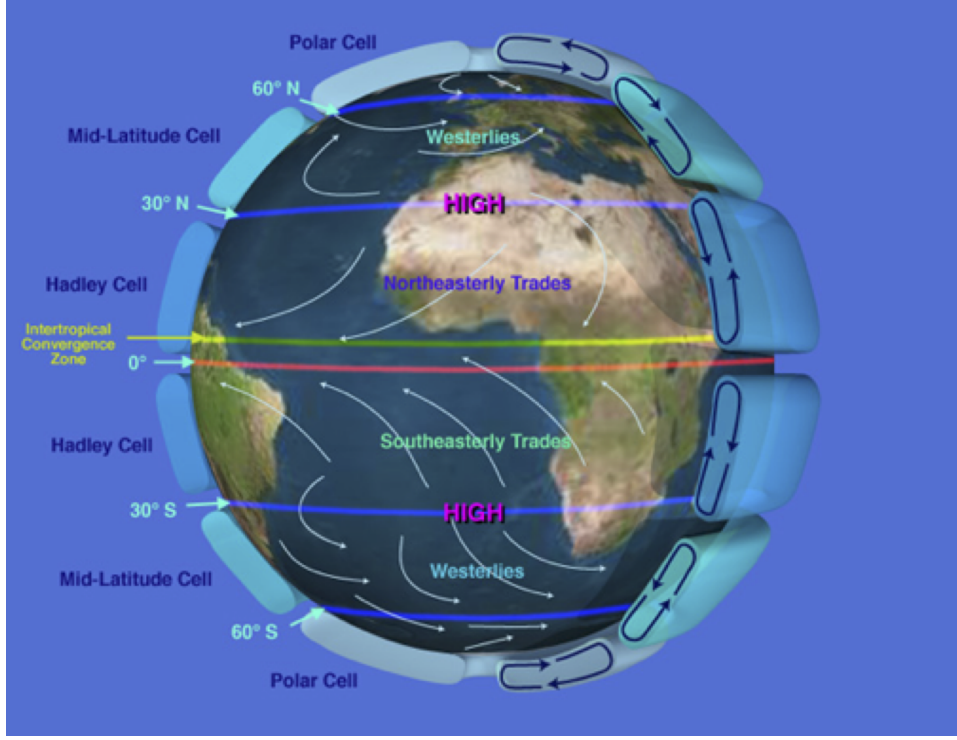


Figure 5.6: Schematic of the large-scale circulation. Source: UCAR.

may represent, for example, heat, moisture or momentum can be computed from the following bulk formula,

$$\overline{w'\phi'_{\text{sfc}}} = C_d U_s (\phi_{\text{sfc}} - \phi), \quad (5.23)$$

with C_d turbulent drag coefficient that depends on the vertical stability and the roughness of the surface. For flow over the ocean $C_d \approx 10^{-3}$. The wind speed U_s and ϕ are typically evaluated at a height of 10 m. Since the no-slip condition states that at the ground surface the wind must be zero, we can express the momentum fluxes as,

$$(\overline{u'w'_{\text{sfc}}}, \overline{v'w'_{\text{sfc}}}) = -C_d U_s (U, V). \quad (5.24)$$

At some height h above the ground surface there will be no turbulence with zero values for the momentum fluxes. This implies that the turbulent flux term in Eq. (5.12) may be approximated by

$$-\frac{\partial \overline{u'w'}}{\partial z} = -\frac{C_d U_s}{h} U. \quad (5.25)$$

If we define $k_f \equiv C_d U_s / h$, the turbulent fluxes can be expressed as

$$-\frac{\partial \overline{u'w'}}{\partial z} = -k_f U \quad , \quad -\frac{\partial \overline{v'w'}}{\partial z} = -k_f V. \quad (5.26)$$

With aid of the parameterization for the turbulent flux, and with use of the definition of the geostrophic wind Eq. (5.15), we can write the stationary momentum equations as follows,

$$V - V_g - k_f U = 0, \quad , \quad -U + U_g - k_f V = 0. \quad (5.27)$$

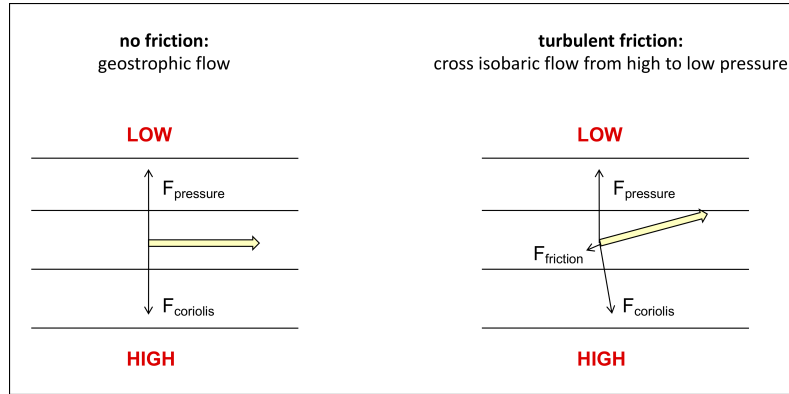


Figure 5.7: A schematic representation of cross isobaric flow due to turbulent friction.

The horizontal wind can be expressed in terms of the geostrophic wind,

$$U = \frac{U_g}{1 + k_f^2} - \frac{k_f}{1 + k_f^2} V_g \quad , \quad V = \frac{V_g}{1 + k_f^2} + \frac{k_f}{1 + k_f^2} U_g. \quad (5.28)$$

In the absence of turbulent friction ($k_f = 0$) we recover the solutions of geostrophic balance. For $k_f > 0$ we find that turbulent friction decreases the wind speed as

$$U_s = \sqrt{\frac{U_g^2 + V_g^2}{1 + k_f^2}} \leq |\vec{U}_g|. \quad (5.29)$$

Fig. 5.7 illustrates schematically the effect of turbulent friction for the situation in which the geostrophic forcings $U_g = 0$ and $V_g \neq 0$. For frictionless flow $U = 0$. However, for $k_f > 0$ we find that $U \neq 0$, which indicates that cross-isobaric flow occurs.

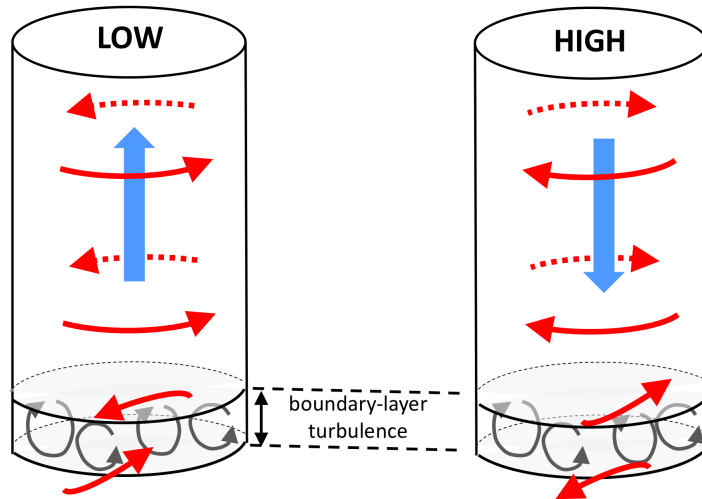


Figure 5.8: A schematic representation of Ekman pumping in a synoptic low and high pressure system (adapted from Marshall and Plumb (2016)).

The presence of this ageostrophic wind component results in the large-scale divergence (or convergence) of the flow that, in turn, drives the large-scale vertical motions as schematically depicted in Fig. 5.8. Because the magnitude of the turbulent friction controls the strength of the cross-isobaric flow, it impacts the evolution of (anti) cyclones at synoptic scales. Although the mean vertical velocity is small, typically of the order of $\sim \text{cm s}^{-1}$, it has a very strong impact on cloud formation. Indeed, if air moves upward, such as occurring in a low pressure system, its cooling will increase its relative humidity, which may give rise to saturation and cloud formation. Clear skies are often present in high pressure systems in which the air is slowly subsiding.

The vertical velocity that is driven by surface momentum fluxes is often called **Ekman pumping** after the Swedish oceanographer who was the first to derive an analytical solution for wind-driven horizontal transport in the ocean. Ekman's solution for ocean flow, which involves the ratio of the densities of air to water, is widely used as a powerful diagnostic tool that relates the strength of Ekman pumping in the ocean to the curl of the wind stress exerted at the Ocean's surface. Because the density of water is about a factor of 1000 larger than that of air, the typical vertical velocities in the ocean are of the order of several tens of meters per year.

Chapter 6

Atmospheric Stability

Fig. 6.1 shows the observed vertical profiles of temperature and dry static energy. These profiles are typical for clear sky conditions during daytime when the sun is heating the ground surface, which in turn heats the air just above giving rise to convection. The air in the surface layer is characterized by a decrease in s_{dry} . In the layer above s_{dry} is vertically well mixed, and is approximately constant with height. This **mixed layer** structure is the result of turbulent eddies that mix and homogenise the air up to the inversion layer. In the free troposphere s_{d} increases with height, and this layer is devoid of turbulence. We will use the thermodynamic properties of adiabatic air parcels to explain how the temperature stratification of the atmosphere controls whether air parcels may rise spontaneously or not.

The stability of the atmosphere will be derived from considering the acceleration due to the buoyancy of an air parcel if it is vertically displaced. If we denote the parcel's properties with respect to its environment with a prime, $\phi' = \phi_p - \bar{\phi}$, its buoyancy can be expressed as (see Eq. (4.11)),

$$\frac{dw'}{dt} = \frac{T_{v,p} - \bar{T}_v}{\bar{T}_v} g = \frac{T'_v}{\bar{T}_v} g = \frac{\theta'_v}{\theta_v} g. \quad (6.1)$$

The last term is obtained by multiplying by a factor including the Exner function, Π/Π , as defined

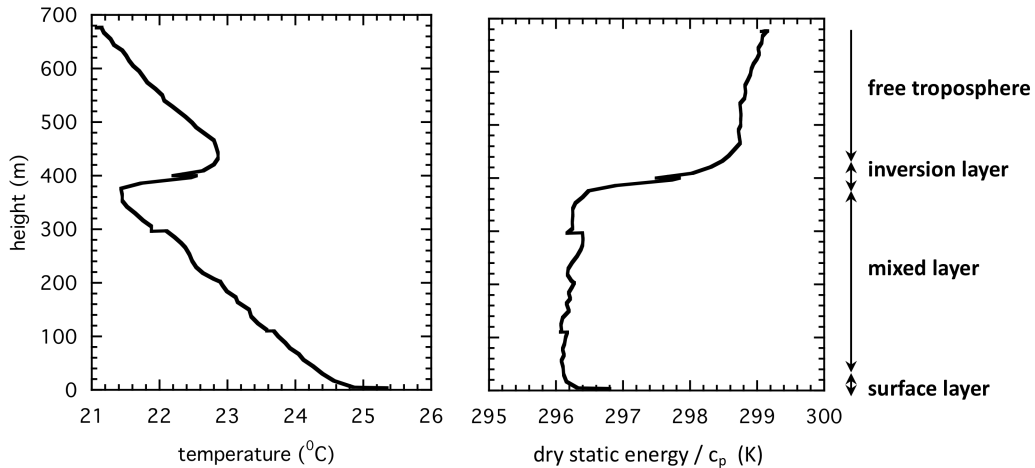


Figure 6.1: The temperature profile as observed from a tethered balloon during daytime at Cabauw (left). The plot on the right shows the dry static energy divided by c_p , which is approximately equal to the potential temperature.

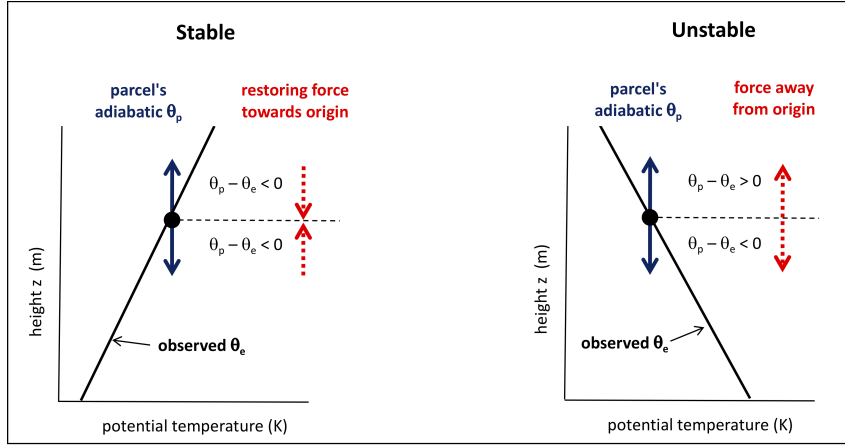


Figure 6.2: Schematic showing the forces acting on an adiabatic air parcel that is vertically displaced for a stable (left) and unstable (right) stratification. The parcel's potential temperature is indicated with a subscript 'p'. The observed vertical profile is indicated by a subscript 'e' and is assumed to be representative for the mean of the environment ($\bar{\theta} = \theta_e$).

in Eq. (2.54). In the absence of moisture we can write

$$\frac{\theta'_v}{\theta_v} = \frac{\theta'}{\bar{\theta}} \approx \frac{s'_{\text{dry}}}{\bar{s}_{\text{dry}}}. \quad (6.2)$$

6.1 Stability of the dry atmosphere

We will first study a situation without moisture. Fig. 6.2 shows an example of the buoyancy force acting on a vertically displaced adiabatic air parcel. Here we recall that an adiabatic parcel does not mix with its environment and does not absorb heat. Energy conservation dictates that its values for θ or s_{dry} will be constant with height.

Let us assume that the mean potential temperature varies linearly with height with slope

$$\gamma_\theta = \frac{d\bar{\theta}}{dz}, \quad (6.3)$$

we may express it as $\bar{\theta} = \theta_p + \gamma_\theta z'$, where z' is the height with respect to the origin of the disturbed air parcel. We may rewrite the vertical momentum equation as

$$\frac{dw'}{dt} = \frac{d^2 z'}{dt^2} = \frac{g}{\bar{\theta}} \theta' = \frac{g}{\bar{\theta}} \gamma_\theta z'. \quad (6.4)$$

If we ignore variations of $\bar{\theta}$ with height, we obtain for $\gamma_\theta > 0$,

$$z'(t) = c_1 \cos(\ell t) + c_2 \sin(\ell t), \quad (6.5)$$

with frequency

$$\ell = \sqrt{\frac{g}{\bar{\theta}} \frac{d\bar{\theta}}{dz}}. \quad (6.6)$$

For $\gamma_\theta > 0$ the buoyancy force is directed towards to origin of the parcel, and this restoring force gives rise to an oscillation of the disturbed air parcel. This is called a stable stratification, with ℓ the Brunt-Väisälä frequency. By contrast, for $\gamma_\theta < 0$ we obtain

$$z'(t) = c_1 e^{\ell t} + c_2 e^{-\ell t}, \quad \ell = \sqrt{-\frac{g}{\bar{\theta}} \frac{d\bar{\theta}}{dz}}. \quad (6.7)$$

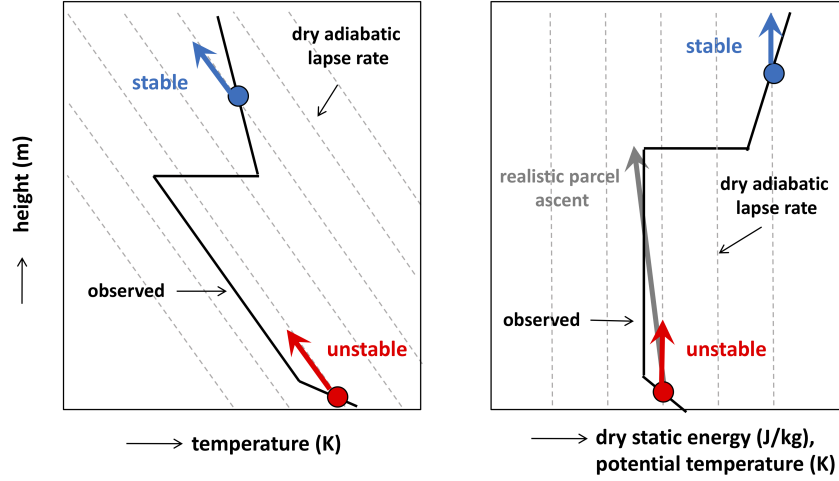


Figure 6.3: Atmospheric stability from a temperature (left) and a dry static energy or potential temperature perspective (right). The thick black lines depict schematically their observed profiles. The thin dashed lines indicate dry adiabatic profiles. The blue and red arrows show the values of adiabatically displaced parcels. The thick grey arrow indicates more realistic values of parcel ascent. Because the water vapor specific humidity is also constant with height for an adiabatic parcel, the diagram would look identical if the temperature T would be replaced by the virtual temperature T_v . Likewise, the dry static energy and the potential temperature may be substituted by the virtual potential temperature.

The first term indicates a vertical acceleration that is due to the buoyancy force that is directed away from the origin of the parcel. We have therefore derived the following stability criteria,

$$\text{stable} \quad \frac{dT}{dz} > -\frac{g}{c_p}, \quad \frac{ds_{\text{dry}}}{dz} > 0, \quad \frac{d\theta_v}{dz} > 0 \quad (6.8)$$

$$\text{unstable} \quad \frac{dT}{dz} < -\frac{g}{c_p}, \quad \frac{ds_{\text{dry}}}{dz} < 0, \quad \frac{d\theta_v}{dz} < 0 \quad (6.9)$$

Fig. 6.3 captures the main features of T and s_d in a mixed layer. If an adiabatic air parcel is displaced vertically from the surface layer its positive buoyancy will cause an upward acceleration up to the inversion layer. Once it reaches the free troposphere the parcel will be colder than its environment causing a downward acceleration. No convection can be triggered in the free troposphere due to its stable stratification. As we will see later the only exception is when moist air becomes saturated and latent heat is released.

Although adiabatic parcels are never observed in practice, the above consideration well explains observations in terms of the onset of convection and the lack of turbulence in the free troposphere. The thick grey arrow in Fig. 6.3 depicts a more realistic view of parcel ascent. Due to lateral mixing of air with its environment the difference in the thermodynamic properties between the parcel and its environment will gradually weaken. At some height its buoyancy will have become equal to zero. Because the parcel has gained vertical velocity it will be able to keep rising, even it has achieved a negative buoyancy. The latter is due to fact that in reality the upper part of the mixed layer slightly deviates from a dry adiabatic profile due to the presence of the warm inversion layer. However, once the rising air has reached the inversion layer, its large negative buoyancy will act to strongly damp its upward motion. This will ultimately give rise to a weak descending motion. It has been observed that during this stage air from the free troposphere is mixed downwards into the mixed layer. This process of **entrainment** is not only an important means for the growth of the mixed layer depth, but as it mixes relative warm and dry air from the free troposphere it is also important for the thermodynamic evolution of the mixed layer.

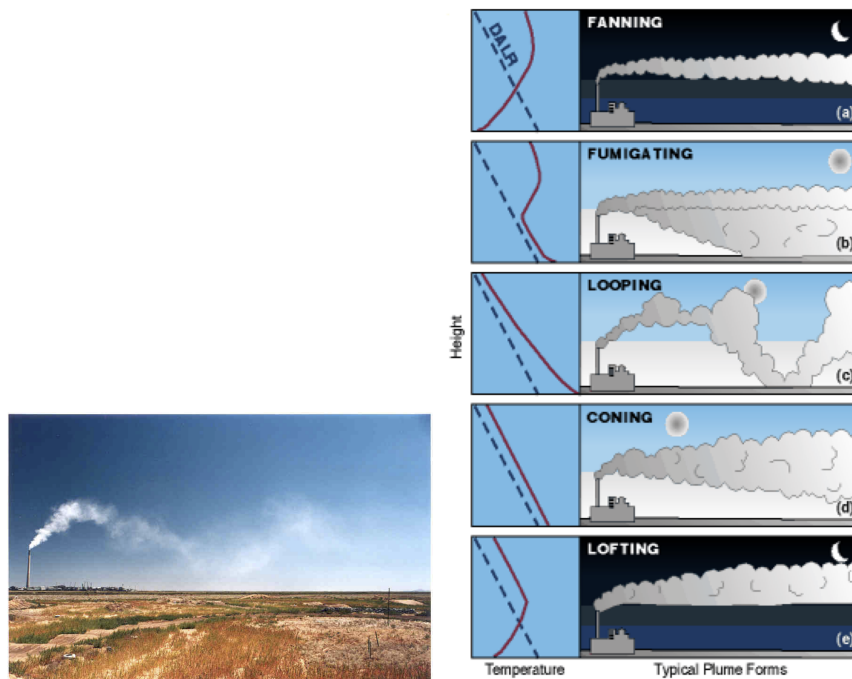


Figure 6.4: Photograph that makes the presence of updraft and downdrafts visible. The schematic on the right shows five different conditions of the vertical temperature profile (red lines) and the dry adiabatic temperature lapse rate (DALR). Copied from David Whiteman, University of Utah.

Application: Stability dependent dispersion of smoke

Fig. 6.4 shows a photograph of a smoke plume during convective conditions. The presence of both updrafts and downdrafts is clear from the variations in the plume elevation heights. The updrafts rising from the surface layer can be explained from the adiabatic theory. The downdrafts, however, are the result of conservation of mass, which dictates that *what goes up must come down*. This flow structure of upward and downward motions acts to efficiently stir the air. The schematic in Fig. 6.4 illustrates the impact of the atmospheric stability on the dispersion of a smoke plume. If smoke is released in a stable atmosphere, there will be only a little dispersion in the vertical direction (fanning). The lack of dilution causes the smoke concentration in the plume to be rather high. In the fumigating case convection stirs the smoke throughout the mixed layer, where the presence of a thermal inversion limits the upward dispersion. Under conditions of low inversion height air quality may turn poor as emissions will pile up in a shallow mixed layer. In case of a very strong surface layer instability the presence of individual plumes make be reflected in the undulations of the smoke plume. If the atmosphere is neutrally stratified (coning), the dispersion is stronger than for the neutral case, but weaker than for unstable case.

6.2 Stability of the moist atmosphere

A schematic description of some important definitions in cumulus classification is given in Fig. 6.5. The solid black line indicates the virtual potential temperature of the mean state. If the surface layer is unstably stratified air parcels may accelerate upwards. At the **level of neutral buoyancy** (LNB) the parcel has the same value of θ_v as its environment. Because the air parcel has obtained an upward vertical velocity (inertia) it can overshoot into the stable layer where it is gradually decelerated. If the air keeps rising its temperature decreases and the parcel may become saturated

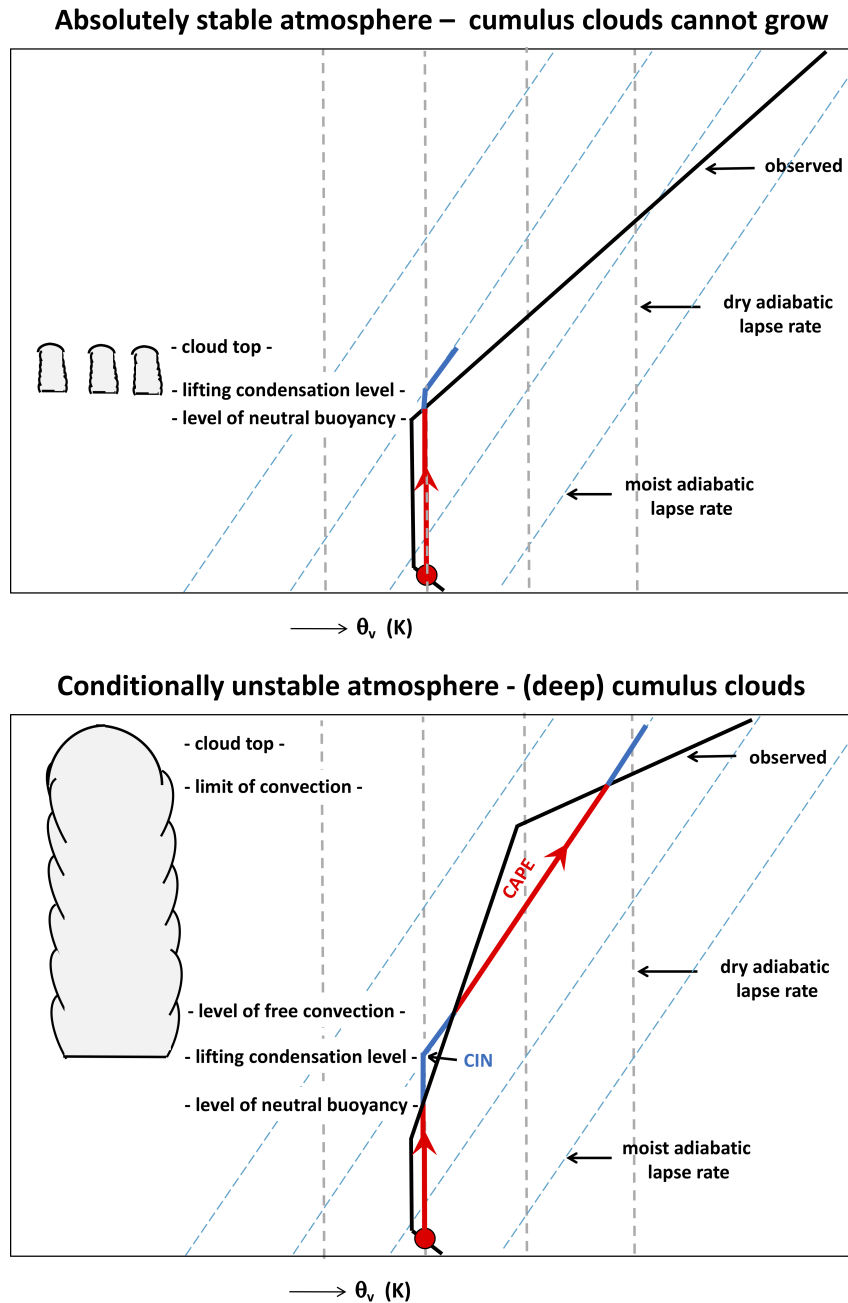


Figure 6.5: Schematic showing the relation between the mean vertical profile of θ_v (solid black lines) and cloud formation. The grey dashed lines indicate adiabatic profiles of dry adiabatic parcels, and the blue dashed lines the moist adiabatic profiles of θ_v . In the lower layer the parcel's θ_v will follow the dry adiabatic profile, but above the cloud base its θ_v increases with height due to the release of latent heat. See text for an explanation.

with water vapor. This height defines the cloud base and is also denoted as the **lifting cloud condensation level** (LCL). Above the LCL the saturated air parcel will follow the moist-adiabatic lapse rate.

From this stage there are two possible scenarios. If the vertical gradient of θ_v of the environment is larger than the moist-adiabatic lapse rate, the cloud parcel will remain negatively buoyant with respect to its environment. As a result its vertical motion will be damped and its vertical growth will be limited. Such a cloud is called a *forced* cloud. In contrast, when the vertical gradient of θ_v of the environment is less than the moist-adiabatic lapse rate, the cloud may reach the **level of free convection** (LFC). At this level the cloud is exactly neutrally buoyant with respect to its environment, but above it can gain vertical momentum again by a positive buoyancy excess up to the height where it reaches the **limit of convection** (LOC). Again, the vertical velocity the cloudy air parcel has obtained allows it to overshoot such that the actual cloud top is often observed above the LOC. This specific cloud type is able to vent air into the free atmosphere. For a cumulus cloud obeying this pattern the term *active* cloud is used. A necessary condition for its formation is a **conditionally unstable** atmosphere,

$$\text{conditional instability} \quad 0 < \frac{d\bar{\theta}_v}{dz} < \left(\frac{d\theta_v}{dz} \right)_{\text{moist adiabat}} \quad (6.10)$$

$$\text{absolute stability} \quad \frac{d\bar{\theta}_v}{dz} \geq \left(\frac{d\theta_v}{dz} \right)_{\text{moist adiabat}} \quad (6.11)$$

The **convective available potential energy** (CAPE) is a quantity that gives a measure of the instability of the atmosphere. It is estimated from the vertical velocity equation assuming a moist adiabatic rising air parcel which positive buoyancy is in balance with the vertical advection term. If we ignore pressure effects and lateral mixing ($u = v = 0$) we can write

$$\frac{1}{2} \frac{\partial w^2}{\partial z} = \frac{g}{\bar{\theta}_v} (\theta_{v,\text{ma}} - \bar{\theta}_v), \quad (6.12)$$

where $\theta_{v,\text{ma}}(z)$ represents the moist adiabatic virtual potential temperature of the parcel. This equation can be integrated between the level of free convection (LFC) and the limit of convection (LOC) to give (see its schematic depiction in Fig. 6.5),

$$\frac{1}{2} (w_{\text{LOC}}^2 - w_{\text{LFC}}^2) = \frac{g}{\bar{\theta}_v} \int_{\text{LFC}}^{\text{LOC}} (\theta_{v,\text{ma}} - \bar{\theta}_v) dz \equiv \text{CAPE}. \quad (6.13)$$

If we assume that w_{LOC}^2 is negligibly small, we can define the convective velocity scale w_{CAPE} . It can be interpreted as a conversion of potential energy into kinetic energy,

$$w_{\text{CAPE}} = 2\sqrt{\text{CAPE}}. \quad (6.14)$$

If we have surface observations of temperature and humidity we can use this to compute an adiabatic profile of θ_v . If an observed vertical profile of $\bar{\theta}_v$ is available the CAPE can be computed. This is a highly relevant quantity for meteorologists. For example, as a rule of thumb thunderstorms may develop for $\text{CAPE} > 2000 \text{ J kg}^{-1}$.

Part II

Part II. Clear and Cloud-Topped Atmospheric Boundary Layers

Chapter 7

Preface

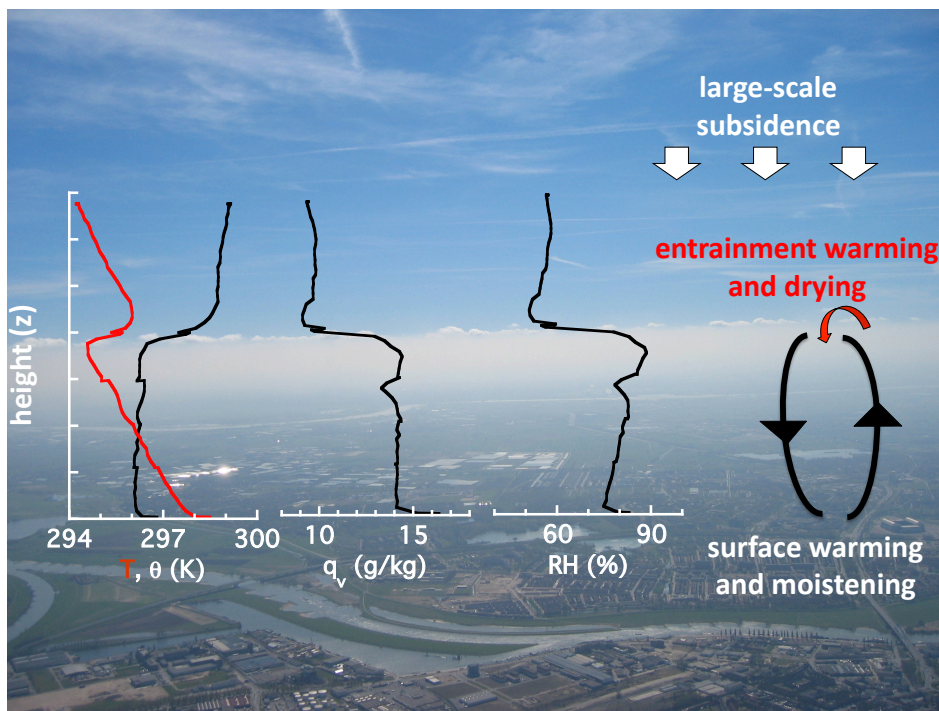


Figure 7.1: Tethered balloon observations of (a) the temperature T (red line) and the potential temperature θ , (b) the specific humidity q_v and (c) the relative humidity RH . The data were collected on 23 August 2001, between 10:12 and 10:35 UTC, at Cabauw in the Netherlands. The data have been superposed on a representative photograph of a convective boundary layer above the city of Rotterdam as observed from a glider by Adriaan Schuitmaker on another date.

Figure 7.1 shows a distinct layer of haze, whose top appears very sharp and very homogeneous in the horizontal directions. The photographer took advantage of rising thermals that buoyed his glider up to the top of the haze layer. The figure also shows typical observations of the vertical thermodynamic structure of a clear convective atmosphere during daytime. The temperature profile follows a dry adiabatic lapse rate up to the thermal inversion layer in which the temperature strongly increases. This thermal inversion layer can have depths of just several tens of meters, and sharply

marks the relatively warm and dry free tropospheric air from the air in the layer below. The potential temperature and the specific humidity in the boundary layer are fairly well mixed which is due to the stirring and homogenizing effect of turbulence. For this reason the convective boundary layer (CBL) is often called the mixed layer. It is frequently observed over land during daytime as a result of a heating of the ground surface by solar radiation which triggers convective plumes. Note that the relative humidity is not constant in the mixed layer but increases with height. From the photograph it can be seen that high RH values at the top of the mixed layer can give rise to a distinct layer of haze. This is due to aerosol deliquescence, i.e. the process of aerosols absorbing moisture from the atmosphere until they dissolve in the absorbed water. This gives rise to a more efficient scattering of light particularly at RH values above 80%. Another indicator of a high RH is the presence of a few scattered shallow clouds.

The thermal inversion layer acts like some kind of lid in the sense that it prohibits thermals to rise much further, which explains why air pollutants that are emitted near the ground surface tend to accumulate in the mixed layer especially on clear days, as subsidence and warm air aloft inhibit vertical mixing through the troposphere. In the remainder of the text the inversion or inversion layer is loosely used to refer to the thermal inversion layer. If rising plumes penetrate the inversion layer, their negative buoyancies at this height will strongly damp their upward vertical velocities. In fact, they will ultimately sink thereby mixing some warm and dry air from just above the inversion layer into the boundary layer, a process which is referred to as **entrainment**. The thermodynamic evolution of the boundary layer can actually be calculated straightforwardly from the fluxes at the ground surface and the entrainment flux at the top of the mixed layer. Such a bulk approach, which is called a mixed-layer model (MLM), considers the vertically integrated budget equations for heat and moisture thereby effectively treating the turbulent atmospheric boundary layer as a single slab (Tennekes 1973).

The MLM not only allows to predict the possible formation of clouds at the top of the mixed layer, but it will be explained that it also can be applied to study the temporal evolution of the cloud-topped boundary layer. The applicability of the MLM can even be pushed further to investigate how large-scale conditions such as the surface temperature or the large-scale divergence of the wind control the stratocumulus amount.

Chapter 8

The clear convective boundary layer

Since the early sixties many studies have been devoted to understand the temporal evolution of the mixed layer. Early studies were dedicated to the ocean mixed layer in which the buoyancy depends on the salinity and temperature. The dynamical structure of the buoyancy-driven mixed layer in the ocean is identical to the clear CBL in the atmosphere.

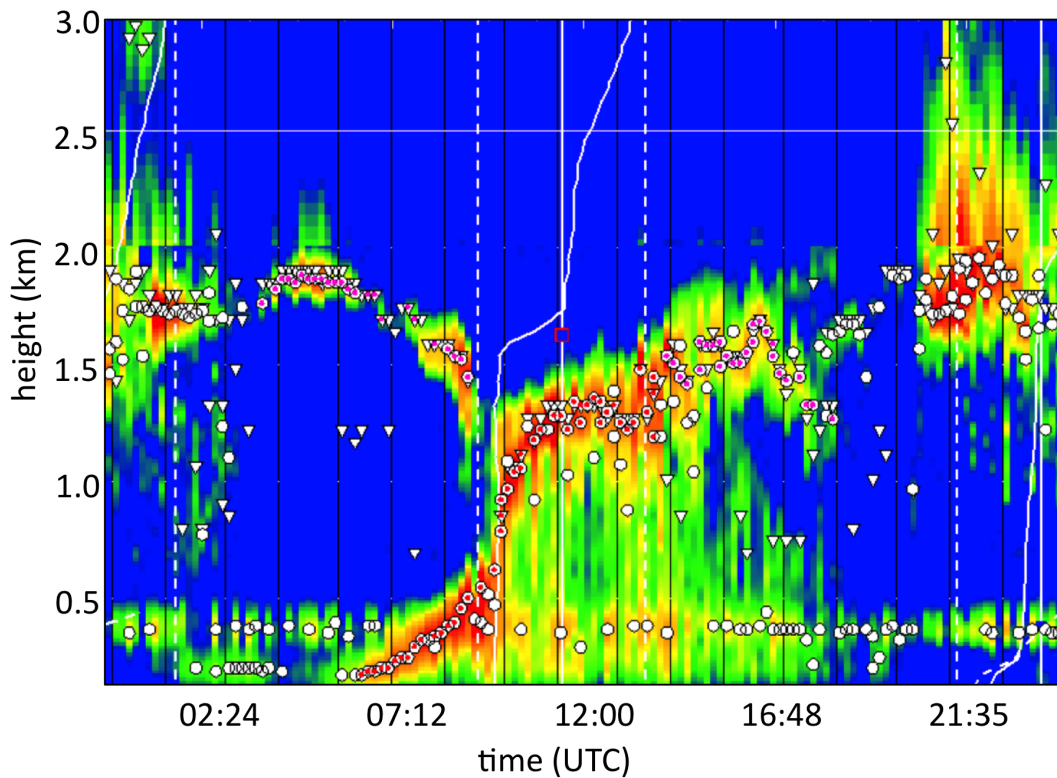


Figure 8.1: CBL evolution as observed from a lidar at Cabauw, in the Netherlands, 5 May 2008. Local time is two hours later than the UTC. The red colors can be interpreted as the top of the mixed layer. Plot kindly provided by Henk Klein Baltink (KNMI).

Figure 8.1 shows a typical example of the mixed-layer height h evolution over land as observed at the meteorological measurement station Cabauw, in the Netherlands. In the early morning h

rapidly deepens with time, after which it reaches an approximate steady state during the afternoon. During the night a two layer structure is seen. The lower layer is associated with the nocturnal stable boundary layer which is cooled from the surface. Just below 2 km the observations indicate the residual mixed layer, which is a result of convective mixing and entrainment during the preceding daytime period.

The surface energy balance (SEB) is determined by net fluxes of solar and infrared radiation, SW_{net} and LW_{net} , respectively, turbulent fluxes of heat and moisture, SHF and LHF, respectively, and the energy flux into the ground G ,

$$\text{SHF} + \text{LHF} + SW_{\text{net}} + LW_{\text{net}} + G = 0. \quad (8.1)$$

Fig. 8.2 shows an example of observations during a day with clear skies. The albedo of the grass surface is minimum around local noon at a value of about 0.19. The effect of the heating of the ground surface is evident from the increase in the upwelling infrared radiation flux, which for a black body emitter is given by $LW_{\text{up}} = \sigma T_{\text{sfc}}^4$. In any case the ground surface is emitting more longwave radiation than is absorbed from the atmosphere, such that for the clear sky case shown, the net longwave radiation at the surface is negative and of the order of 100 Wm^{-2} . An interesting feature of Cabauw is its high soil humidity. This results in a very strong evaporation, and a relatively small SHF. Their ratio is characterized by the **Bowen ratio**,

$$B \equiv \frac{\text{SHF}}{\text{LHF}} = \frac{c_p \overline{w' T'_{\text{sfc}}}}{L_v \overline{w' q'_{\text{sfc}}}}. \quad (8.2)$$

Fig. 8.3 shows a polder in the Netherlands and a desert area. For moist surfaces $B \ll 1$. Another limit is a soil that is almost free of moisture like the Sahara desert where $B \rightarrow \infty$. The onset of clouds during daytime is strongly controlled by the value of B .

8.1 Evolution of the boundary-layer depth

During daytime solar radiation heats up the ground surface. This results in a gradual increase of the surface temperature. At some time the surface layer may become unstably stratified, resulting in rising warm air parcels. Observations collected over land typically show a growth of the boundary layer depth h with time during daytime. Here we will discuss and quantify the mechanisms explaining the evolution of h due to entrainment and large-scale subsidence.

Entrainment

Figure 8.4 nicely shows that if the convective plumes hit the inversion layer, the vertical motion will be strongly damped, basically because of its negative buoyancy (as boundary layer air is colder than the inversion layer). The strong upward vertical motions cause the air to overshoot into the inversion, where the boundary-layer air will mix with inversion layer air, and the negative buoyancy of the mixed air will ultimately push it down into the boundary layer. The main point is that in this way the relatively warm and air from just above the inversion layer will be mixed downwards into the boundary-layer causing its warming, drying in addition to its deepening. The growth rate of the boundary layer depth due to turbulent mixing is called **entrainment** w_e ,

$$\left(\frac{\partial h}{\partial t} \right)_{\text{entrainment}} = w_e. \quad (8.3)$$

We recognize that entrainment must have dimensions of velocity.

Large-scale subsidence

In practice the mean vertical velocity \bar{w} in the atmosphere is small, but in any case usually nonzero. This is due to the turbulent friction in the boundary layer, which gives rise to the Ekman pumping

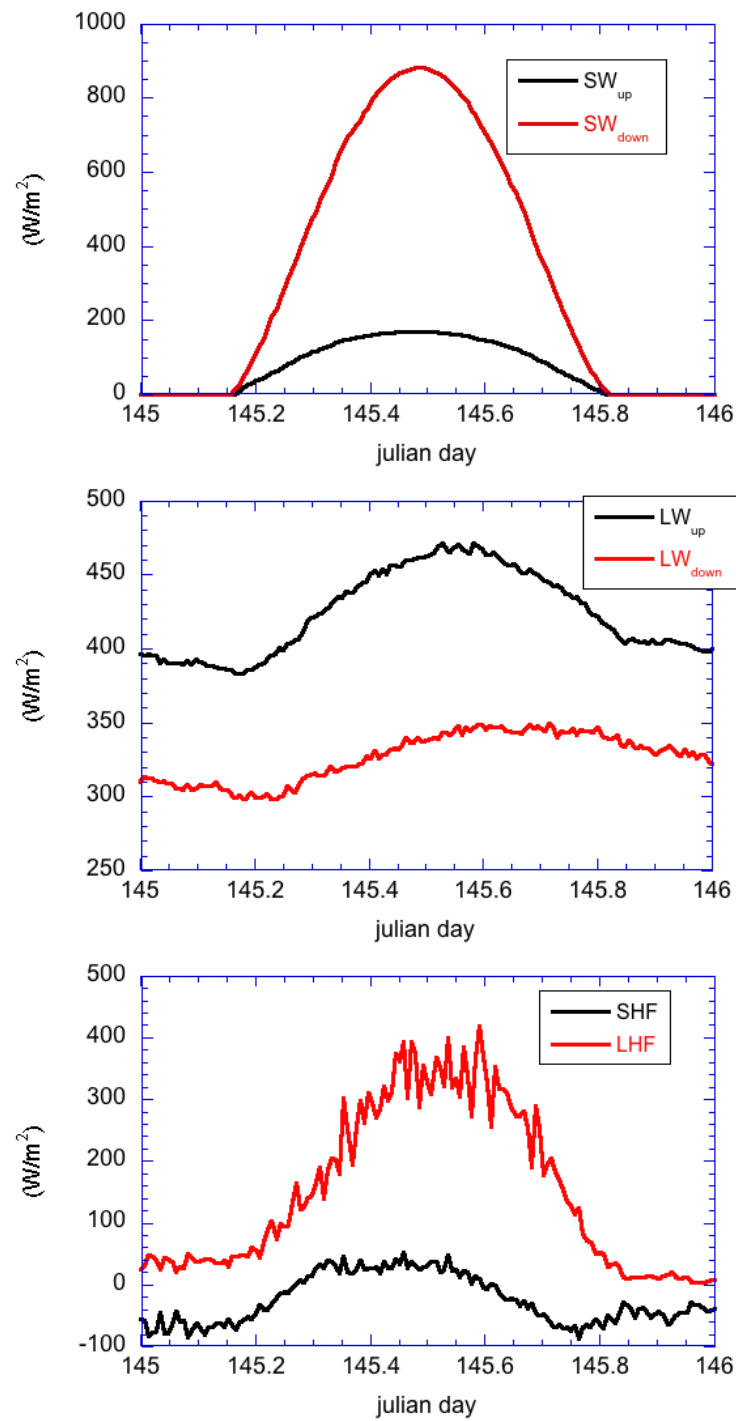


Figure 8.2: The upward and downward shortwave and longwave radiation fluxes, and the sensible and latent heat fluxes as observed during 24 May 2012 at Cabauw.



Figure 8.3: Photographs of areas with a very dry and very moist soil.

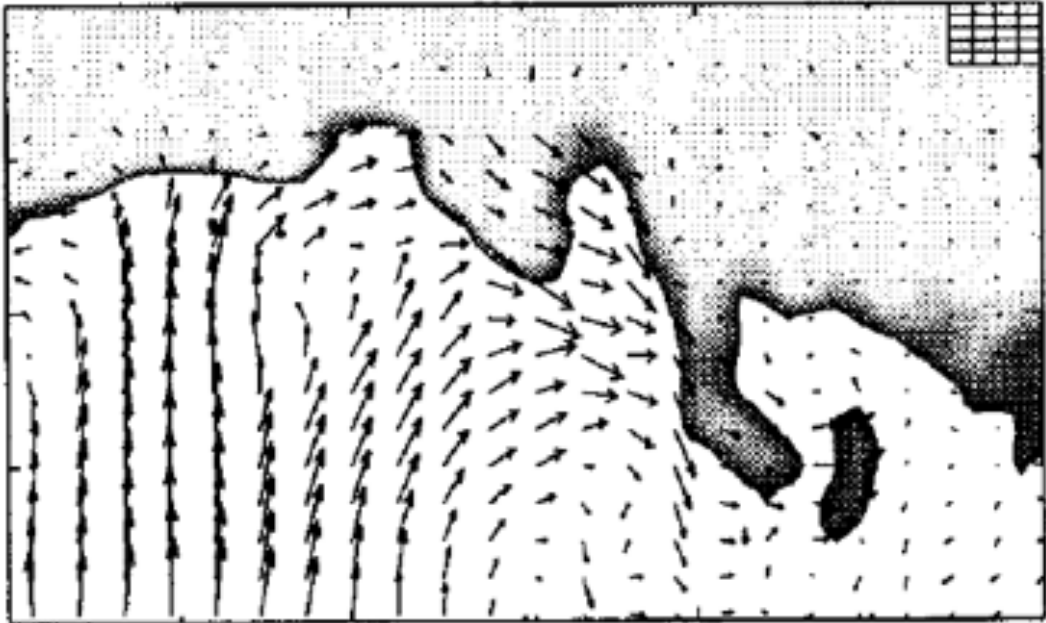


Figure 8.4: Flow field at the top of a convective boundary layer capped by a thermal inversion as obtained from a large-eddy simulation (Sullivan et al. 1998).

discussed in Chapter 5. This implies that the boundary layer depth h will not only depend on the entrainment velocity w_e , but also on the large-scale vertical velocity \bar{w} ,

$$\frac{dh}{dt} = w_e + \bar{w}_h. \quad (8.4)$$

This tendency equation is actually another way of expressing conservation of mass, where $w_e > 0$ represents a measure of the volume of air that is mixed per unit horizontal area per unit time into the boundary layer by turbulent eddies. The large-scale subsidence \bar{w} is driven by a large-scale divergence of the horizontal winds (D),

$$\bar{w}(z) = - \int_0^z D(z) dz = - \int_0^z \left(\frac{\partial \bar{u}}{\partial x} + \frac{\partial \bar{v}}{\partial y} \right) dz. \quad (8.5)$$

This means that if there is a divergence in the horizontal air flow (i.e. a net outflow, which is typically present under conditions of a high pressure system), conservation of mass dictates that

the removal of mass out of the boundary layer must be accompanied by a compensating large-scale subsiding velocity, $\bar{w} < 0$, which acts to contract and lower the boundary-layer top. As an analogy, one may compare this process with opening the drain in a bathtub such that the removal of water causes its surface level to decrease or a bucket with holes in its sides.

8.2 Turbulence

To illustrate the effect of convection on the boundary layer evolution and the entrainment flux Figure 8.5 presents large-eddy simulation results of the horizontal slab-mean profiles for θ_v and the virtual potential temperature flux $\overline{w'\theta'_v}$ at intervals of 2 hours. The case was driven by a constant surface buoyancy flux and the large-scale subsidence was set to zero. The boundary-layer deepens with time due to the entrainment air from just above the inversion. The virtual potential temperature flux varies linearly with height. The key notion of the figure is that the minimum value of $\overline{w'\theta'_v}$ at the top of the boundary layer is a constant fraction of the surface value,

$$\overline{w'\theta'_v}|_h = -A\overline{w'\theta'_{v,\text{sfc}}}, \quad (8.6)$$

with $A \approx 0.2$.

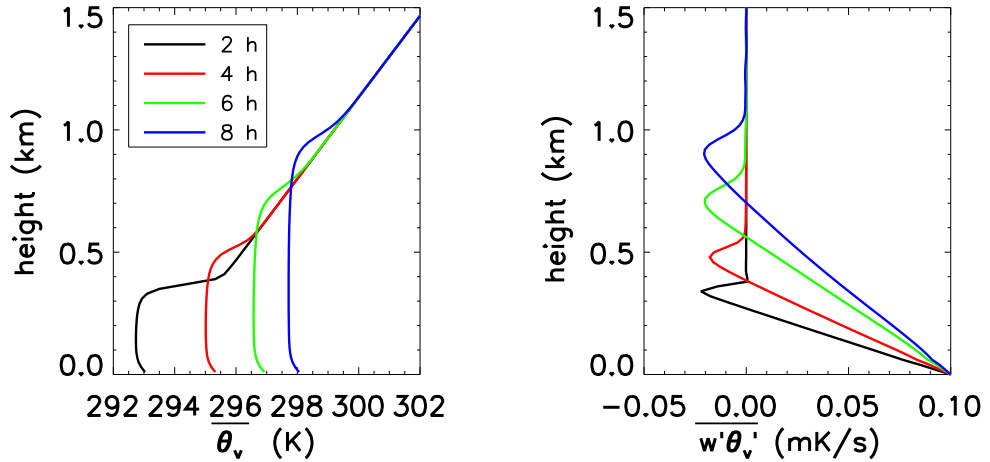


Figure 8.5: Large-eddy simulation results of a CBL driven by a constant surface buoyancy flux. The lines show the results at $t=2, 4, 6$ and 8 hrs for (a) θ_v and (b) $\overline{w'\theta'_v}$.

A typical feature of the clear convective boundary layer is the presence of turbulent eddies that act to stir and homogenize the air in the boundary layer. Like the vertical mean profile of $\overline{\theta_v}$ turbulent mixing causes the slab mean values of so-called conserved variables to become approximately constant with height. For this reason the CBL is sometimes simply called the **mixed layer**. We recall that a conserved variable is a quantity which value remains constant under vertical adiabatic displacements, meaning that the air parcel does neither absorb heat from radiation nor mixes with air from its environment. For the CBL the potential temperature and the water vapor specific humidity are conserved variables, and consequently the virtual potential temperature (Eq. 8.19) too. Let us indicate these variables by the variable ϕ , with $\phi \in \{q_v, \theta, \theta_v\}$.

For convenience we repeat the budget equation for the horizontal slab mean value $\overline{\phi}$ in the presence of turbulence acting as the only means of transport,

$$\left(\frac{\partial \overline{\phi}}{\partial t}\right)_{\text{turb}} = -\frac{\partial \overline{w'\phi'}}{\partial z}, \quad (8.7)$$

where we assumed a horizontally homogeneous boundary layer allowing to ignore the changes of the horizontal fluxes in the horizontal directions, i.e. $\partial \overline{w'\phi'}/\partial x \approx 0$.

Quasi-steady state

The fact that at times t and $t + \Delta t$ the boundary layer is and remains vertically well mixed indicates that the change in the slab-mean value $\overline{\phi}$ is constant *at any height in the mixed layer*. In other words, if the vertical gradient of ϕ does not change with time we can write

$$\frac{\partial}{\partial t} \frac{\partial \overline{\phi}}{\partial z} = \frac{\partial}{\partial z} \frac{\partial \overline{\phi}}{\partial t} = -\frac{\partial^2 \overline{w'\phi'}}{\partial z^2} = 0, \quad (8.8)$$

where we changed the order of differentiation. This condition is referred to as a **quasi-steady state**. It has a distinct consequence for the shape of the vertical flux profiles. From an integration of Eq. (8.8) we conclude that the vertical gradient of the flux is constant,

$$\frac{\partial \overline{w'\phi'}}{\partial z} = c_1. \quad (8.9)$$

Since the change of the flux with height (often called the divergence of the flux or simply the **flux divergence**) is equal to the tendency of $\overline{\phi}$, this solution states that at any height in the turbulent boundary layer the change in $\overline{\phi}$ will be the same. A second integration yields

$$\overline{w'\phi'} = c_1 z + c_2, \quad (8.10)$$

which indicates that the flux varies linearly with height, similar to what is found in Fig. 8.5. The constants can be expressed in terms of the values of the fluxes at the surface ($z = 0$) and at the top of the mixed layer ($z = h$),

$$\overline{w'\phi'} = \overline{w'\phi'}_{\text{sfc}} \left(1 - \frac{z}{h}\right) + \overline{w'\phi'}_h \left(\frac{z}{h}\right). \quad (8.11)$$

To predict the change of $\overline{\phi}$ with time it therefore suffices to know the fluxes at the surface and the top of the mixed layer. It is a beautiful result in the light of the fact that the flux $\overline{w'\phi'}$ is a result of turbulent transport, a phenomenon that is known to behave chaotically. However, despite this apparent complexity the vertical turbulent transport of conserved variables for vertically well mixed layers can be simply described by a linear function of height. On the basis of these notions we will discuss that even the magnitude of fluxes at the top of the boundary layer ($\overline{w'\phi'}_h$) can be well predicted, which paves the way to predict the tendency of the slab-mean value of ϕ .

The flux-jump relation

For an infinitesimally thin inversion layer the flux at the boundary layer top is equal to

$$\overline{w'\phi'}_h = -w_e \Delta \phi. \quad (8.12)$$

This equation states that the flux at the top of the mixed layer is proportional to the jump of ϕ across the inversion and the entrainment velocity. The validity of the **flux-jump relation** will be explained from a simple conceptual model. The appendix presents a more rigorous mathematical derivation following VanZanten et al. (1999).

Fig. 8.6 shows how entrainment affects the vertical profile of a quantity ϕ with time. Here we take a zero surface flux, $\overline{w'\phi'}_{\text{sfc}} = 0$, and we assume that turbulence maintains the boundary layer in a vertically well-mixed state. Due to entrainment the boundary layer grows at a rate of $w_e = \Delta h / \Delta t$. The assumption of a zero surface flux implies that the vertically integrated amount of ϕ will be constant in time, which can be expressed as,

$$\int_0^{h+\Delta h} \phi_{\text{ml}}(z) dz = \text{constant} \iff \phi_{\text{ml}}^t h + \phi_{h+\Delta h} \Delta h = \phi_{\text{ml}}^{t+\Delta t} (h + \Delta h). \quad (8.13)$$

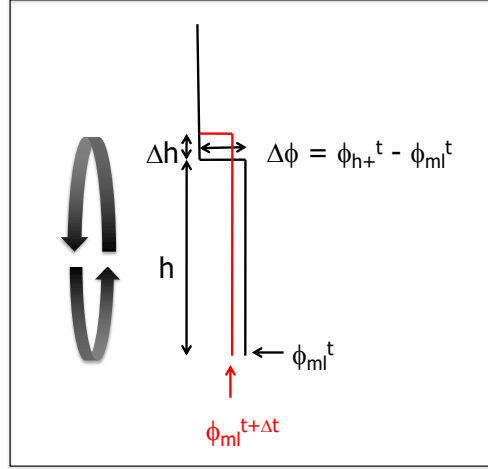


Figure 8.6: A conceptual model illustrating how entrainment of air from just above the inversion layer causes its growth by an amount Δh and affects the change of an arbitrary conserved variable ϕ in the mixed layer (denoted by the subscript 'ml', ϕ_{ml}) from time t to $t + \Delta t$, as indicated by the black and red lines, respectively. See text for details.

The temporal change of ϕ_{ml} in the boundary layer can now be expressed as

$$\frac{\partial \phi_{ml}}{\partial t} = \frac{\phi_{ml}^{t+\Delta t} - \phi_{ml}^t}{\Delta t} = \frac{\phi_{ml}^t h + \phi_{h+} \Delta h}{(h + \Delta h) \Delta t} - \frac{\phi_{ml}^t}{\Delta t} = -\frac{(\phi_{ml}^t - \phi_{h+}) \Delta h}{(h + \Delta h) \Delta t}. \quad (8.14)$$

For small $\Delta h/h$, and an inversion jump $\Delta \phi = \phi_{h+} - \phi_{ml}$, we can approximate

$$\frac{\partial \phi_{ml}}{\partial t} = -\frac{\phi_{ml}^t - \phi_{h+}}{h} \frac{dh}{dt} = \frac{w_e \Delta \phi}{h}, \quad (8.15)$$

where we used $\Delta h/\Delta t \approx dh/dt$, in and the absence of large-scale subsidence $dh/dt = w_e$. Since in the absence of a surface flux

$$\frac{\partial \phi_{ml}}{\partial t} = -\frac{\overline{w' \phi'_h} - \overline{w' \phi'_{sfc}}}{h} = -\frac{\overline{w' \phi'_h}}{h} \quad (8.16)$$

we identify

$$\overline{w' \phi'_h} \equiv -w_e \Delta \phi. \quad (8.17)$$

which is known as the **flux-jump relation**.

For a CBL the entrainment velocity depends on the surface buoyancy flux and the inversion stability.

Entrainment parameterization for the CBL

Entrainment causes the boundary layer to grow. One could argue that the entrainment rate may likely depend on the intensity of turbulence. Likewise, one might reason that the entrainment rates may depend on the strength of the inversion layer as measured by its temperature jump. Despite the fact that turbulence is a 'chaotic' process, entrainment in the CBL is one of the few quantities in the atmosphere whose scaling behavior is well known.

We found from Figure 8.5 that the minimum value of the virtual potential temperature flux at the top of the boundary layer is a constant fraction of the surface value, as expressed by Eq. (8.6). With aid of the flux-jump relation (10.28) we can now write the entrainment velocity as

$$w_e = A \frac{\overline{w' \theta'_{v, sfc}}}{\Delta \theta_v}. \quad (8.18)$$

Here the surface flux virtual potential temperature flux is the main driver of turbulence, and the strength of the inversion layer is quantified by the jump $\Delta\theta_v$. For convenience we repeat the definition of θ_v for moist, cloud-free air,

$$\theta_v = \theta(1 + \epsilon_I q_v). \quad (8.19)$$

Since $\epsilon_I \approx 0.608$ and because q_v is on the order of 0.01 kg/kg, we conclude that the magnitude of $\Delta\theta_v$ is determined mainly by the difference of the potential temperature across the inversion layer.

However, because θ_v depends both on the potential temperature and the specific humidity, its vertical flux depends on the fluxes of the latter two quantities,

$$\overline{w'\theta'_v} = A_d \overline{w'\theta'} + B_d \overline{w'q'_v}, \quad (8.20)$$

with $A_d \approx 1 + \epsilon_I \overline{q_v}$ and $B_d \approx \epsilon_I \overline{\theta}$. If the fluxes of heat (SHF) and moisture (LHF) are given in units of Wm^{-2} , then we can write

$$\overline{w'\theta'_v} = \frac{A_d}{\rho c_p} \text{SHF} + \frac{B_d}{\rho L_v} \text{LHF}. \quad (8.21)$$

The factors $A_d/\rho c_p \approx 8 \cdot 10^{-4}$ and $B_d/\rho L_v \approx 6 \cdot 10^{-5} \text{ m}^3 \text{K/J}$. Over sea the LHF may be one order of magnitude larger than the SHF. For such a situation they have an almost equal effect on the surface buoyancy flux, and, in turn, on the entrainment rate.

Example. Consider a situation without moisture, $\text{SHF} = 100 \text{ Wm}^{-2}$ and a temperature jump of 5 K across the inversion. If $q_v = 0$, we have $\Delta\theta_v = \Delta\theta = \Delta T/\Pi$, with Π the Exner function according to Eq. 2.54. If the inversion height is located below a pressure level of 900 hPa, approximating $\Pi \approx 1$ yields an acceptable error of less than 3% in $\Delta\theta_v$ ¹. We then find $w_e = 1.6 \text{ cm s}^{-1}$.

8.3 Summary and outlook

In this chapter we have highlighted some key aspects of the clear convective boundary layer (CBL). A CBL develops as a result of a heating of the ground surface by solar radiation. This leads to the formation of convective plumes which transport moisture and heat from the surface to the top of boundary layer. By their inertia the plumes can overshoot into the warm inversion layer that caps the boundary layer. This causes some mixing of air from just above the inversion layer into the boundary layer. This process is called entrainment and causes a growth of the boundary-layer height. The turbulent eddies act as a stirring agent that makes the mean profiles of conserved variables like q_v , θ and θ_v vertically well mixed. For this reason the convective boundary layer is often called the mixed layer.

- The growth of the boundary-layer height depends on the entrainment velocity w_e and the large-scale vertical motion \overline{w} . In a high-pressure system $\overline{w} < 0$ which tends to push down the inversion layer height.
- Entrainment causes the boundary-layer height h to grow. It is one of the few quantities whose scaling behaviour is known. Its magnitude can be well predicted from the surface virtual potential temperature flux and the inversion jump $\Delta\theta_v$.
- In the absence of sources and sinks like radiation or precipitation turbulent fluxes of the (virtual) potential temperature or the specific humidity will be simple linear functions of height. This notion follows from the fact that if a vertically well mixed structure is maintained, then temporal changes for those quantities must be constant with height.
- For thin inversion layers the flux at the top of the boundary layer h of a quantity ϕ is given by the flux-jump relation, which is the product of the entrainment velocity and the jump of ϕ across the inversion, $\overline{w'\phi'_h} = -w_e \Delta\phi$.

¹In boundary-layer studies it is sometimes allowed to approximate Π to be equal to unity, *but never* when it concerns *vertical* variations of potential temperature. In the latter case such an approximation will yield an incorrect measure of vertical stability.

- The main reason to have spent relatively much attention to the clear convective boundary layer is that an understanding of the impact of surface and entrainment fluxes of heat and moisture on the relative humidity paves the way for being able to predict cloud formation. Indeed, this will occur if the relative humidity at the top of the boundary layer hits saturation.

Because θ_v depends on both the temperature and humidity, its surface flux depends on the fluxes of both heat and moisture. Because the sum of the sensible and latent heat fluxes is controlled by the net flux of radiation at the surface minus the heat flux into the soil, and because their contribution to $\overline{w'\theta'_{v\text{sf}}}$ has unequal weights, the precise partitioning of the turbulent fluxes into SHF and LHF matters for the magnitude of the entrainment velocity.

Much of what has been discussed in this chapter can be applied to stratocumulus-topped boundary layers. Like the CBL, these cloud layers are capped by a sharp thermal inversion and they are affected by cloud-top entrainment. However, because phase changes of water and radiation play an important role these processes need to be included.

Chapter 9

Boundary-layer clouds



Figure 9.1: Photographs of shallow cumulus (left) and stratocumulus (right).

Stratus, stratocumulus and shallow cumulus, as shown in Fig. 9.1, are all classified as boundary layer clouds. Stratus and stratocumulus are layered clouds having cloud fractions close to unity. The formal distinction between stratus and stratocumulus is the cloud optical thickness (τ), where $\tau > 23$ ($\tau < 23$) defines stratus (stratocumulus). However, in practice this definition is usually not that strictly applied. Even in the scientific literature it is not uncommon to find that a cloud type is called stratus instead of stratocumulus, and vice versa. Shallow cumulus can be characterized by its broken structure and small cloud fraction.

Satellite retrievals as compiled in Figure 9.2 show that there is a very persistent presence of stratocumulus clouds in the subtropical areas west of the American continent and Africa. Figure 9.3 shows a satellite image of stratocumulus off the coast of California. The presence of stratocumulus in the subtropics can be understood by considering the mean flow pattern in subtropics (see Figure 9.4). Due to the large-scale subsidence in the descending branch of the Hadley circulation the observed boundary layers in the subtropical regions are usually relatively shallow. The boundary layers are capped by a stable temperature inversion that acts to trap the moisture that is evaporated from the sea surface. This supports the formation and maintenance of horizontally extended stratocumulus fields. The surface winds transport air from the subtropics towards the equator. Along this path the sea surface temperature gradually increases and a subsequent transition from stratocumulus to cumulus takes place.

Figure 9.5 shows the cloud albedo, defined as the ratio of the upward to the downward solar radiative flux at the top of the cloud layer according to Eq. (1.2). As the definition of the cloud optical depth τ will be given in the Chapter on radiation the cloud layer depth is shown at the top of the figure. The key message of the plot is that a cloud layer with a depth of more than about 300 m will reflect more than 50% of the downward solar radiation back to space. This strong reflectivity make stratocumulus a key cloud regime controlling the Earth's climate. This notion led to the statement by Randall et al. (1984) that *a mere 4% increase in the area of the globe covered*

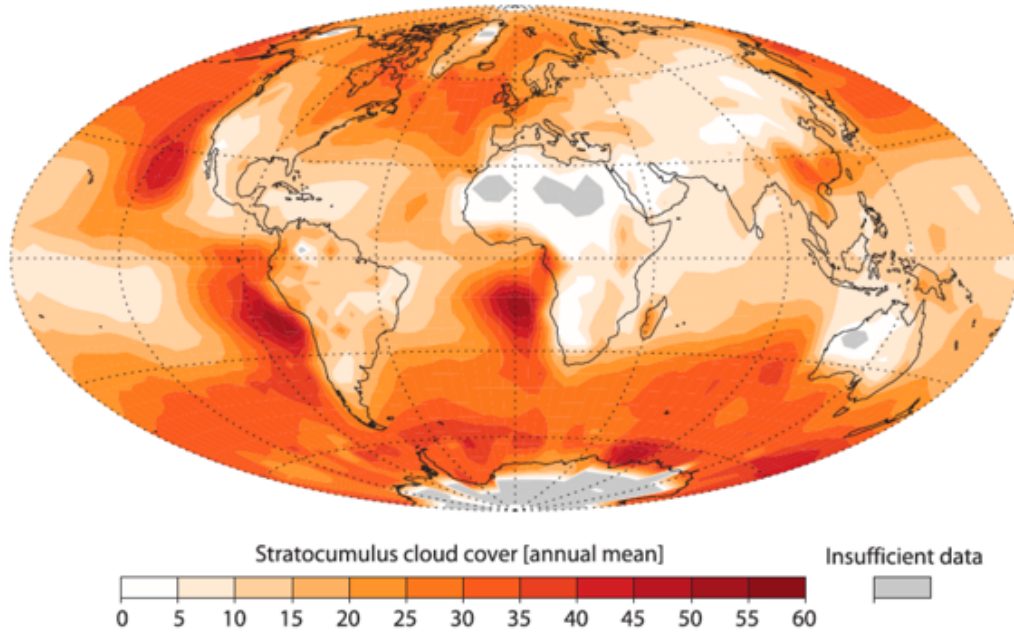


Figure 9.2: Annual mean stratocumulus cover (Wood 2012).

by low level stratus clouds would be sufficient to offset the 2-3 K predicted rise in global temperature due to a doubling of CO_2 . Unfortunately, it appears that global climate models predict an opposite, diminishing trend in the global stratocumulus amount under global warming conditions, thereby amplifying the latter (Bony and Dufresne 2005).

The increase in the downwelling longwave radiation is due to the presence of cloud water. If the depth of stratus or stratocumulus exceeds 100 m, they are optically thick and emit radiation as a black body as opposed to a clear atmosphere which emits longwave radiation as a grey body. As a consequence, more infrared radiation is emitted downwards from the cloud top than is received and absorbed from the atmosphere above, as is illustrated from aircraft observations shown in Figure 9.6. The largest jump in the downward longwave radiation takes place in a shallow layer of several tens of meters thick near the cloud top. In this layer local radiative cooling rates exceeding more than 8 K h^{-1} are not exceptional. It causes radiatively cooled air parcels to sink downwards, thereby redistributing the colder temperatures throughout the boundary layer. There is also a small jump at cloud base which leads to warming. The strong increase in the downwelling longwave radiation flux in the presence of low clouds has a strong impact on the surface temperature evolution in the sense that it reduces the cooling of the ground surface. This is the main reason that nights with clear skies are typically colder than under cloudy skies, for which reason clouds are sometimes said to 'act as a blanket'.

Extended stratus cloud decks frequently observed in the Arctic region. In particular during the dark winter period Arctic stratus has a strong damping effect on surface cooling due to its blackbody emission of downward longwave radiation. Figure 9.7 displays observations at the SHEBA (Surface Heat and Energy Balance of the Arctic Ocean) ice camp during the Arctic spring. It clearly shows that the net longwave radiation at the surface increases sharply by an amount of about 60 W m^{-2} during the presence of a cloud layer that extends down to the surface. Note that the figure shows the *liquid* water path while the temperature during the observations was below freezing, which implies that the cloud must have consisted of *supercooled* liquid water.

The radiative cooling of the stratocumulus cloud top generates turbulence that causes conserved

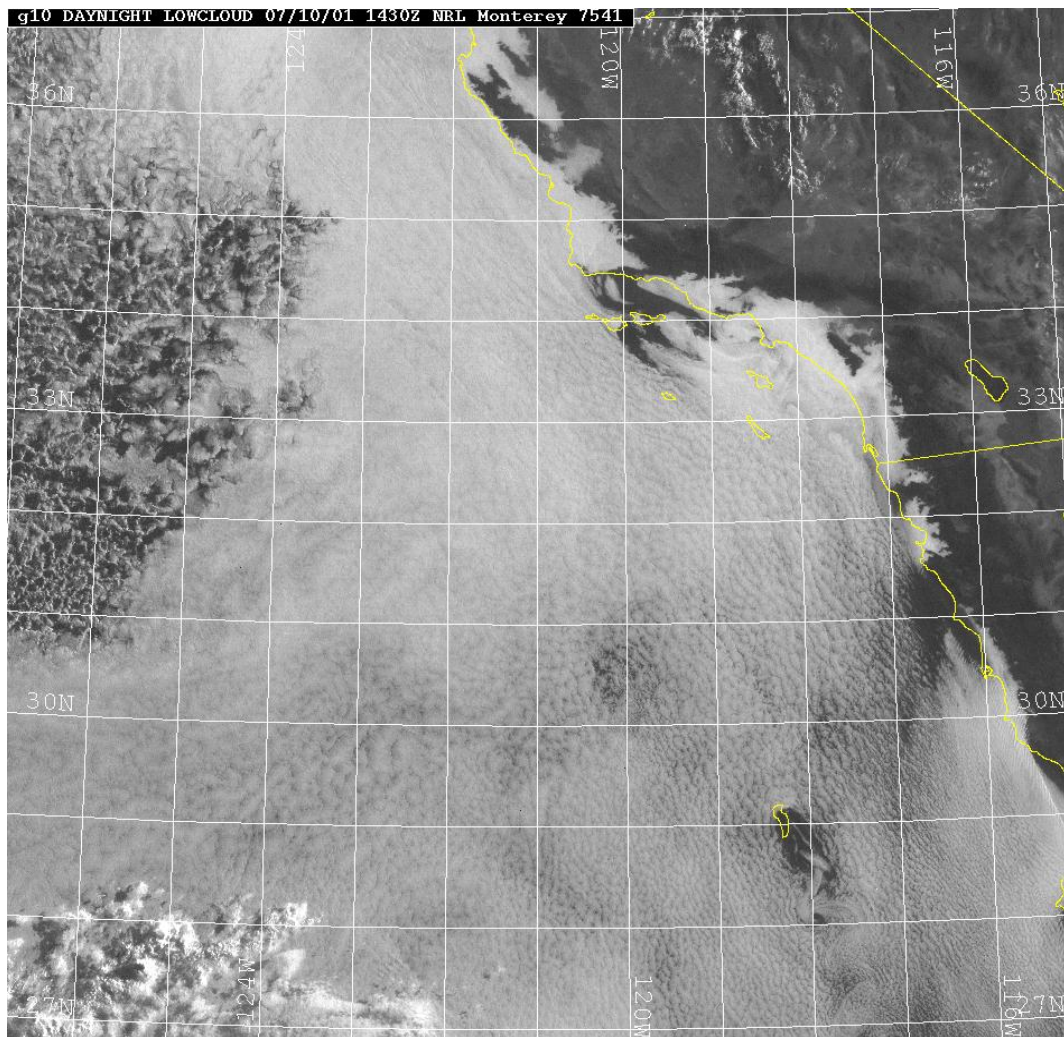


Figure 9.3: Satellite image of an horizontally extended field of stratocumulus clouds ($\sim 1100 \times 1100\text{km}^2$) off the coast of California. Stratocumulus often hinders aircraft operations in San Francisco.

variables such as the liquid water potential temperature and the total specific humidity to become vertically well mixed (see Figure 9.8 for a schematic illustration). From the cloud base to the cloud top the total water specific humidity exceeds the saturation value, i.e. $q_t > q_{\text{sat}}$, and due to latent heat release effects the virtual potential temperature approximately follows the wet-adiabatic lapse rate. The cloud top is capped by a strong stable inversion layer in which the temperature can increase by more than $10 \sim 15^\circ\text{C}$ over a vertical distance of less than 50 m.

During daytime, a significant amount of solar radiation is absorbed by the cloud layer. The solar absorption extends deeply into the cloud layer. As a result, the cloud layer can get warmer more rapidly than the subcloud layer, causing a very small virtual potential temperature jump near the cloud base. In that case the cloud layer becomes stably stratified with respect to the subcloud layer, and the transport of heat and moisture into the stratocumulus cloud by convective eddies driven from the surface is effectively reduced and sometimes even cut off. Radiative cooling will maintain the generation of convection from the cloud top, which results in two well-mixed turbulent

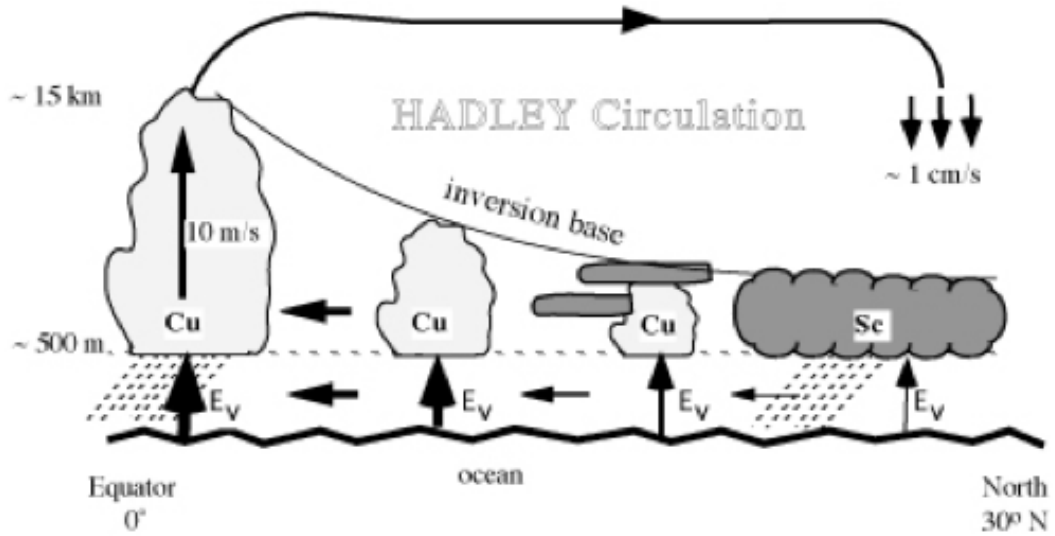


Figure 9.4: Schematic cross section through the trades and ITCZ illustrating the circulation and moistening of the subcloud layer and cloud layer. ' E_v ' indicates the surface moisture flux, and 'sc' and 'cu' denote stratocumulus and cumulus clouds, respectively. Figure by Hans Cuijpers.

layers that are *decoupled* and only interact weakly. Decoupling may lead to a breakup of the cloud because, firstly, solar radiative absorption will cause evaporation of cloud liquid water, and secondly, the cloud layer will dry out if entrainment of dry air at the cloud top continues while the moisture supply at the cloud base by the surface-driven eddies is reduced significantly. Even if these two processes do not lead to a full dissipation of the cloud layer, they will at least cause a change in the cloud structure. Because of the diurnal cycle of the sun, the cloud amount and cloud fraction will be maximal before and near sunrise while the minimal cloudiness occurs around local noon. Other mechanisms that can cause a temperature jump near cloud base are evaporation of drizzle below cloud base and the subsequent cooling of the subcloud layer.

The subcloud layer of a cumulus-topped boundary layer is also vertically well-mixed. This does not apply to the cloud layer in which the virtual potential temperature profile is in between the dry and the wet-adiabatic lapse rate. Note that in the cloud layer the mean specific humidity is lower than the saturation value ($q_t < q_{sat}$).

Typical examples of vertical profiles for the buoyancy fluxes are displayed in Figure 9.9. In the clear convective boundary the buoyancy flux is approximately linear with height, and the minimum value at the boundary-layer top is due to the downward turbulent mixing (entrainment) of warm air from above the inversion layer. In stratocumulus the longwave radiative cooling explains the sharp jump in the buoyancy flux profile near the cloud top as the cooling produces cold air parcels that sink downwards. The sharp increase in the buoyancy flux that occurs near the cloud base is resulting from latent heat release by condensation of cloud liquid water. Thus both latent heat release effects and longwave radiative cooling act to generate a positive buoyancy flux in the cloud layer. The minimum flux at the cloud top is also due to the entrainment of warm air from above the inversion. In the case of cumulus convection, the buoyancy flux is negative near the top of the subcloud layer. At these levels only the strongest thermals that have sufficient upward momentum can rise through and become saturated. Above this level the release of latent heat causes the virtual potential temperature difference with respect to the environment to become positive again.

An accurate representation of boundary-layer clouds in weather forecast and climate models is problematic. This can be clearly illustrated from a climate model intercomparison project (CMIP5). Figure 9.10 shows that global climate models experience great difficulties simulating eastern boundary regions, with one of the most notable shortcomings being warm sea-surface temperature biases

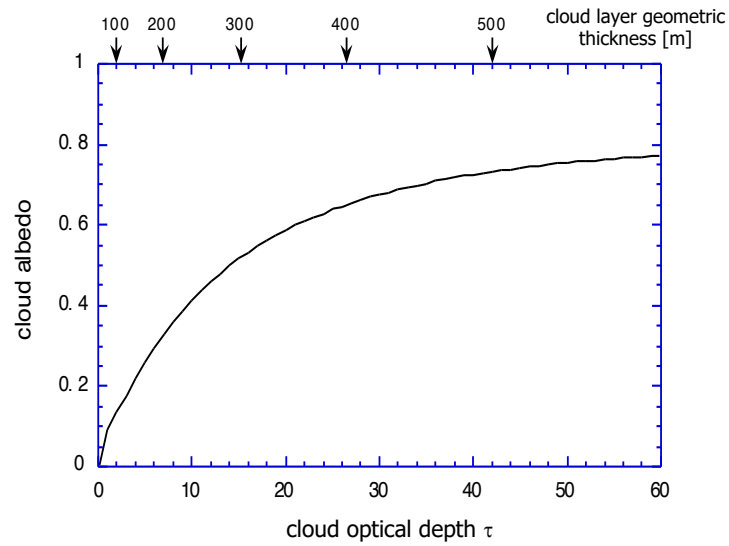


Figure 9.5: The cloud albedo as a function of the cloud optical depth τ . The corresponding cloud geometric depth is shown at the top of the figure.

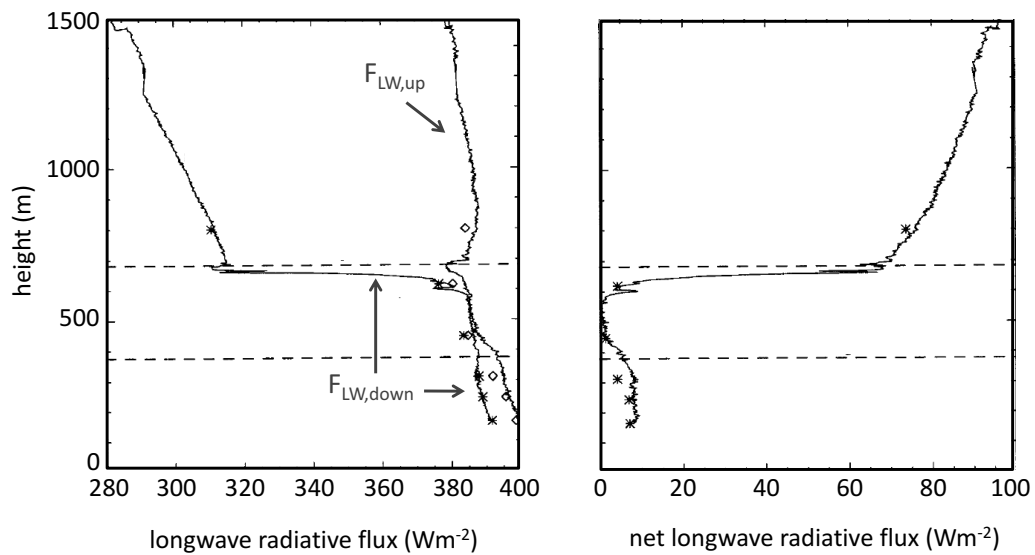


Figure 9.6: The observed upward and downward longwave radiation (left panel) and the net longwave radiation (right panel, same vertical scale as right panel) as a function of height in a stratocumulus-topped boundary layer during ASTEX. The asterisks '*' and the diamonds '◇' represent mean values during a horizontal aircraft leg (± 60 km), and the line indicates results from a slant profile. From Duynkerke et al. (1995)

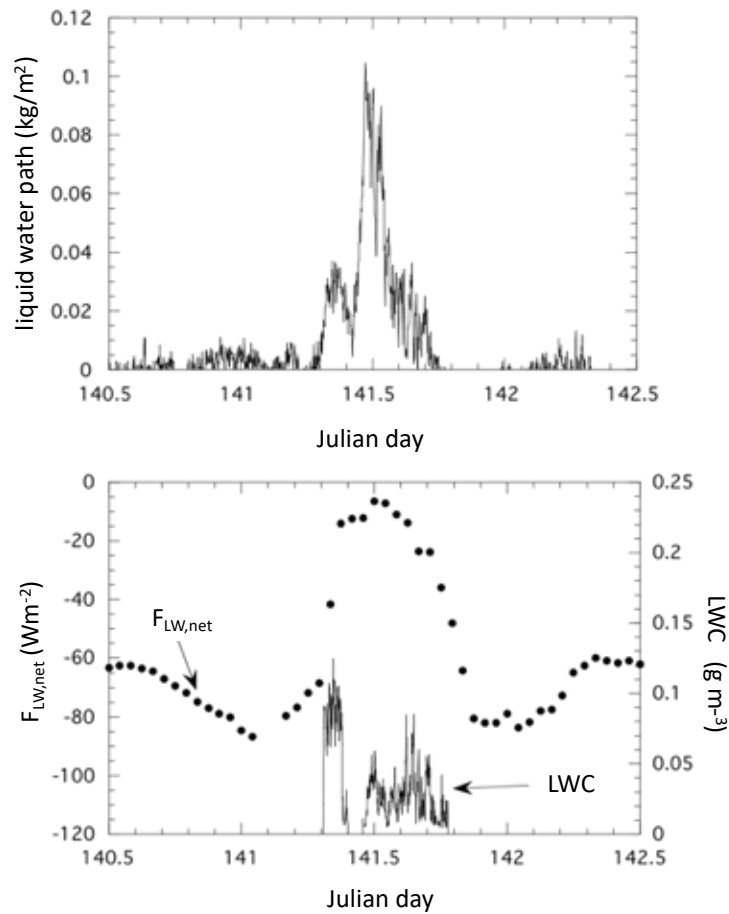


Figure 9.7: Time series of the liquid water path (upper panel) and the net longwave radiation and liquid water content (LWC) in fog at 2 m above the surface (lower panel). The liquid water path data were obtained with a microwave radiometer and were kindly provided by Dr. J. Liljegren. The measurements were made from 20 to 22 May 1998 (Julian day 140 to 142) at the SHEBA ice camp (76°N, 166°W)

that often exceed 5 K. One of the reasons is that stratocumulus cloud decks and their effects on shortwave radiation are underpredicted in these models. This deficiency is in particular relevant for the simulation and the prediction of the El Niño - Southern Oscillation (ENSO). An important reason that explains the systematic stratocumulus cloud bias is the rather coarse vertical resolution Δz applied in global models, in the boundary layer usually more than 100 m. In any case Δz is much larger than the inversion layer thickness, or the thickness of the radiatively cooled layer at the top of the stratocumulus. An obvious consequence is that large-scale models cannot faithfully capture the sharp inversion layers capping stratocumulus.

Figure 9.11 shows a case of an underpredicted stratocumulus clouds deck by the the German weather forecast model COSMO, which was also missed by most of the other European weather forecast models. This led to some severe problems in the fields of renewable energy and traffic. Energy companies wish to get an accurate prediction of solar radiation (in addition to wind speed) as this information is vital to establish the remainder of the electricity demand that needs to be generated by power plants. The airport of Schiphol complained about the poor quality of the

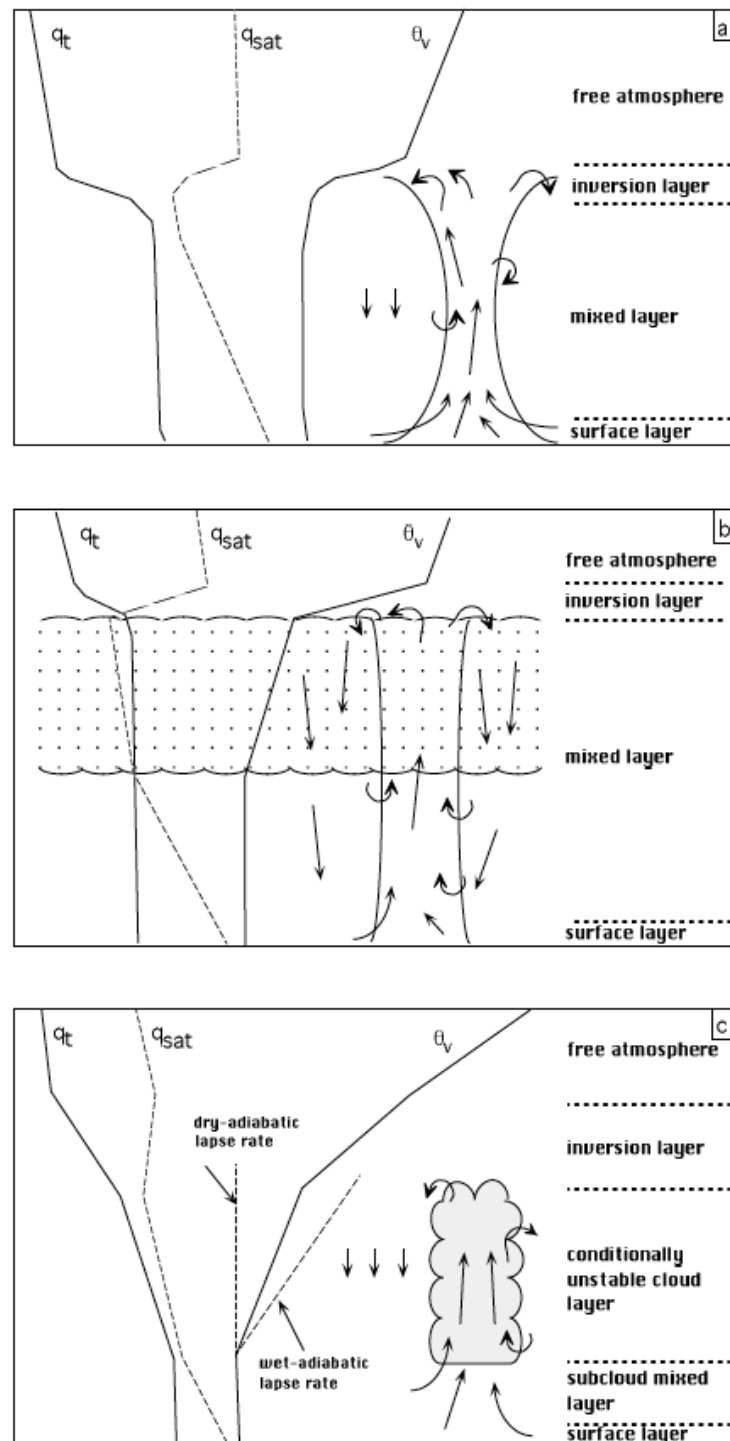


Figure 9.8: Schematic of typical mean profiles for the total specific humidity q_t , the saturation specific humidity q_{sat} and the virtual potential temperature θ_v in a) the clear convective boundary layer, b) stratocumulus and c) cumulus. From Heus et al. (2010)

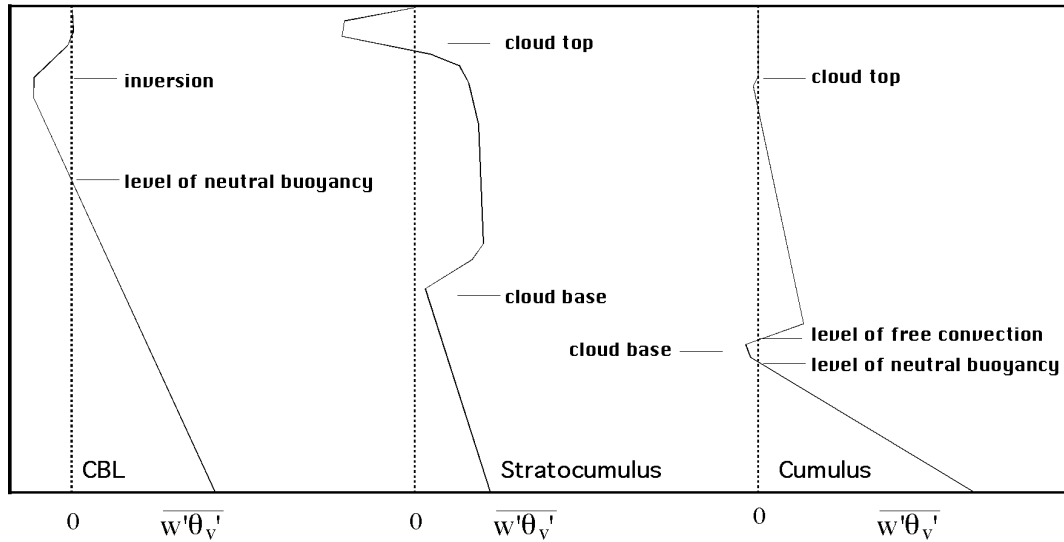


Figure 9.9: Schematic of typical virtual potential temperature flux ($\overline{w'\theta_v'}$) profiles in the clear convective boundary layer (left), stratocumulus (middle), and cumulus (right).

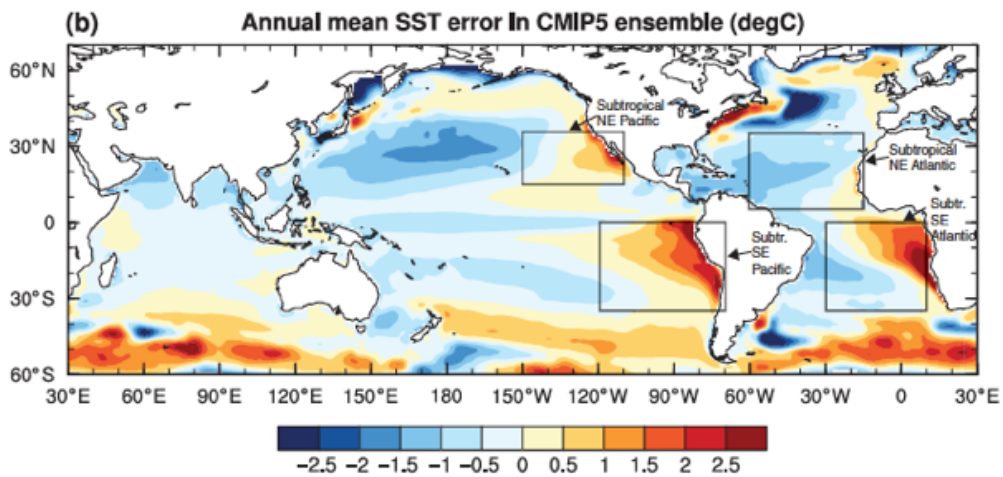


Figure 9.10: Errors in the sea surface temperature computed from an ensemble of climate model results by Richter (2015).

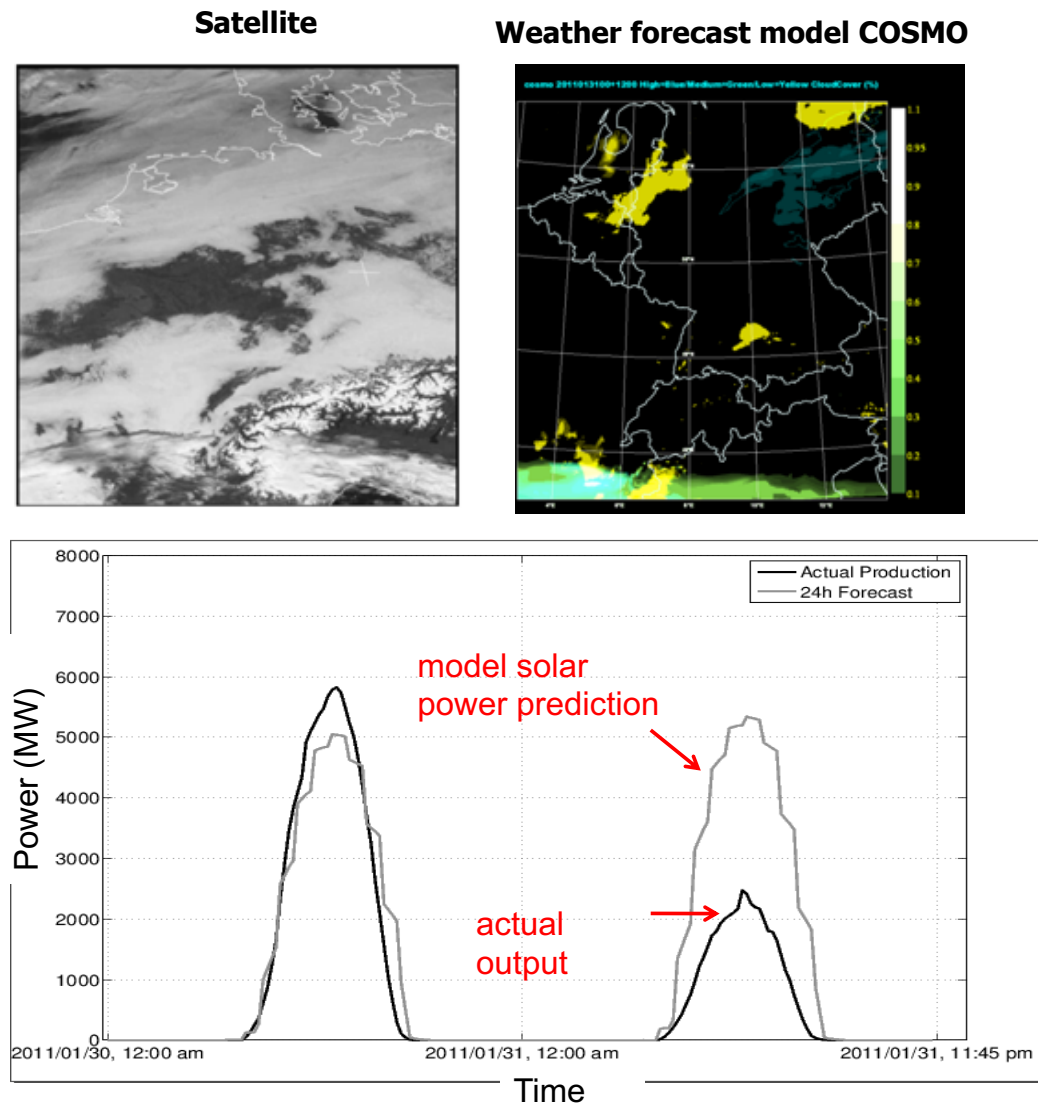


Figure 9.11: Example of a stratocumulus deck over the Netherlands and Germany (upper left plot), the prediction of the cloud deck (yellow colors in the upper right plot) by the German weather forecast model COSMO, and a comparison of the predicted solar power with the actual output (lower plot) for 30 January 2011.

weather forecast as this wintertime cloud deck could possibly produce freezing rain which could have a severe impact on aviation.

9.1 Summary and outlook

Clouds are key to weather and climate due to their impact on the radiative fluxes. Here we have focused on stratocumulus clouds that, despite their relatively shallow vertical extent, have a large albedo. We have also seen that stratocumulus clouds tend to increase the downwelling longwave

radiation. The overall net effect of stratocumulus on the global climate is dominated by their shortwave albedo that tends to cool the Earth. Regionally there may be exceptions to this rule, for example in the Arctic. During winter there is no solar radiation, and the presence of stratus causes an enhancement of the downward longwave radiative flux, which in turn strongly reduces the cooling of the sea ice.

Global climate models have difficulties in faithfully capturing the subtropical stratocumulus cloud decks, but also weather forecast models sometimes underpredict them. This is partly due to their limited vertical extent, which makes them difficult to capture as large-scale models apply relatively coarse vertical grid sizes.

Because stratocumulus clouds are important to both weather and climate has made them subject of quite a few intensive fields experiments as well as modeling intercomparison studies with turbulence resolving models like large-eddy simulation models.

Chapter 10

Mixed-layer model

The fact that the mean vertical profiles of θ and q_v are approximately constant with height in the CBL can be used to build a simple conceptual model for this type of boundary layer. To this end let us denote the mean mixed-layer value of any arbitrary conserved variable by ϕ_{ml} , and the values at the surface and just above the inversion layer as ϕ_{sfc} and ϕ_{h^+} , respectively. Fig. 10.1 shows a schematic depiction of a clear CBL with depth h .

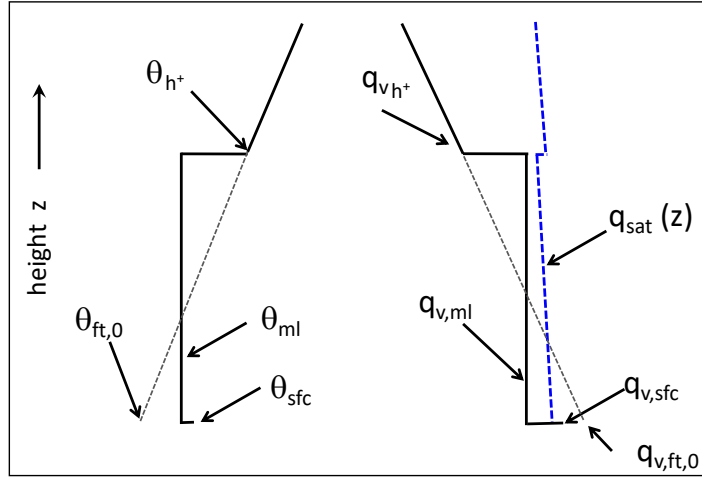


Figure 10.1: Schematic of the vertical profiles of the potential temperature, specific humidity, and saturated specific humidity. See text for details.

If turbulence is the only acting physical process, then the temporal change of ϕ_{ml} will be determined by the change of the turbulent flux across the boundary layer. For this case the turbulent flux will be a linear function of height and is therefore determined by its values at the ground surface and the top of the boundary layer. Let $\bar{\phi}(z) = \phi_{ml}$ in the boundary layer. This allows to write

$$\frac{d\phi_{ml}}{dt} = -\frac{\partial \overline{w'\phi'}}{\partial z} = -\frac{\overline{w'\phi'}_h - \overline{w'\phi'}_{sfc}}{h} = \frac{w_e \Delta\phi + \overline{w'\phi'}_{sfc}}{h}, \quad (10.1)$$

where we used the linear flux profile Eq. (8.11) and the flux-jump relation (10.28).

Because the inversion jump is defined by the difference of the values of ϕ just above the inversion layer at h^+ and the boundary-layer value, $\Delta\phi = \phi_{h^+} - \phi_{ml}$, we can express the time derivative of the inversion jump as,

$$\frac{d\Delta\phi}{dt} = \frac{d\phi_{h^+}}{dt} - \frac{d\phi_{ml}}{dt} \quad (10.2)$$

Let us assume a constant vertical gradient of $\gamma_\phi \equiv (d\bar{\phi}/dz)_{ft}$ in the free troposphere (indicated by subscript 'ft'). With aid of the slope parameter γ_ϕ we can express the free tropospheric profile as

$$\bar{\phi}(z) = \phi_{ft,0} + \gamma_\phi z \quad \text{for } z \geq h^+, \quad (10.3)$$

where the quantity $\phi_{ft,0}$ is the extrapolated value of the free tropospheric profile of $\bar{\phi}$ to the surface. The value of ϕ_{h^+} depends on the height of the boundary layer, so its temporal change depends on the change in height of the boundary layer, and hence entrainment,

$$\frac{d\bar{\phi}_{h^+}}{dt} = w_e \frac{d\bar{\phi}}{dz} = w_e \gamma_\phi. \quad (10.4)$$

Because large-scale subsidence advects the height of the inversion layer, but does not modify the magnitude of the inversion jump, Eq. (10.4) also applies to cases with large-scale subsidence.

The last equation gives the evolution of the boundary-layer depth,

$$\frac{dh}{dt} = A \frac{\overline{w'\theta'_{v,sfc}}}{\Delta\theta_v} + \bar{w}_h, \quad (10.5)$$

where we used the entrainment parameterization (8.18). Eqs. (10.1), (10.2) and (10.5) comprise the mixed-layer model (MLM). It is typically applied to the potential temperature θ and the specific humidity q_v . Those two variables are actually necessary to compute the vertical profile of the virtual potential temperature that is needed to calculate the entrainment velocity.

Equilibrium boundary-layer height

The observations shown in Fig. 8.1 indicate a period with only a weak growth of h . Given the theory above, we can determine the conditions that explain a constant boundary layer height with time. This will be achieved if there is a balance between entrainment and large-scale subsidence, $dh/dt = 0$. For negligibly small vertical variations in the large-scale divergence

$$\bar{w}(z) = -Dz, \quad (10.6)$$

and subsequently the equilibrium boundary layer depth h_{eq} can be obtained from

$$h_{eq} = \frac{A}{D} \frac{\overline{w'\theta'_{v,sfc}}}{\Delta\theta_v}. \quad (10.7)$$

The equilibrium mixed-layer height is thus controlled by the large-scale divergence D , the surface buoyancy flux, and the thermal inversion stability as measured by the jump $\Delta\theta_v$. From this solution we can infer the conditions that favor a shallow boundary layer. Because air pollutants that are emitted near the surface will be distributed across the boundary layer depth h , small values for h will yield typically yield higher concentrations of air pollution (see Fig. 10.2). Shallow boundary layers can be expected for strong subsidence as measured by a large value of D , a large jump $\Delta\theta_v$ that indicates a very stable inversion layer, or a relatively small value for $\overline{w'\theta'_{v,sfc}}$.

Hydrostatic pressure in a moist mixed layer

An important application is the capability of the MLM to predict and understand the formation of clouds. What is needed as input parameters to the MLM are the surface values of the SHF and LHF, and the initial vertical profiles of θ and q_v . The large-scale divergence is typically taken from a large-scale weather forecast model. To assess whether clouds will form the relative humidity needs to be diagnosed, which, in turn, according to Eqs. (2.18) and (2.19) requires the vertical profiles of temperature and pressure. We recall that in the mixed layer the potential temperature and the specific humidity are constant with height, but the temperature decreases with height according to

$$\gamma_T \equiv \frac{dT}{dz} = -\frac{g}{c_p}, \quad (10.8)$$

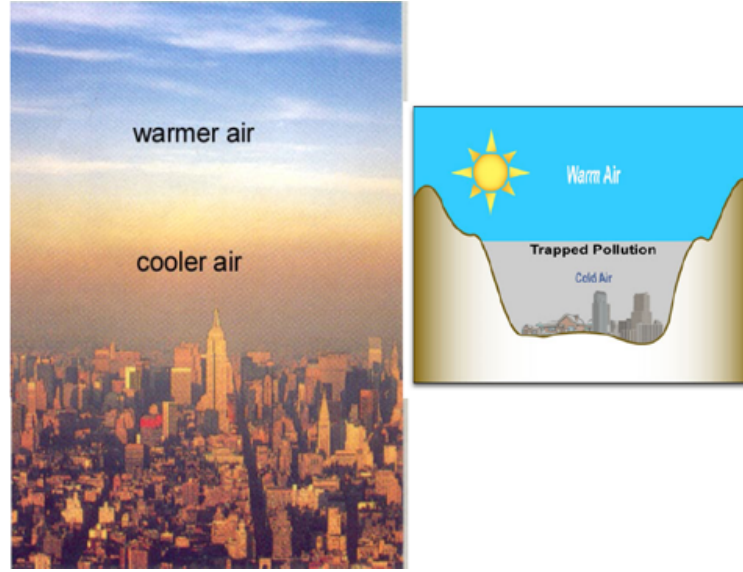


Figure 10.2: Photograph and schematic of a polluted clear, shallow atmospheric boundary layer.

and consequently

$$\gamma_{T_v} \equiv \frac{dT_v}{dz} = -(1 + \epsilon_I q_{v,ml}) \frac{g}{c_p}. \quad (10.9)$$

The latter quantity is needed to evaluate the pressure with aid of the gas law and hydrostatic equation, Eqs. (2.11) and (2.27), respectively. By eliminating ρ we obtain an expression that gives the vertical variation of the pressure as a function of the temperature,

$$\frac{\partial \ln p}{\partial z} = -\frac{g}{R_d T_v}. \quad (10.10)$$

Since T_v varies linearly with height an analytic solution can be obtained. Let $T_v(z) = T_{v\text{sfc}} + \gamma_{T_v} z$. We can then write

$$\frac{\partial \ln p}{\partial z} = -\frac{g}{R_d(T_{v\text{sfc}} + \gamma_{T_v} z)} \iff d \ln p = -\frac{g}{\gamma_{T_v} R_d} d \ln(T_{v\text{sfc}} + \gamma_{T_v} z). \quad (10.11)$$

Integration from the ground surface $z = 0$ upwards to height z yields

$$\ln \left(\frac{p(z)}{p_{\text{sfc}}} \right) = -\frac{g}{\gamma_{T_v} R_d} \ln \left(1 + \frac{\gamma_{T_v} z}{T_{v\text{sfc}}} \right) = \ln \left(1 + \frac{\gamma_{T_v} z}{T_{v\text{sfc}}} \right)^{-\frac{g}{\gamma_{T_v} R_d}} \quad (10.12)$$

The logarithm can be omitted to give

$$p(z) = p_{\text{sfc}} \left(1 + \frac{\gamma_{T_v} z}{T_{v\text{sfc}}} \right)^{-\frac{g}{\gamma_{T_v} R_d}} \quad (10.13)$$

This equation is valid for any layer with constant lapse rate of temperature.

How to code a mixed-layer model?

Here the sequence of steps to be taken is presented.

1. Initialize the model by prescribing the constant mixed-layer values for q_v and θ , their jumps across the inversion, and their vertical profiles in the free troposphere.

2. Determine the surface fluxes of heat and moisture. This may be done with aid of a bulk formula like Eq. (5.23), you may specify the fluxes on the basis of observations, or you may prescribe them on the basis of an educated guess.
3. Calculate the entrainment velocity w_e from Eq. (8.18). Diagnose the virtual potential temperature profile from Eq. (8.19), and calculate $\overline{w'\theta'_{\text{sfc}}}$ with aid of Eqs. (8.20) or (8.21).
4. Use the flux-jump relation Eq. (10.28) to compute the fluxes of q_v and θ at the top of the mixed layer.
5. Discretize Eq. (10.1) to compute the updated values of θ_{ml} and $q_{v,\text{ml}}$ at time $t + \Delta t$ based on information known at time t ,

$$\phi_{\text{ml}}^{t+\Delta t} = \phi_{\text{ml}}^t + \left(\frac{w_e \Delta \phi^t + \overline{w'\phi'_{\text{sfc}}}}{h^t} \right) \Delta t \quad (10.14)$$

Your time step should be sufficiently small such that the solution will not depend on the value of Δt .

6. Compute the updated boundary-layer depth from

$$h^{t+\Delta t} = h^t + (w_e + w_h) \Delta t. \quad (10.15)$$

7. To inspect whether clouds will have formed you will need to compute the relative humidity. This requires the computation of the pressure from Eq. (10.13). This in turn allows to compute the temperature from Eq. (2.52) and the saturation specific humidity with aid of Eqs. (2.18) and (2.19).

Despite its simplicity, the MLM has been demonstrated to capture observations very well and it is therefore considered to be a very powerful tool for research.

10.1 Summary and outlook

An MLM can also be applied to stratocumulus-topped boundary layers. Like the CBL, these cloud layers are capped by a sharp thermal inversion and they are affected by cloud-top entrainment. However, because phase changes of water and radiation play an important role these processes need to be included as a source term in the heat equation, which is usually used in terms of a conserved variable for moist adiabatic processes like the liquid water potential temperature θ_1 or the dry static energy s_1 , according to Eq. (2.47).

The conservation equations for heat and moisture are given by, respectively,

$$\frac{\partial \overline{\theta_1}}{\partial t} = - \frac{\partial \overline{w'\theta'_1}}{\partial z} - \frac{1}{\rho c_p \Pi} \frac{\partial F_{\text{rad}}}{\partial z}, \quad \frac{\partial \overline{q_t}}{\partial t} = - \frac{\partial \overline{w'q'_t}}{\partial z} \quad (10.16)$$

In a mixed-layer framework they read,

$$\frac{\partial \theta_{1,\text{ml}}}{\partial t} = \frac{w_e \Delta \theta_1 + \overline{w'\theta'_{1,\text{sfc}}} - \Delta F_{\text{rad}} / \rho c_p \Pi}{h}, \quad \frac{\partial q_{t,\text{ml}}}{\partial t} = \frac{w_e \Delta q_t + \overline{w'q'_{t,\text{sfc}}}}{h}. \quad (10.17)$$

Entrainment in stratocumulus depends mainly on the radiative forcing according to

$$w_e = \eta \frac{\Delta F_{\text{rad}}}{\rho c_p \Delta \theta_1}, \quad (10.18)$$

with η an efficiency factor close to unity, and F_{rad} the change of the net radiation flux across the cloud layer. Recall that according to Eq. (8.18) the entrainment in the CBL depends on the surface buoyancy flux, where the latter is the main forcing of boundary-layer turbulence.

Appendix A: The vertically integrated budget equation for conserved variables

The bulk model equations can be derived from the Reynolds averaged budget equation for any arbitrary conserved variable φ , which for horizontally homogeneous conditions read,

$$\frac{\partial \bar{\varphi}}{\partial t} = -\bar{w} \frac{\partial \bar{\varphi}}{\partial z} - \frac{\partial \overline{w' \varphi'}}{\partial z} - \frac{\partial F_{\varphi}^{\text{sfc}}}{\partial z}, \quad (10.19)$$

where F_{φ}^{sfc} represents the horizontal slab mean value of the vertical flux of, for example, drizzle or radiation.

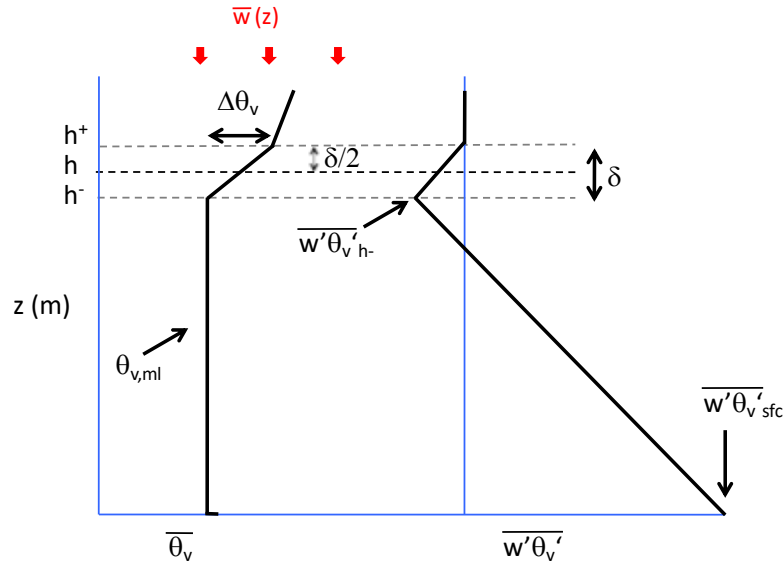


Figure 10.3: Schematic of the vertical mean profiles of θ_v and the virtual potential temperature flux $w' \theta_v'$ in the CBL. Adapted from vanZanten et al., 1999 (VanZanten et al. 1999).

Figure 10.3 shows a schematic of the CBL structure for θ_v , where the subscript 'ml' is used to denote the mixed layer mean value of any quantity. A MLM assumes that conserved variables are vertically well mixed in the boundary layer, and that the depth of the inversion layer δ is infinitesimally thin.

As a first step towards the MLM equations we will integrate Eq. (10.19) from the surface (sfc)

to the top of the boundary layer h^- to give

$$\int_0^{h^-} \frac{\partial \bar{\phi}}{\partial t} dz = -\overline{w' \phi'}_{h^-} + \overline{w' \phi'}_{\text{sfc}} - F_{\phi}^{\text{src}}|_{h^-} + F_{\phi}^{\text{src}}|_{\text{sfc}}. \quad (10.20)$$

Note that because of our assumption of a constant value of $\bar{\phi}$ in the mixed layer, the subsidence term has vanished. In MLMs the surface flux is usually computed from a simple bulk formula like Eq. (5.23). At this point the flux at the top of the boundary layer $\overline{w' \phi'}_{h^-}$ needs to be specified.

It is possible to express $\overline{w' \phi'}_{h^-}$ as a function of the entrainment rate. We will again integrate the budget equation (10.19), but now from the base (h^-) to the top (h^+) of the inversion layer,

$$\int_{h^-}^{h^+} \frac{\partial \bar{\phi}}{\partial t} dz = - \int_{h^-}^{h^+} \bar{w} \frac{\partial \bar{\phi}}{\partial z} dz + \overline{w' \phi'}_{h^-} - F_{\phi}^{\text{src}}|_{h^+} + F_{\phi}^{\text{src}}|_{h^-}. \quad (10.21)$$

Above the thermal inversion layer there is no turbulence such that $\overline{w' \phi'}_{h^+} = 0$. Because the inversion layer height is time dependent we will need to invoke Leibniz' rule of integration,

$$\begin{aligned} \frac{d}{dt} \left(\int_{z_0(t)}^{z_1(t)} \varphi(z, t) dz \right) &= \int_{z_0(t)}^{z_1(t)} \frac{\partial}{\partial t} \varphi(z, t) dz \\ &+ \varphi(z_1, t) \frac{dz_1}{dt} - \varphi(z_0, t) \frac{dz_0}{dt}, \end{aligned} \quad (10.22)$$

to give

$$\int_{h^-}^{h^+} \frac{\partial \bar{\phi}(z, t)}{\partial t} dz = \frac{d}{dt} \left[\int_{h^-}^{h^+} \bar{\phi}(z, t) dz \right] - \Delta \phi \frac{dh}{dt}. \quad (10.23)$$

where we neglected the time rate of change in the thickness of the inversion layer relative to the time rate of change in its height. This is mathematically equivalent to assuming a more stringent condition of a fixed inversion layer depth $\delta = h^+(t) - h^-(t)$. We define the operator $\Delta_{z_1}^{z_2} \varphi \equiv \varphi_{z_2} - \varphi_{z_1}$ to denote the difference of φ between two arbitrary heights z_1 and z_2 . However, for the special case of the inversion jump we will simply use Δ ,

$$\Delta \phi \equiv \bar{\phi}_{h^+} - \bar{\phi}_{h^-}. \quad (10.24)$$

If $\bar{\phi}$ is assumed to vary linearly with height in the inversion layer, $\bar{\phi} = \phi_{\text{ml}} + \Delta \phi (z - h^-) / \delta$, then we can directly evaluate the following integral,

$$\frac{d}{dt} \left[\int_{h^-}^{h^+} \bar{\phi}(z, t) dz \right] = \delta \frac{\partial (\phi_{\text{ml}} + \Delta \phi / 2)}{\partial t}, \quad (10.25)$$

and likewise the integral including the large-scale subsidence,

$$\int_{h^-}^{h^+} \bar{w} \frac{\partial \bar{\phi}}{\partial z} dz = \bar{w}_h \Delta \phi, \quad (10.26)$$

where we used $\bar{w}_{h^-} \approx \bar{w}_h$. With aid of Eqs. (8.4), (10.23), (10.25) and (10.26) the budget equation (10.21) becomes,

$$\delta \frac{\partial (\phi_{\text{ml}} + \Delta \phi / 2)}{\partial t} = \overline{w' \phi'}_{h^-} + w_e \Delta \phi - \Delta F_{\phi}^{\text{src}}. \quad (10.27)$$

Eq. (10.27) can be strongly simplified by taking the limit $\delta \rightarrow 0$ to yield

$$\overline{w' \phi'}_{h^-} = -w_e \Delta \phi. \quad (10.28)$$

This expression is often referred to as the 'flux-jump relation' and states that the turbulent flux at the top of the boundary layer is proportional to the entrainment rate w_e and the inversion jump of φ .

Bibliography

- Albrecht, B. A., D. A. Randall, and S. Nicholls, 1988: Observations of marine stratocumulus clouds during fire. *Bull. Amer. Meteorol. Soc.*, **69** (6), 618–626.
- Bony, S. and J.-L. Dufresne, 2005: Marine boundary layer clouds at the heart of tropical cloud feedback uncertainties in climate models. *Geophys. Res. Lett.*, **32**, doi:doi:10.1029/2005GL023851.
- Bretherton, C. S., M. E. Peters, and L. E. Back, 2004: Relationships between water vapor path and precipitation over the tropical oceans. *J. Climate*, **17** (7), 1517–1528.
- Crewell, S., et al., 2004: The BALTEX bridge campaign: An integrated approach for a better understanding of clouds. *Bull. Amer. Meteorol. Soc.*, **85** (10), 1565–1584.
- Dufresne, J.-L. and S. Bony, 2008: An assessment of the primary sources of spread of global warming estimates from coupled atmosphere–ocean models. *J. Climate*, **21** (19), 5135–5144.
- Duykerke, P. G., H.-Q. Zhang, and P. J. Jonker, 1995: Microphysical and turbulent structure of nocturnal stratocumulus as observed during ASTEX. *J. Atmos. Sci.*, **52**, 2763–2777.
- Emanuel, K. A., 1994: *Atmospheric Convection*. Oxford University Press, New York.
- Garratt, J. R., 1994: *The atmospheric boundary layer*. First paperback ed., Cambridge University Press, Cambridge, 316 pp.
- Heus, T., et al., 2010: Formulation of the dutch atmospheric large-eddy simulation (DALES) and overview of its applications. *Geosci. Model Development*, **3**, 415–444, doi:10.5194/gmd-3-415-2010.
- Liou, K.-N., 2002: *An introduction to atmospheric radiation*, Vol. 84. Elsevier.
- Marshall, J. and R. A. Plumb, 2016: *Atmosphere, ocean and climate dynamics: an introductory text*, Vol. 21. Academic Press.
- Randall, D. A., J. A. C. Jr, D. H. Lenschow, C. W. Fairall, and R. A. Kropff, 1984: Outlook for research on subtropical marine stratiform clouds. *Bull. Amer. Meteorol. Soc.*, **65**, 1290–1301.
- Richter, I., 2015: Climate model biases in the eastern tropical oceans: Causes, impacts and ways forward. *Wiley Interdisciplinary Reviews: Climate Change*, **6**, 345–358.
- Stephens, G. L., et al., 2012: An update on earth’s energy balance in light of the latest global observations. *Nature Geoscience*, **5** (10), 691.
- Stull, R. B., 1988: *An Introduction to Boundary Layer Meteorology*. Kluwer Academic Publishers, Dordrecht, 666 pp.
- Sullivan, P. P., C.-H. Moeng, B. Stevens, D. H. Lenschow, and S. D. Mayor, 1998: Structure of the entrainment zone capping the convective atmospheric boundary layer. *J. Atmos. Sci.*, **55**, 3042–3064.
- Tennekes, H., 1973: A model for the dynamics of the inversion above a convective layer. *J. Atmos. Sci.*, **30**, 558–567.

- VanZanten, M. C., P. G. Duynkerke, and J. W. M. Cuijpers, 1999: Entrainment parameterization in convective boundary layers. *J. Atmos. Sci.*, **56**, 813–828.
- Wallace, J. M. and P. V. Hobbs, 2006: *Atmospheric science: an introductory survey*, Vol. 92. Elsevier.
- Wood, R., 2012: Stratocumulus clouds. *Mon. Weather Rev.*, **140**, 2373–2423.